APRIL 1958

VOLUME 2 (1958) No. 3

GREGG M. SINCLAIR LIBRARY
UNIVERSITY OF HAWAII
8-7-63

NUCLEAR INSTRUMENTS

A JOURNAL ON ACCELERATORS, INSTRUMENTATION AND TECHNIQUES IN NUCLEAR PHYSICS

EDITOR K. SIEGBAHN - UPPSALA

CONTENTS

J. FLINTA, Pulsed high-intensity ion source (Part I) 219

R. PAULI and J. FLINTA, Pulsed high-intensity ion source (Part II) 227

R. B. MURRAY, Use of Li^6I (Eu) as a scintillation detector and spectrometer for fast neutrons 237

O. ALMÉN, G. BRUCE and A. LUNDÉN, Electromagnetic isotope separator in Gothenburg . . 249

C. CERNIGOI, G. PAULI and C. POIANI, On the pulse shape in a cylindrical ionization chamber 261

E. BUJDOSÓ and L. MEDVECZKY, Apparatus for processing nuclear emulsions 270

J. S. FRASER and J. C. D. MILTON, Automatic-recording apparatus for fission-fragment time-of-flight measurements 275

M. J. POOLE, G. DEAN and W. HOWE, Pulsed beam deflection system for a linear electron accelerator 282

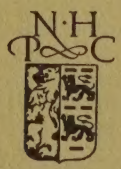

NORTH-HOLLAND PUBLISHING COMPANY - AMSTERDAM

NUCLEAR INSTRUMENTS

A journal on accelerators, instrumentation and techniques in nuclear physics

EDITOR: K. SIEGBAHN, UPPSALA

EDITORIAL BOARD:

J. B. ADAMS (CERN)
E. AMALDI (Rome)
H. L. ANDERSON (Chicago)
K. T. BAINBRIDGE (Cambridge, Mass.)
C. J. BAKKER (CERN)
P. R. BELL (Oak Ridge)
R. E. BELL (Montreal)
A. BERTHELOT (Saclay)
H. BRINKMAN (Groningen)
S. DE BENEDETTI (Pittsburgh)
M. DE HEMPTINNE (Louvain)
A. DE-SHALIT (Rehovoth)
M. DEUTSCH (Cambridge, Mass.)
S. DU TOIT (Pretoria)
B. S. DŽELEPOV (Leningrad)
W. GENTNER (CERN)
P. C. GUGELOT (Amsterdam)
H. HALBAN (Paris)
O. HAXEL (Heidelberg)
P. HUBER (Basel)
D. J. HUGHES (Brookhaven)
S. KIKUCHI (Tokyo)
J. KOCH (Copenhagen)
M. S. KOZODAEV (Moscow)
S. LIVINGSTON (Cambridge, Mass.)
E. M. MCMILLAN (Berkeley)
M. G. MEŠČERJAKOV (Moscow)
P. B. MOON (Birmingham)
M. L. OLIPHANT (Canberra)
W. PAUL (Bonn)
A. S. RAO (Bombay)
G. SALVINI (Rome)
P. SAVIĆ (Belgrade)
P. SCHERRER (Zürich)
CH. SCHMELZER (CERN)
H. W. B. SKINNER (Liverpool)
R. TANGEN (Blindern)
D. TAYLOR (Harwell)
V. I. VEKSLER (Moscow)
O. WERNHOLM (Stockholm)
G. VON DARDEL (CERN)
R. R. WILSON (Cornell)
S. D. WINTER (Saclay)

Contributions may be sent to the Editor, Professor K. Siegbahn, Institute of Physics, the University of Uppsala, either directly or through the intermediary of one of the members of the Editorial Board of the country or region in which the author is working. Contributions may be written in English, French or German, with an abstract in English.

Books for review should be sent to Professor Siegbahn.

Nuclear Instruments is published in bi-monthly issues. The subscription price of a volume of 360 pages is $ 17.00 (130 s), postage free.

Subscriptions should be sent to the publishers, North-Holland Publishing Company, P.O.Box 103, Amsterdam or to any subscription-agent. Subscriptions for U.S.A. are to be sent exclusively to Interscience Publishers, Inc., 250 Fifth Avenue, New York, 1 N.Y.

No part of this issue may be reproduced in any form, by print, photoprint, microfilm or any other means without written permission from the publisher. Reprints, photoprints or microfilms are obtainable at cost from the publisher.

PARTICLE ACCELERATORS

in Nuclear Physics, Chemistry, and Biology

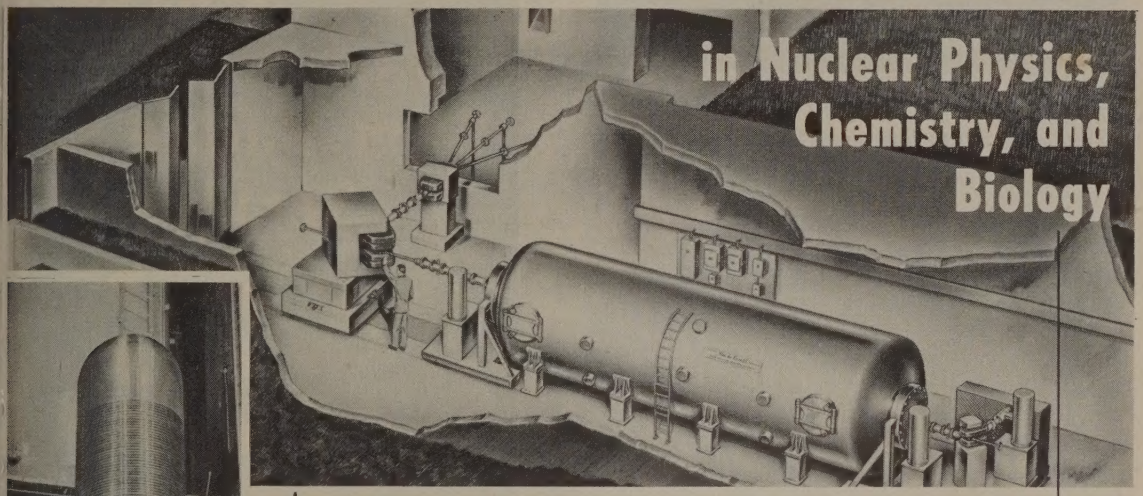

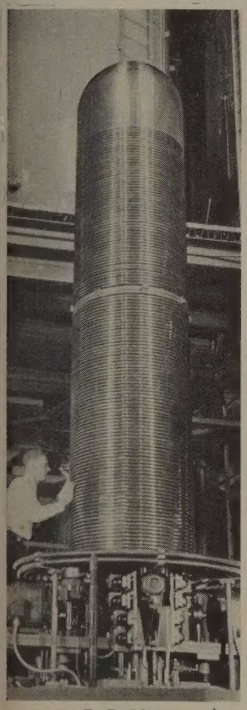

5.5 Mev Van de Graaff Model CN

This machine, widely used for neutron cross-section studies and nuclear-energy-level determinations, will be displayed at the Second International Exhibition of the Peaceful Uses of Atomic Energy, in Geneva, Switzerland.

10-Mev Tandem Van de Graaff® Positive-ion Accelerator, Model EN. Designed for nuclear research at the Chalk River establishment of Atomic Energy of Canada Limited, this is the first of three high-energy machines being built by HIGH VOLTAGE for installation in various parts of North America. With this new design, physicists will, for the first time, be able to explore with precision the binding-energy physics of higher atomic numbers.

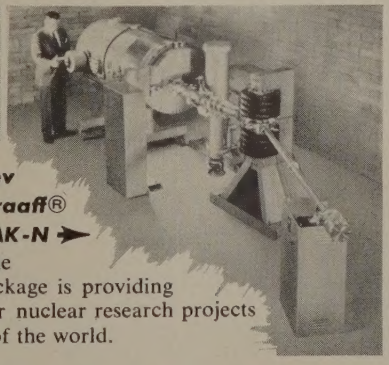

2-Mev Van de Graaff® Model AK-N

This versatile research package is providing the basis for nuclear research projects in all parts of the world.

0.25-Mev Van de Graaff®, Model XN-250

The most recent development in particle accelerators, this new, low-energy machine is designed as a pulsed-neutron source for use with subcritical assemblies in reactor research and teaching.

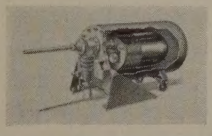

Van de Graaffs®

1 Mev – Model JN
Economical neutron source for reactor research

1 Mev – Model JS
Simplified electron source for transistor and crystal research

2 Mev Model AK-N
Precise, multiple-purpose instrument for general physics research and teaching

2 Mev Model AK-S
Moderate-power electron source for quantitive radiation research

3 Mev – Model KN
Powerful neutron source and effective instrument for binding-energy physics

5.5 Mev - Model CN
Ideal positive-ion accelerator for broad-range nuclear research programs

10 Mev – Model EN
New, precise, high-energy, tandem accelerator for binding-energy investigation of heavy nuclei

Microwave Linear Electron Accelerators – 5 to 50 Mev Linacs
A series of high-energy, high-powered electron accelerators for research and production

WRITE or CABLE
High Voltage Servicing Co. Ltd.
60 Carpenter's Wood Drive
Chorley Wood
Rickmansworth Herts, England

HIGH VOLTAGE ENGINEERING CORPORATION
BURLINGTON MASSACHUSETTS

LELAB METAL-WALLED G-M TUBES

for anti-coincidence applications where uniformity counts !

Lelab Counter Tubes are individually constructed, filled, and tested. Each is fabricated almost entirely of metal. All components are confined within the diameter of the tube shell to permit close stacking.

Compare our low prices on these superior tubes!

(Makers of Lelab [Robinson-Selverstone Type] Probe Counters for neurosurgery and where a fine needle-like probe for highly localized measurements is useful.)

Write for complete information

H. W. Leighton Laboratories

York & Sunset Lane-Hatboro, Pa. U.S.A.

FOR SCINTILLATION & PROPORTIONAL COUNTING

Non-overloading linear Amplifiers

MODELS 108 and 108 p

* GAIN–40,000, continuously variable
* RISE TIME–0.2 microsecond
* ACCEPTS + AND — PULSES

Tremendous Dynamic Range

EXCEEDS 1,000,000 (0.1 mv to 100 V)

Excellent linearity for small pulses in the presence of tremendous overloads that paralyze other amplifiers. PULSE HEIGTSELECTOR (Supplied only on Model 108 P—Precision trigger-type).

MODEL 108 . . . $ 545.00 — MODEL 108 p . . . $ 525.00

Precision High Voltage Supply

MODEL 515 . . . $ 385.00

* 500–1500 volts, 1 m.a. (2 m.a. to 1 KV)
* Continuously variable
* Polarity switch makes this highly regulated supply equivalent to two separate precision instruments
* Drift less than .01% over several hours; less than .02% per day Regulation .0002% per % change in line voltage for line voltages between 70 and 140
* Precision voltage divider for precise reading of output voltage
* 4½" panel meter. Dual teflon connectors

RADIATION INSTRUMENT CO.

P.O. BOX 733 SILVER SPRING, MARYLAND, U.S.A.

NCA

WORLDWIDE Film Badge Service

for Beta
Gamma X-rays
and Neutrons

Available in clip-on, wrist, or ring style, for isotope and X-ray laboratories, medical and dental offices, and industrial plants. Write or 'phone for Bulletin N20, containing complete information and prices.

- Low Cost
- Prompt, Reliable Reports
- Provides Permanent Records
- Covers Wide Range of Energies and Exposures
- 5 Filters for Highest Accuracy

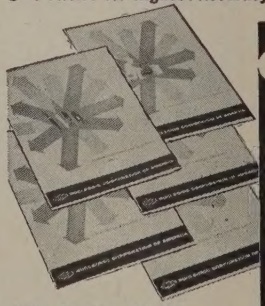

NCA

Your One Source of Nucleonic Equipment for Every Field

#101. Uranium and Oil Exploration Equipment
#102. Atomic Education Equip't.
#103. Nuclear Laboratory Equip't.
#104. Medical Radioisotope Equipment
#105. Geiger, Proportional, and Scintillation Detectors

Send now for above new catalogs

Dept. N17

NUCLEONIC

Corporation of America

196 Degraw St B'klyn 31, N. Y.

MAin 4-7370

NCA

FOR
STEAM AND NUCLEAR
POWER STATIONS

BROWN BOVERI

One of the four 150-MW steam turbines for a large power station

Brown, Boveri & Co., Ltd., Baden (Switzerland)

Representatives in most countries

A complete scintillation service . . .

PLASTIC, LIQUID, AND CRYSTAL PHOSPHORS

* PLASTIC PHOSPHOR N.E. 102, light output 65% anthracene, available in all sizes and shapes up to one ton, in thin sheet form, in fine tubes for the constructions of scintillation flow counters, or as filaments for the construction of scitnillation nuclear track chambers, (Bulletin 11).
* BORON POLYESTER PLASTIC PHOSPHOR N.E. 400 and N.E. 401 for neutron detection.
* LOADED LIQUID SCINTILLATORS in bulk or encapsulated, containing Pb for extreme X-ray sensitivity, and Gd, B or Cd for neutron detection (Bulletins 9 and 9a).
* SCINTILLATING GELS for efficient internal counting of suspended materials, (Bulletin 9).
* SCINTILLATION CHEMICALS of higest purity P.B.D., POPOP, T.P.B., p-terphenyl, PPO, D.P.H., alpha-N.P.O., vinyltoluene, styrene, xylene, toluene, and methyl borate (Bulletin 10).
* LIGHT PIPES of polyvinyltoluene and polystyrene.
* HARSHAW SODIUM IODIDE CRYSTALS. Exclusive concessionaire for Great Britain.

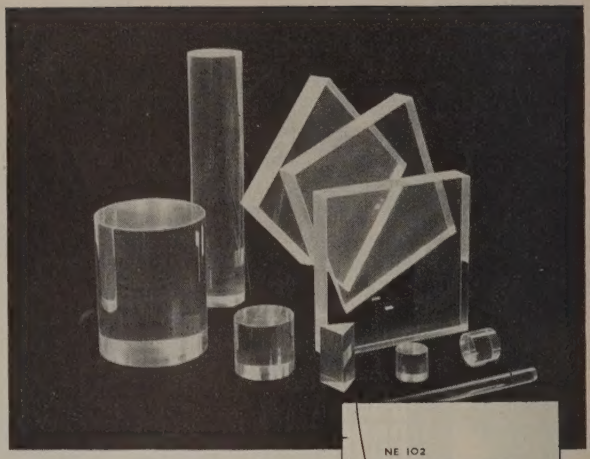

NEW LINE OF PRECISION NUCLEAR INSTRUMENTS

* Non Overloading Linear Pulse Amplifier N.E.5202 of the Fairstein type (Bulletin14).
* Pre-Amplifier and Cathode Follower N.E. 5202. A
* Single Channel Pulse Height Sorter N.E. 5102.
* Shielded Scintillation Head Unit N.E. 5501.
* Highly Stabilised EHT Supply N.E. 5301.
* Complete assembly for C14 and tritium counting, N.E. 8301.
* Complete Human Body Counter Installation N.E. 8101.
* Multi-Channel Scintillation Spectrometer 8201 for Industrial Traçer Investigations.
* Scintillometers for Geophysical Exploration.
* Differential pulse height distributions for Cs^{137} gamma ray. The plastic and crystal samples have volumes of several cc's.

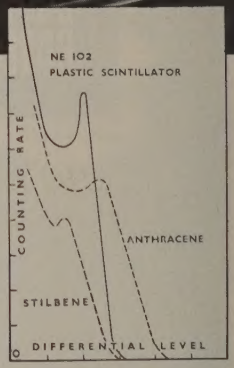

Write now for Bulletins 9, 9a, 10, 11, 12, 13, 14 and 1958 PRICE LIST

Nuclear Enterprises (G.B.) Ltd.

Bankhead Medway, Sighthill, Edinburgh — Scotland — Tel.: CRA 4513

Associate Company: Nuclear Enterprises Ltd. — 1750 Pembina Highway — Winnipeg — Canada

---

general radiological

Manufacturers of complete neutron flux monitoring systems for Reactors.

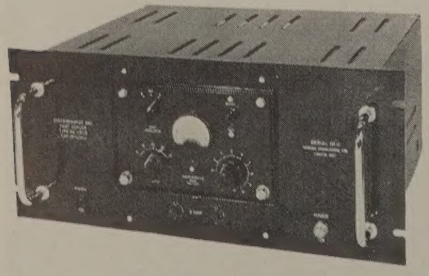

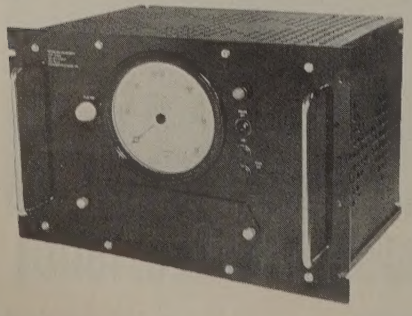

NE. 030 Discriminator and Fast Prescaling Unit for low flux counting channel of Nuclear Reactor Control circuits.

Max. average count rate 7×10^5 c/s. Resolution time $^1/_4$ μ/sec. Built-in test oscillator. Output used to drive:–

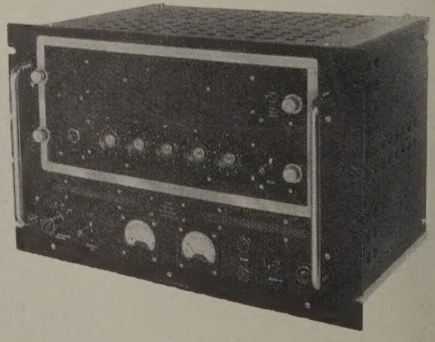

NE. 002 Scaler Unit.

Nominal Resolution time 5 μ/sec. Max. displayed count 1×10^7. Outputs $\div 1 \div 10 \div 100$ used to drive: –

NE. 003 Logarithmic Ratemeter. Resolution Time $^1/_4$ μ/sec. Meter display of 1×10^6 counts.

These units are normallly preceded by NE. 041 Pulse Amplifier, and followed by NE. 057 Reactivity Meter

general radiological ltd

15/18 Clipstone Street - London - W.1.

INTERNATIONAL

advertise

YOUR NUCLEAR PRODUCTS IN

sell

YOUR NUCLEAR PRODUCTS

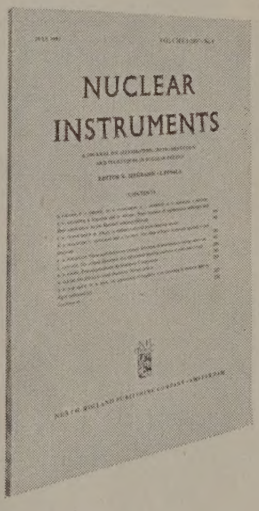

reap

YOUR NUCLEAR SALES
REWARDS

world wide

KEY NUCLEAR MANAGEMENT
NUCLEAR SCIENTISTS
NUCLEAR ENGINEERS
NUCLEAR PRODUCTION
PERSONNEL

SUBSCRIBE TO

you reach

THE WHOLE
NUCLEAR SALES WORLD IN

Entirely international in scope Nuclear Instruments is the one nuclear scientific journal that has an established subscription clientele through-out the whole world-where-ever nuclear men are at work—they want your nuclear products—they need your nuclear products—advertise in Nuclear Instruments and tell them WHAT – HOW – WHERE they can get your nuclear products

GO INTERNATIONAL WITH YOUR SALES PROGRAM TODAY WRITE

WILLIAM F. BAARS - ADVERTISING MANAGER NORTH-HOLLAND PUBLISHING COMPANY

P.O. BOX 103 – AMSTERDAM, HOLLAND

INTERNATIONAL

THE DEKATRON

COLD-CATHODE DECADE SCALING TUBE

"Scaling equipment has also undergone a number of changes in recent years and probably the most significant was the introduction of the decade scaling tubes. In general the introduction of such tubes has simplified circuits and allowed improved reliability, and in some cases it has resulted in a reduction in cost. The Dekatron tube, manufactured by Ericsson Telephones Ltd., is now very popular and deservedly so, and is used in many scaling and timing equipments."

. . . DENIS TAYLOR, M.SC., PH.D., M.I.E.E., F.INST.P. REVIEW ARTICLE "NUCLEAR POWER YEAR BOOK" 1957-58.

SCALING UNIT Type 1221

OTHER PRODUCTS INCLUDE

Industrial Counting Equipment
Batching Equipment
Survey Meters
Radiation Monitors
Field Ratemeters
Laboratory Ratemeters
Quench Units
E.H.T. Power Units
Custom-built Counting Units
Reactor Instrumentation

Write now for your copy of "ELECTRONIC & NUCLEONIC INSTRUMENTS"

As originators and sole manufacturers of the DEKATRON, and having developed most of its associated circuitry, we believe that we know best how to put it to work to meet your requirements. Illustrated is the well-known Ericsson Scaling Unit which was developed in conjunction with the Atomic Energy Research Establishment (Harwell) for reliable general purpose scaling.

Your complete supply source for

ELECTRONIC AND NUCLEONIC INSTRUMENTS

ERICSSON

INSTRUMENT DIVISION

HIGH CHURCH STREET, NEW BASFORD, NOTTINGHAM. Tel. 75115

ERICSSON TELEPHONES LTD. HEAD OFFICE: 22 LINCOLN'S INN FIELDS, LONDON, W.C.2

E79B

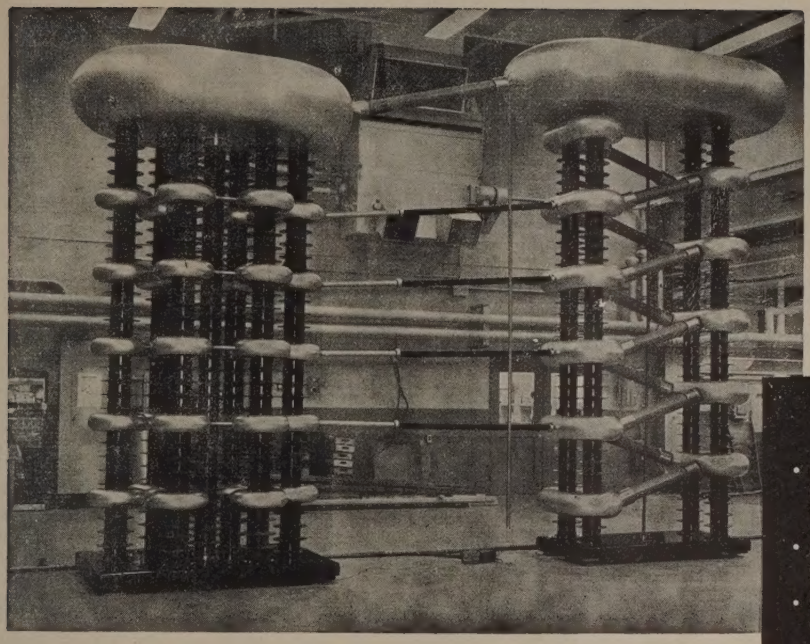

Stabilized
H.V. supply 800 kV/8 mA

(Photo by courtesy of
the Brookhaven
National Laboratory,
Upton L.I., N.Y., U.S.A.)

PHILIPS *equipment for*
Nuclear Physics and Atomic Energy

This Cockcroft-Walton generator will serve as a pre-injector for the 25 BeV Alternating Gradient Synchrotron under construction at the Brookhaven National Laboratory.
A similar installation is used at the Atomic Energy Research Authority at Harwell, England for injection into a proton linear accelerator.

- Synchro-cyclotrons for various final energies.
- Linear electron accelerators.
- Cockcroft-Walton accelerators.
- Radiation measuring and detection equipment.
- Area monitoring instrumentation.
- Civil defence instruments.
- Reactor control instrumentation.
- Geiger counter tubes.
- Radio-active isotopes.
- Air liquefiers.
- Generators for very high d.c. voltages.

PHILIPS

PHILIPS

Nuclear Equipment

For further information please apply to one of the following addresses:

N.V. PHILIPS' GLOEILAMPENFABRIEKEN,
Scientific Equipment Department, Eindhoven - Holland
PHILIPS ELECTRICAL LTD.,
Research and Control Instruments Division, Shaftesbury Avenue, London W. C. 2
PHILIPS ELECTRONICS INC.,
Instruments Division, 750, South Fulton Avenue, Mount Vernon N.Y. U.S.A.

Cary / instrument abstracts

Applied Physics Corporation/Pasadena/California

Radioactivity Measurements Made Faster, Cheaper with Vibrating Reed Electrometer

Measurement of radioactivity in radioisotope determination, reactor control, air contamination studies, oil well logging, and other problems involving precise measurement of small currents, voltages and charges, such as precise pH determination and mass spectrometry, can now be made faster, simpler and cheaper by using the Cary Model 31 Vibrating Reed Electrometer.

Unusually high sensitivity plus high zero stability and ease of installation and operation are responsible for the greater speed and savings. The Model 31 detects as little as 10^{-17} amperes, and measures up to 10^{-6} amperes with a precision of 1%. Zero drift is less than 0.2 mV in 24 hours and less than .02 mV per hour.

C^{14}, H^3 DETERMINATIONS SIMPLIFIED

One widespread application in which the Model 31 has been of particular value is in determining C^{14}, H^3, and S^{35}. Wilzbach and his coworkers at Argonne National Laboratory have developed procedures* which simplify these determinations in a wide variety of organic compounds. Samples are converted directly to a gas suitable for measurement with an ionization chamber and the Model 31. This simple procedure eliminates the necessity for use of a precipitate, with its inaccuracy and time-consuming, tedious preparation.

Since as little as 10^{-12} curies of radioactivity can be detected, use of expensive "tagged" materials can be greatly reduced, often enough to return the cost of the instrument in a relatively short time.

The Model 31 can be used in any laboratory and does not require costly, vibration-free mountings or other special conditions of installation or operation. For additional information on the Model 31, write for bulletin NU-1 today. It gives you details on applications, references, performance, operating principle, specifications, modifications, accessories.

*Wilzbach, Brown, Kaplan, Science, **118**, 522-523 (1953)
Wilzbach, Van Dyken, Kaplan, Anal. Chem., **26**, 880 (1954)
Wilzbach, Sykes, Science **120**, 494-496 (1954).

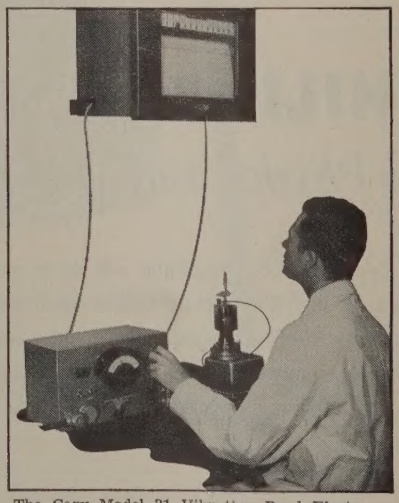

The Cary Model 31 Vibrating Reed Electrometer is capable of detecting a current as small as 1.0 X 10^{-17} amperes originating in a high impedance source. Charges as small as 5 X 10^{-16} coulombs and voltages as small as .02 mV can be measured.

CARY MODEL 36 VIBRATING REED AMPLIFIER IMPROVES MASS SPECTROMETER PERFORMANCE

The Cary Vibrating Reed Amplifier, Model 36, is being used in an increasing number of mass spectrometer installations where high molecular weight analyses make rapid scanning of mass numbers desirable. The Model 36 combines rapid response with high sensitivity. Response is critically damped, with an 0.1 sec. natural period (98.6 percent response in 0.1 second). Thus a range of 100 mass numbers can be accurately scanned in as little as one minute. Sensitivity and range are such that as little as 10^{-15} amperes and up to 10^{-11} amperes can be measured to a reproducibility of 0.2 percent without change of range. The stability of the Model 36 is superior too–zero drift is less than 10^{-15} amperes.

The Model 31 is preferred for mass spectrometer applications where extreme response speed is not required, such as isotope determinations. Sensitivity of the Model 31 is 10^{-17} amperes, and like the 36 it has high stability–less than 5 x 10^{-17} amperes zero drift.

NUCLEAR INSTRUMENTS 2 (1958) 219–226; NORTH-HOLLAND PUBLISHING CO. – AMSTERDAM

PULSED HIGH-INTENSITY ION SOURCE†

PART I

JAN FLINTA

A. B. Atomenergi, Stockholm

Received 16 October 1957

The first part of this publication deals with the limitations of the discharge current, extraction of ions and focusing of large ion current beams. Three types of ion sources are described and their data are given.

The second part†† deals with detailed investigation of the characteristics of the discharge of the Penning type. For this purpose a special ion source was build which allowed for the exchange of all inner parts.

1. Introduction

That large ion currents can be extracted from ion sources have been reported by a number of authors. Ion sources of the so called Penning discharge type, where electrons from cold cathodes oscillate in an axial magnetic field between the cathodes, are described by [1–5]). The same type of ion sources but using electrons from a hot cathode are described by [6–12]). An ion source with hot cathode but without magnetic field is described by ref. [13]).

The below investigations were made in order to develop an ion source planned for a 300 kV accelerator for high intensity neutron generation.

The second part is concerned with the investigations of the behaviour of the discharge and with the description of the cold cathode ion sources constructed for this study, and their performance and general properties are discussed.

2. The Discharge Pressure

According to David Bohm (ref. [12]) p. 87) both ion and electron currents between the surface of the plasma and the cathode are space-charge-limited if the issue current exceeds 10 mA/cm². For both these currents:

$$j = k \frac{1}{\sqrt{M}} \frac{V^{3/2}}{X^2} \qquad (1)$$

where V = the voltage between plasma and cathode, and X = the distance between plasma and cathode. M = the mass of the charged particles in the current.

For the Penning type discharge arrangement (see fig. 1) is

$$2 \cdot j_e = \tfrac{1}{2} j_+ \cdot \sqrt{M/me} \qquad (2)$$

where M and me = the mass of the ions and electrons and $\frac{1}{2} j_+$ = the ion current that strikes one of the cathodes and j_e = the oscillating electron current momentarily noted,

† The work was done at A. B. Atomenergi, Stockholm.

†† See following article, Nuclear Instruments 2 (1958) 227.

[1]) P. C. Veenstra, H. M. Jengerius, C. N. Paris and F. P. G. Valckx, Physica **XVIII** (1952) 378.

[2]) R. Keller, Helv. Phys. Acta **22** (1949) 78; R. Keller, Helv. Phys. Acta **23** (1950) 627.

[3]) F. M. Penning, J. H. A. Moubis, Physica **4** (1937) 1190.

[4]) P. Lorrain, Can. J. of Res. **25A** (1947) 338.

[5]) J. D. Gow and J. S. Foster, Jr., Rev. Sc. Instr. **24** (1953) 606.

[6]) H. Heil, Z. Phys. **120** (1943) 212.

[7]) A. Th. Finkelstein, R. S. I. **11** (1940) 94.

[8]) R. B. Setlow, R. S. I. **20** (1949) 558.

[9]) H. Atterling, Arkiv för M., A. och Fysik, Band **35A** (1948) No. 32.

[10]) J. Kistemaker and H. L. Douwer Dekker, Physica **XVI** (1950) 198; J. Kistemaker and C. J. Zilverschoon, Physica **XVII** (1951) 43.

[11]) P. C. Veenstra and J. M. W. Milatz, Physica **XVI** (1950) 528.

[12]) A. Guthrie and R. K. Wakerling, The characteristics of electrical discharges in magnetic fields (National Nuclear Energy Series, Div. 1 – Vol. 5. McGraw-Hill Book Co. Inc., N.Y., 1949).

[13]) W. Scott, Jr., Phys. Rev. **55** (1939) 954.

which have to be accounted for twice. The current is limited by saturation of the emission of ions or electrons, the last case gives the unequal sign in eq. (2). For a full discussion of the factors involved the reader is referred to Bohm's article.

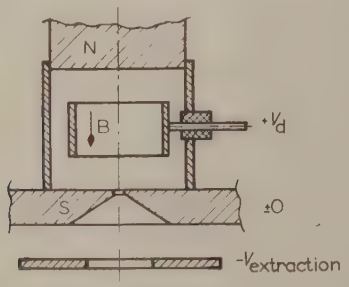

Fig. 1. A cold cathode discharge chamber used as an ion source described in section 6a.

The ions consumed at the cathodes must be replaced by ionisation in the gas caused by the electrons. Assume that λ is the mean free path for an oscillating electron to produce an ionisation collision, and that the secondary electrons from ionisation gain too little energy to give accountable contribution to the ion production which then will be:

$$j_+ = j_e \cdot \frac{2S}{\lambda} \tag{3}$$

where S = the path of the oscillating electrons between the two cathodes, that is practically the same as the distance between the cathodes. From (2) and (3) the condition for equilibrium is found:

$$\frac{1}{\lambda} = \frac{2}{S}\sqrt{\frac{m_e}{M}}. \tag{4}$$

Since λ is inversely proportional to the gas pressure this equality gives the minimum discharge pressure p. We can write

$$p = \frac{1}{\lambda} \cdot f(V) \tag{5}$$

where $f(V) = 0.4$ Torr·cm mean value for a few hundred volts of the max. electron energy, V. Numerically an oscillating electron discharge in atomized deuterium gas with cathode surfaces 2 cm apart can be sustained at a minimum pressure of about 6×10^{-3} Torr in agreement with Allen[14]). This minimum pressure, however, will ultimately depend on the cathodes, for it will be higher when V is increased because $f(V)$ increases with V. But as stated below in section 3, the anode voltage, V, is inversely proportional to the effective secondary emission factor γ at the cathode which however depends on V (see section 4 below).

Eq. (4) indicates that the pressure needed is lower for heavy molecules, other factors being the same. It was observed that the introduction of water or mercury vapour in a hydrogen discharge lowers the working pressure appreciable, probably due in part to this effect.

3. The Operating Potential

Using a hot cathode capable to produce $\sqrt{M/m_e}$ more electrons than ions striking it, for conditions similar to those in eq. (2), the electron does not need to oscillate. In this case the anode voltage should, for lowest pressure be held at a potential giving the electrons an energy corresponding to the highest ionisation efficiency. For atomized hydrogen maximum lies at 100 eV.

With oscillating electrons their initial energy is consumed by collisions. These collisions must for each oscillating electron lead to N ions. For a self maintaining discharge N ions strike the cathode for each emitted electron available for oscillating. For a cold cathode N is the inverted value of the effective secondary emission factor γ. Thus the anode voltage V_a must be N times the effective ionisation potential V_{eff}, or for the cold cathode:

$$V_a = \frac{1}{\lambda} \cdot V_{eff}. \tag{6}$$

The effective ionisation potential including radiation losses is 2 to 3 times the net value or about 40 eV per produced ion for hydrogen. If the hydrogen discharge current is 10 times the cathode emission current the anode voltage will be about 400 volts, provided that the magnetic field is strong enough to keep the oscillating electrons away from the anode ring,

[14]) N. I. Allen, Proc. Phys. Soc. 65 (1952) 697.

until they have expended all their energy in collisions. The dependence on the magnetic field is fully investigated in ref. [12]).

4. The Cathode

The advantage of a high emitting hot cathode with pulsed drift is that the discharge will start immediately at the rise of the anode voltage pulse even at the very shortest pulses. A hot cathode will consume some hundred watts per Amp. electron emission. Several different types of cathodes have been tried in this laboratory but have been found to have either too short a life (thin cathode wires or coated cathodes surfaces) or too large a heat dissipation (bare tungsten and the La B/ cathode reported by Lafferty[15])). A "Philips L-cathode"[16]) has not yet been available for test, but would probably be suitable for this application.

A cold cathode, however, has a long life and in spite of the great peak discharge power the heat dissipation can be kept small during the impulsed operation. An advantage is that the ion density on the cathode is much greater than that using a high emitting hot cathode provided the anode current is the same. The cathode emission consists of the electrons released by the ion bombardment, producing on the average γ electrons per ion. Backus (ref. [12]) p. 348) gives some values for Cu (0.1 to 1.5 for ion energies from 700 to 3000 eV). As shown in section 3 the anode voltage needed is high for small effective: electron to ion ratio. With cold cathodes this ratio is γ and it increases for increasing voltage. Thus a balance will be reached for some voltage. A monomolecular oxide layer sometimes reduces the work function for electron emission making γ large but is easily destroyed by bombardment with a large current of energetic ions. When the oxide layer on Mg and Al cathodes is destroyed and thereby γ is reduced, the anode voltage must be increased 10 times to about 3 000 volts as expected from section 3. It has been reported (ref. [12]) p. 368) that a cathode of Os + 10% ThO_2 needs 200 volts, being self-regenerating, but a practical cathode of this material has not yet been developed.

As uranium was available, we decided to test it as a cathode material, since it was expected to have a low work function for electrons because of its place in the periodic system and since it has a high reflection coefficient for electrons about 80% because of its high atomic number. The high reflection coefficient is necessary for the electron economy in a discharge where the electrons oscillate in a magnetic field between two cathodes N and S (fig. 1). An emitted electron from one of the cathodes has an initial energy which will make it strike the other electrode if no energy is given to the gas. If the reflection coefficient is high, the electron has a large chance of being reemitted.

Uranium hydrolyses easily, and is also a little radioactive, which may be of some importance, especially for the ignition. The test was successful. At a pressure of 0.003 Torr with $B = 1\,500$ gauss and large discharge current the anode voltage was 500 volts.

The state of the particles which strike the cathode is of some importance. Atoms in excited or metastable states give a high γ, and it was for example found during an investigation of the composition of the ion beam[19–22]), that it was advantageous to add Hg vapour to the gas in the discharge chamber which will be described in a following part of the article.

5. Focusing

The spread of the ion beam due to space charge repulsion is the most important factor in the focusing of intense ion beams at relatively low acceleration voltages. The contours of an ion beam of energy V volts and current i A injected with parallel trajectories into a field free region are given by Fowler and Gibson[17]). For deuterium atomic ions one can write:

$$z/r_0 = 1.48 \times 10^{-3} \, (V^{3/2}/i)^{1/2} \cdot Y(r/r_0) \ , \qquad (7)$$

[15]) J. M. Lafferty, J. of Appl. Phys. **22** (1951) 299.
[16]) Philips Cathode, Phil. Tekn. Rev. **11** (No. 12) 50.
[17]) R. D. Fowler and G. E. Gibson, Phys. Rev. **46** (1934) 1083.

where z = the axial coordinate, r = radius of the beam, r_0 = radius at $z = 0$, where the beam is parallel, Y = a function tabulated by Jahnke and Emde (ref. [18]) p. 32).

The form of the trajectories is given in fig. 2 for various values of $V^{3/2}/i$.

The origin for the motion in the z-direction has been taken at the point where the trajectories are parallel and the beam has its minimum radius r_0. The motion of the ions can be either downwards or upwards. The axes are normalized to r_0.

If the motion is upwards this corresponds to an accelerating tube in 8 steps.

It follows that an ion beam of given intensity

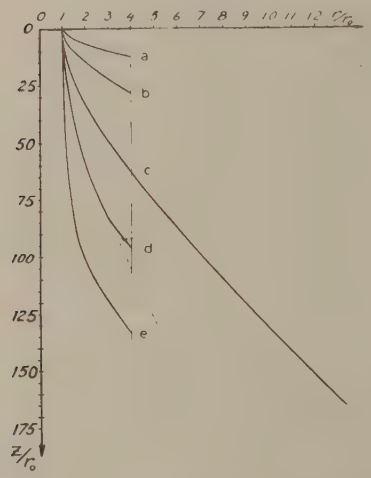

Fig. 2. The contours for ion beams of the same current but different energies (table 1) in a field free space are given normalized to the minimum radius, r_0. The z-axis is the centre line of the beam.

and final energy can be brought to its minimum radius r_0; this dimension is depending on the distance between source and target. If this distance is large it is necessary to use a very wide and strongly convergent beam. A beam with a large diameter may be obtained with a retarding field electrostatic lens, fig. 3. In this the energetic ions, which have been drawn out

[18]) Jahnke and Emde, Tables of Functions (Dover Publ., New York, 1945) p. 32.

of the source by the high potential extraction electrode, are slowed down by the retarding

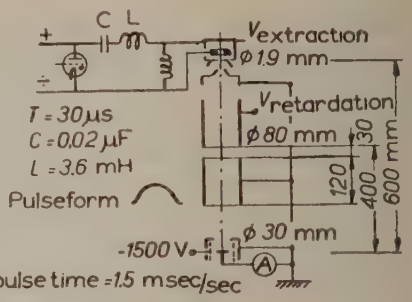

Fig. 3. (a) The arrangements of the focusing and accelerating system using a retarding field electrostatic lens directly under the outlet of the ion source. The collector of the Faraday cage is connected to earth via the µA meter, A. (b) The impulse aggregate for the discharge supply. The charge potential is max. 3 kV. The condensator, C, is discharged through the ion source and the inductor, L, 50 times per sec by means of the thyratron.

electrode to a suitable low energy, some keV, and then again accelerated by the accelerating electrode.

TABLE I

The trajectories (a)–(e) in fig. 2 correspond to the following ion energies, for ion currents in the range 0.9–100 mA

Ion current mA	0.9	2.5	6.7	18	50	100
Beam Trajectory	Ion energy keV					
(a)			2.3	4.6	9.2	15
(b)	1.8	3.5	7.	14	28	44
(c)	5	10	19.5	39	78	120
(d)†	10	19.5	39	78	156	250
(e)††	50	100	200	400	800	1300

† The ions have half the energy in the region $Z/r_0 =$ 84–96. Assuming the motion being upwards it corresponds to an accelerating tube in 2 steps. The focusing in the gap is not accounted for.

†† The energy of the ions is changed along the Z-axis as follows:

1/8 of total energy in range $Z/r_0 =$ 116–133
. . . . . .
. . . . . .
7/8 of total energy in range $Z/r_0 =$ 17–34
8/8 of total energy in range $Z/r_0 =$ 0–17.

The extraction electrode can be very short. The retarding electrode should be about 1.5 times the lens diameter which shall be taken the same as the beam diameter as determined from the diagram fig. 2. The extraction voltage is kept constant and equal to the acceleration voltage on the first acceleration electrode. Variations of the focusing of the strongly convergent beam that emerges from the retarding electrode can be achieved by varying the voltage of this electrode. This voltage V_{ret} to the ion source will be held within 10% of the extraction (= acceleration) voltage, V_{acc}.

Experiments with the arrangement of fig. 3, using a beam diameter in the retarding electrode of 8 cm and focusing the beam to a smallest diameter of 1 cm at a distance of 60 cm for different beam currents, required the potentials given in fig. 4.

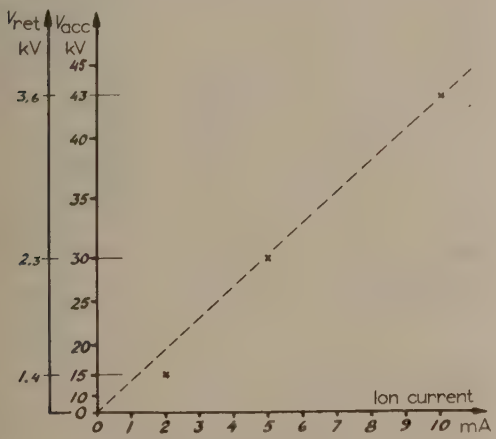

Fig. 4. The 3/2-power of the acceleration voltage, V_{acc}, and of the retardation voltage, V_{ret}, as a function of the ion current.

These experimental arrangements correspond to a case intermediate to curves (c) and (d) of fig. 2, in essential agreement with the results of the measurements.

Although the beam filled almost the whole of the retardation electrode, there were no signs of aberration at the edges of the spot.

With the voltages given in fig. 4 a negligible portion of the ion beam goes to the retarding electrode. The potential of this electrode had to be brought within 3.5 kV of the acceleration voltage before 15% of the beam was intercepted.

Obviously the focusing system can be tested with a small current if the potentials are proportionally lowered according to eq. (7), until a value where the energy spread from the ion source will disturb.

6. The Atomic Ion Content

The atomic ion content of the ion beam is of great importance and is discussed by[19-21]) and (ref. [22]) p. 480). An atomic ion content greater than about 10% can only be obtained if the gas in the discharge chamber is already partly dissociated so that atomic ions can be formed directly from atoms by collisions with electrons. The extent of atoms depends on the equilibrium between on the one hand the recombination of the atoms to molecules on the discharge chamber walls and on the other hand the dissociation by electron and ion collisions with the molecules. The dissociation is therefore proportional to the discharge current density and the recombination is proportional to the speed of diffusion of the atoms. This speed is proportional to the energy transferred by the electrons in the collisions, that is proportional to the anode voltage. The diffusion speed will also decrease at increasing pressure. Therefore the atomic ion content will thus increase with the current density in the discharge and also with the pressure (see figs. 8 and 9).

As mentioned in section 4 the addition of Hg vapour may also increase the atomic content somewhat. Hg has a metastable level at 4.66 eV, which is slightly higher than the dissociation energy of hydrogen, 4.45 eV for H_2 and 4.53 eV for D_2. The transfer of energy from excited Hg atoms to hydrogen molecules thus increases the dissociation of the hydrogen, (see fig. 9).

[19]) P. C. Thoneman, Proc. Phys. Soc. **61** (1948) 483; P. C. Thoneman, M. E. Reinders and N. B. Brinkman, Conference of Ion sources, 16-11-1949, Amsterdam (Foundation for Fundamental Research of Matter, Utrecht, The Netherlands).

[20]) W. Maas, University of Utrecht, 12th April (1948).

[21]) E. S. Lamar and O. Luhr, Phys. Rev. **46** (1934) 87.

[22]) Ruark and Urey, Atoms, Molecules and Quanta (1930).

7. Practical Designs

Following the theoretical considerations of the previous sections, three different types of ion sources have been designed all with cold cathodes. The first two types are of the conventional type with both cathodes at the same potential as in refs. [1–5]), whereas in the third type the lower or extracting cathode is at a high negative potential.

(a) The first type of ion source is very similar to the type developed by Keller and is shown in fig. 5. A magnetic yoke with a magnetron magnet gives a not quite homogeneous magnetic field of 1 500 gauss in the discharge chamber. With aluminium, magnesium or iron cathodes the ion source requires a pressure of 0.01 Torr at about 3 000 volts. The oxide layers on Al and Mg are rapidly destroyed giving the high anode voltage if no oxygen is supplied. The insertion of uranium cathodes reduced the pressure and voltage requirements to 0.002 Torr and 500 volts.

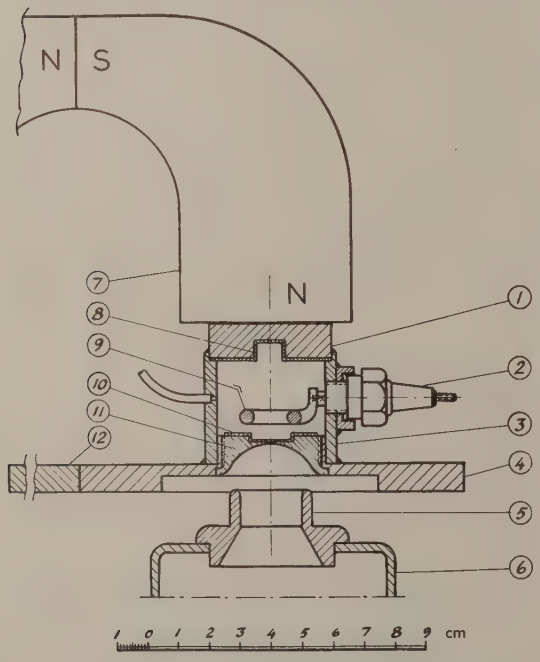

Fig. 5. Cold cathode ion source. (1) Upper pole-piece of soft iron. (2) Anode lead-through (spark plug). (3) Body of ion source (copper) with a copper tube welded on it for cooling. (4) Mounting plate of soft iron. (5) Extraction electrode, changeable. (6) Extraction electrode. (7) "Magnetron" magnet. (8) Recess in upper pole-piece lined with 1.0 mm of uranium metal. Internal dimensions 8 mm in diameter, 6 mm depth. (9) Anode of 2.0 mm molybden wire bent into a ring of 9.0 mm inner diameter. (10) Plate of 1.0 mm uranium metal. The recess with internal dimensions 12 mm in diameter, 2 mm depth. (11) Lower pole-piece of soft iron which can be screwed out. The outlet hole is 2.5 mm in diameter and 0.2 mm long. (12) Magnetic link of soft iron. The other pole of the magnetron magnet rests on a soft iron cylinder standing on the link.

In order to judge the possibility to pulse the ion source with short pulses it is of interest to note that the mean path for the electrons which is about 150 cm in D_2 of 0.002 Torr is traversed in about 0.3 μsec at 500 volts. It will take 0.2 μsec for the D^+ ions to diffuse 1.2 cm from the center of the discharge chamber to the cathode if the diffusion speed corresponds to the energy 25 eV.

(b) The second type was obtained from the first by a drastic reduction of the dimensions of the discharge chamber and a proportional increase of the magnetic field. The magnetic yoke (not shown) is a magnetron magnet giving about 4 000 gauss. The ion source is seen in fig. 6. The operating data were comparable to those of the previous source. With an outlet channel 0.2 cm in diameter and 0.01 cm long the gas consumption was 20 NPT cm³ per hour deuterium (ref.[23])) for the operating pressure 0.004 Torr, the pressure is higher than that of the first type corresponding to the smaller distance between the cathodes according to section 2.

The ion sources were tested with a thyratron pulse generator as indicated in fig. 3b.

The dimensions of the electrode system are shown in fig. 3a.

The results of some measurements made with this arrangement are shown in figs. 7–9.

Since the pulse length was 30 μsec at a repetition frequency of 50 p/sec, and the pulse shape was semisinusoidal, the peak ion current would be about 10^3 times greater than the mean current and may be read from the figure directly in mA. This was checked by examining the voltage over a small series resistance with

[23]) J. E. Flinta, J. S. I. 31 (1954) 388.

an oscillograph. In the same way the discharge peak current was measured to be in the interval 2–7 A. At an acceleration voltage of 25 kV the current shows signs of saturation, but not at

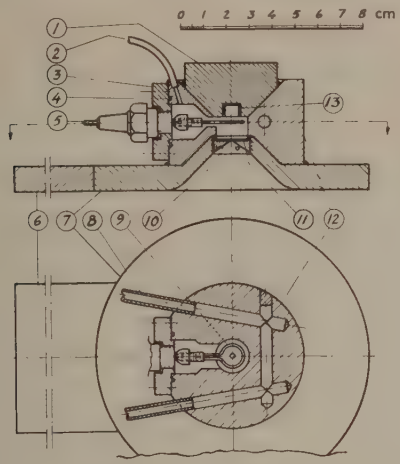

Fig. 6. Cold cathode ion source. (1) Upper pole-piece of soft iron. (2) Copper tube for gas inlet. (3) Removable side-panel carrying anode lead-through. (4) Gasket (a sharp ridge cuts into the sunk 1.0 × 1.0 mm aluminium gasket). (5) Anode lead-through (spark plug). (6) Magnetic link of soft iron (a permanent "Magnetron" magnet rests with one pole on a soft iron cylinder standing on the link and the other pole on the upper pole piece 1). (7) Mounting plate and lower pole piece (soft iron). (8) Channels for cooling-oil bored in body 12. (9) Anode of 1.2 mm tungsten wire bent into a ring of 9.0 mm inner diameter, mounted in a small chuck attached to the centre electrode of the sparking plug. (10) Bottom plate of ion source (soft iron) which can be screwed out. The outlet hole is 1.9 mm in diameter and is counter-sunk on the under-side. (11) Plate of uranium metal 0.6 mm thick and 14 mm diameter. Centre hole 1.9 mm diameter, counter-sunk on upper side. (12) Body of ion source (non-magnetic stainless steel), with discharge chamber 11 mm high and 14 mm in diameter. (13) Recess in upper pole-piece lined with 1.0 mm of uranium metal. Internal dimensions: 8 mm in diameter, 6 mm depth.

higher voltages. As the smallest diameter of the beam was about 3 cm the experimental arrangement corresponds to the region between (b) and (c) in fig. 2, which is quite compatible with the results of the measurements, as may be checked by comparing fig. 7 with table 1. The focusing was regulated with the retarding potential, V_{ret}.

From fig. 6 it will be seen that, with the greatest extraction voltage, about 1.5% of the discharge current is extracted to form the ion

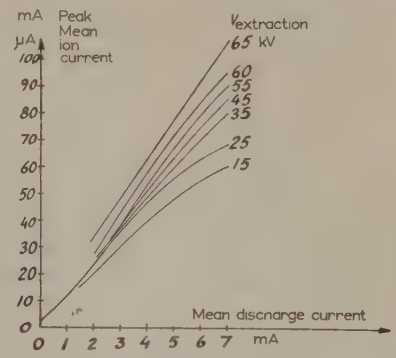

Fig. 7. The peak and mean ion current to the collector in the Faraday cage, fig. 3, as a function of the mean discharge current and with the extraction voltage as a parameter.

beam. This figure is somewhat less than the ratio between the outlet surface and the total cathode surface, depending on the loss of ions to the side walls of the outlet hole because the discharge plasma enters the outlet hole.

Fig. 8 shows the measurements of the atomic ion content made with both the ion sources.

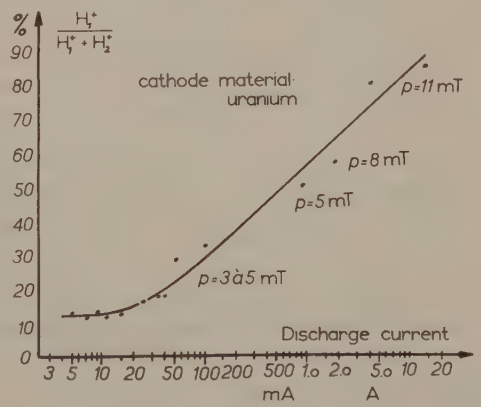

Fig. 8. The atomic ion content of the ion beam as a function of the discharge current.

For discharge current less than 50 mA the measurements are made with continuous discharge, greater currents are pulsed. According to section 6 the atomic ion content increases with the current density in the discharge.

The dependence of the pressure and the addition of Hg-vapour is seen in fig. 9.

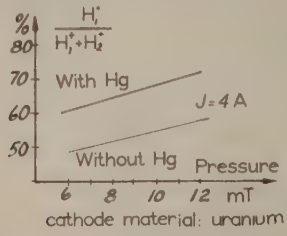

Fig. 9. The atomic ion content of the ion beam as a function of the discharge pressure with constant discharge current 4A (peak), with and without addition of Hg-vapour.

With uranium cathodes it was surprisingly stated that no H_3^+ ions were present contradictorily to other cathode materials where the H_3^+ content usually is 15 to 35% of the total ion current.

(c) The third type of cold cathode discharge which has been studied is shown in fig. 10.

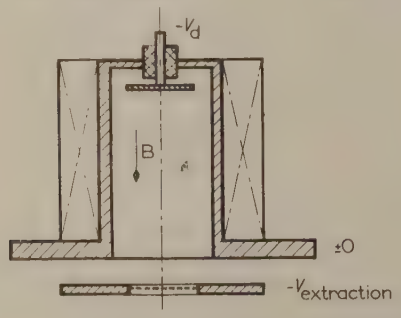

Fig. 10. An asymmetrical cold cathode discharge chamber with the lower cathode removed allowing the extraction high tension to enter into the discharge chamber.

The bottom of the discharge chamber consists of an insulated extracting electrode in the form of a wire grid, through which the ion beam can be extracted. As in type (a) and (b) the discharge is kept together by an axial magnetic field in this case being 220 gauss.

The discharge mechanism is the following. Of the ions in the discharge about 50% are accelerated towards the upper cathode which they strike with an energy of about 500 eV, liberating about 0.1 secondary electrons per ion as in type (a). The remaining half is accelerated towards the extraction electrode which is held at a negative potential of about 20 kV, and part of these ions are intercepted by the grid. The secondary emission ratio for ions in this

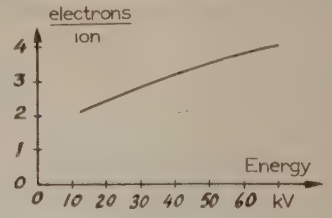

Fig. 11. The secondary electron emission ratio with deuterium ions on tungsten as a function of the energy of the ions.

energy range is measured with deuterium ions on tungsten and is shown in fig. 11.

With a tungsten wire grid we may assume that for each ion intercepted two secondary electrons are liberated. As these secondary electrons strike the upper cathode with an energy of the order of 20 keV about 1.5 tertiary low energy electrons are released per secondary electron. The electrons from the cathode oscillate in the magnetic field between the cathode and the corresponding lower equipotential surface, producing ionisation in the gas until they are captured by the anode.

The advantage of this type of discharge over type (a) is that a larger fraction of the ion current may be extracted due to the large secondary emission factor of the energetic ions at the extraction grid. For this reason the discharge current density is so weak that the limiting conditions in section I are not actual allowing the pressure to be low. A discharge has been sustained at a pressure of 10^{-4} Torr in an ion source where 50% of the downward ion current or 25% of the total ion current were intercepted by the grid. About 4 mA continuous ion beam was collected beneath the ion source. The extraction supply, 30 kV, was loaded with about 12 mA. In this case the extraction grid was bright red.

8. Acknowledgements

The author wishes to express his very best thanks to Dr. G. von Dardel†, leader of the neutron Physics Group, Dr. R. Pauli and Dr. R. Björnerstedt for advise and valuable discussions.

† Now at CERN, Laboratory Group, Geneva, Switzerland.

NUCLEAR INSTRUMENTS 2 (1958) 227–236; NORTH-HOLLAND PUBLISHING CO. – AMSTERDAM

PULSED HIGH-INTENSITY ION SOURCE†

PART II

ROLF PAULI and JAN FLINTA

A. B. Atomenergi, Stockholm

Received 16 October 1957

An investigation of the various factors of importance in the design of a high intensity pulsed ion source has been given in part I††.

On the basis of this study an ion source of the cold cathode or Penning type has been developed. An ion source of this type has been described by Keller and the ion source which is shown in fig. 5, part I, and which will be called type I, is to a large extent a copy of Kellers'. A second ion source (type II) was also built, as shown in fig. 6 of part I, with a smaller discharge chamber and a stronger magnetic field. Later development has been concentrated on the investigation of the characteristics of the discharge, and for this purpose a third ion source (type III) as shown in fig. 1 has been used. The walls of the discharge chamber were made of glass so that the discharge could be seen, and a recess was made in the cathode so that different cathode materials and shapes could be tested. The longitudinal magnetic field which is required by these ion sources was supplied by a permanent magnet of the magnetron type. The magnetic field strength was found by measurements to be about 1 000 gauss for type III (see fig. 1) and can be calculated to be about 1 500 gauss for type I and 4 000 gauss for type II.

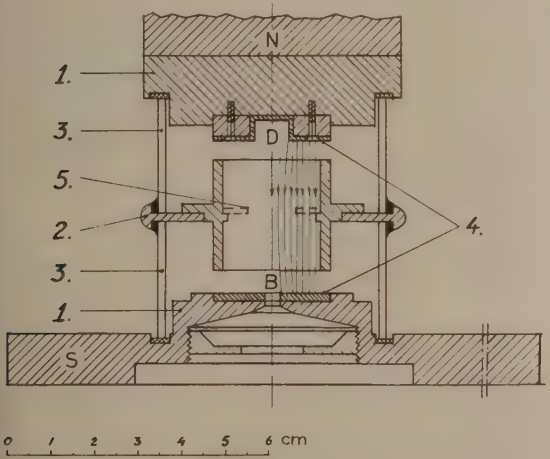

Fig. 1. Ion source type III. (1) Cathodes of soft iron. (2) Magnesium anode. (3) Glass walls. (4) Uranium cathode surfaces. N is the under surface of the permanent magnetron magnet. Magnetic flux density in D is 1 150 gauss, and 900 gauss in B. The convergence of the magnetic field caused by the recess in the upper cathode is shown with broken lines.

1. Pulse Generator

The ion sources were driven by a pulse generator giving pulses of semi sinusoidal form. It consisted of a condenser of 0.1 μF or 0.02 μF, which was discharged by a thyratron through the ion source in series with an inductance which was variable between 0.12 and 3.6 mH. The condenser was charged by a rectifier giving a maximum of 3 000 V. The L and C circuit determined the length and amplitude of the current pulses. Adjustment of the amplitude was also possible by varying the high voltage in the range 1 500 and 3 000 V.

Figs. 2a and 2b show the voltage and current wave forms at the ion sources. The voltage rises at first to the break-down voltage at about 2 000 V and then falls to a value which is constant during the whole discharge period.

† The work was done at A. B. Atomenergi, Stockholm.
†† See preceeding article, Nuclear Instruments 2 (1958) 219.

For a cathode surface of uranium this discharge voltage is about 500 V. The current pulses are sinusoidal.

For the experiments the amplitudes used were between 2 A and 15 A, at pulse lengths between 15 μsec and 60 μsec.

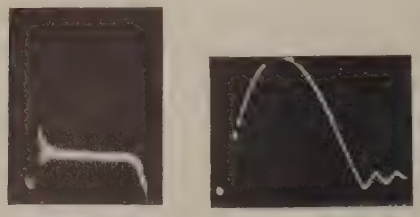

Fig. 2. (a) Voltage across ion source, $V_t = 2\,000$ V, $V_b = 500$ V. (b) Current through ion source $I_p = 5.2$ A, $T = 60$ μsec.

2. Measurements of Ion Current

The ion current from the source was measured by means of the arrangement shown in fig. 3.

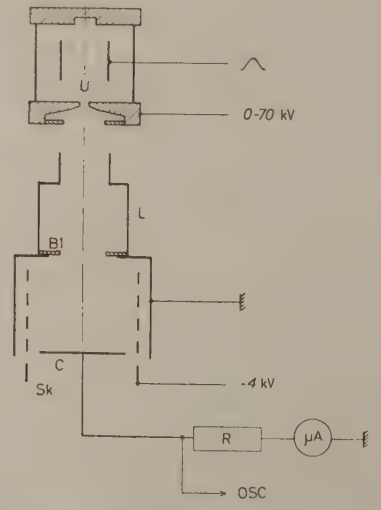

Fig. 3. Arrangement for acceleration and measurement of ion current.

The ions leaving the ion source through the outlet U are accelerated and focused by extraction electrode L. The maximum extraction voltage is 70 kV. Inside the extraction electrode is a removable baffle B 1, so that the aperture angle of the ion bunch passed downwards to the current collector C can be varied between 0° and 2 × 15°.

Secondary electrons from the baffle and the collector are suppressed by the shielding electrode at —4 kV. The waveform of the ion current is measured by a oscillograph connected across a series resistance R of between 200 and 1 000 ohms. The mean value of the ion current is shown by the microamperemeter.

3. Choice of Cathode Shape and Material

A bright spot moving irregularly over the cathode surfaces, was observed during pulsed operation of the ion source when it had aluminium or magnesium cathode surfaces. Electron emission from such a spot is considerably greater than from the other parts of the cathode surfaces, and thus the discharge is concentrated along the lines of magnetic force passing through the bright spot on the cathode.

Since the greater part of the discharge current is concentrated at the bright spot, the source can only give large pulses of ion current when the spot is very close to the outlet hole in the lower cathode. One can then design the cathodes in two ways, either so that the spot is always very close to the outlet hole, or else so that the spot is completely suppressed so that there is an even distribution.

The first alternative was tested in the arrangement shown in fig. 4. The cathodes and

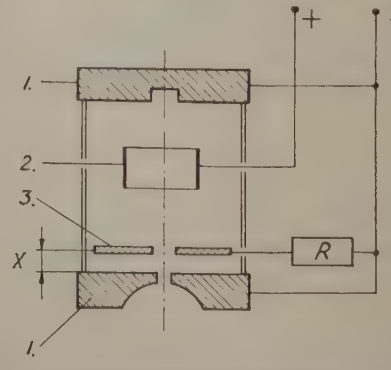

Fig. 4. Ion source with concentrated discharge. (1) Cathodes. (2) Anode. (3) Baffle.

baffle were made of magnesium. The amplitude of the discharge current was about 10 A. A

suitable value for the resistance R was from 10 to 40 ohms and a separation $X = 2.5$ mm was found to be best. At the pressure of 50 mT of D_2 in the ion source, the whole discharge was concentrated through the hole in the baffle down to the outlet in the lower cathode. (Colour of the discharge was purple, indicating a high content of atomic ions.) At lower pressures only a fraction of the discharge pulses passed through the baffle, and at 7 mT the discharge was not concentrated at all but filled the space within the upper cathode and the baffle in a diffuse cloud. When a piece of LaB_6, which is a cathode material giving good emission at 1 500°C, was mounted on the cathode under the aperture in the baffle, it was found that the discharge was concentrated at a lower pressure, but even in this case the discharge was diffuse below 10 mT. It is thus necessary to have a high pressure on the ion source if the discharge is to have the desired form, and the gas consumption is large. For this reason this type of ion source was not studied further.

Cathode materials of high specific resistance should reduce the tendency of the discharge current to concentrate in bright spots. The semi-conductor SiC was tried as cathode, but the discharge was very weak and a large number of very small bright spots appeared. The material has presumably a much too high resistance.

Graphite, which has a moderate specific resistance, was also tried as cathode material, and was found to give a discharge free from bright spots. In order to concentrate the discharge the cathode was made conical as shown in fig. 5. The discharge passes to the part of the cathode where the resistance is smallest, which in this case is a region of about 8 mm in diameter of the thin part round the outlet hole. A small dark thread-like region could be seen reaching up into the discharge from the outlet hole. The graphite was however erroded relatively fast because of the unavoidable thermal strains due to the concentration of the current in the thin part round the outlet, and for this reason this approach was also abandoned.

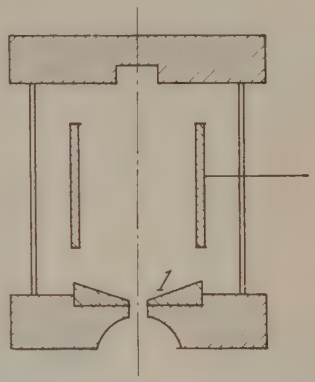

Fig. 5. Ion source with graphite cathode (1).

Later investigations showed that certain cathode materials such as iron and uranium could give discharges free from bright spots. Bright spots occurred with uranium during the first half hour after the ion source was started, but the cathode surfaces were apparently cleaned by the discharge, which then spread itself out evenly over the outlet hole, especially if the cathode was suitably shaped (see table 1). Two different forms of discharge were observed. The discharge was either ellipsoidal, filling the anode (in this case ring 5 of fig. 1 was omitted) or it could be concentrated to a cylindrical plasma of a diameter considerably less than that of the inner surface of the anode (see fig. 6).

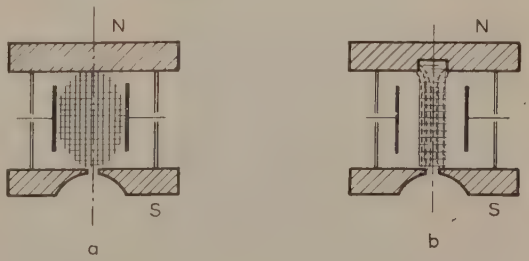

Fig. 6. Different forms of discharge. (a) Ellipsoidal forms of plasma. (b) Cylindrical plasma.

The second of these types of discharge gives the highest value for the yield, defined as the ratio between the ion and the discharge current. If the cathode surfaces are recessed as shown

in fig. 6b, the lines of magnetic force converge towards the centre of the discharge. Electrons emitted from the recess follow the field lines to a certain extent and are concentrated along the axis of the discharge producing the cylindrical plasma.

From this investigation it is concluded that a cylindrical recess in the upper cathode makes it possible to maintain a discharge with cylindrical plasma at a relatively low pressure. A recess in the lower cathode is not necessary. It is also an advantage to use uranium as cathode material since the discharge voltage is then only 500 V.

A disadvantage of the cylindrical recess in the cathode is that the time delay in striking the discharge increases, as discussed below.

Table 1

η (in %)	(a) in mm	(b) in mm	(c) in mm	(d) in mm	
0.5	3	5	—	0	Cylindrical plasma not obtainable
0.9	5	3	—	0	Cylindrical plasma if $p > 8$ mT H_2
0.9	8	5	—	0	Cylindrical plasma if $p > 5$ mT H_2
1.2	8	8	—	0	Cylindrical plasma if $p > 5$ mT H_2
1.1	8	8	12	3	Cylindrical plasma if $p > 5$ mT H_2
1.0	8	8	12	5	Cylindrical plasma if $p > 5$ mT H_2

Yield = ion current/discharge current = η for various shapes of cathode recess
(a) = diameter.
(b) = depth of recess in upper cathode.
(c) and (d) corresponding dimensions for lower cathode.
The outlet hole is at the centre of the $c \times d$-recess. Current amplitude 1.2 A: $T = 60$ μsec. Iron cathodes, inner diameter of the anode 20 mm.

If the pressure in the ion source is varied it is found that a cylindrical discharge can only be maintained if the pressure is higher than a certain value. In order to reduce the gas consumption the cathode recesses should be shaped so as to make this limiting pressure as low as possible. Table 1 shows the result of the investigation of the influence of the dimensions of the recess, measured with an ion source of type III, having an anode with 20 mm internal diameter, and no limiting baffle.

The cathode material may be iron. With magnesium and aluminium the bright spots on the cathodes prevented the development of a true cylindrical plasma, and the ion current yields were considerably lower than 1%, see above. In contrast, uranium was found to be very suitable. Covering a cathode with a 1 mm layer of pure uranium, as shown in fig. 1, made it possible to maintain a discharge at a pressure of about 50% less than that when pure iron was used. Pure iron has also the disadvantage that sputtered fragments held together magnetically may short-circuit the anode and cathode.

4. Types of Discharge

The ion source type III, which was used for measurements which will be described below, has a cylindrical recess of $\varnothing$ 8 × 5 mm² in the upper cathode, and $\varnothing$ 12 × 2 mm² in the lower cathode. The upper cathode was covered with a 1 mm layer of uranium metal which was machined from a uranium bar. A plate of uranium $\varnothing$ 12 × 2 mm² with central outlet hole $\varnothing$ 2 mm was set in the lower cathode, see fig. 1.

If the ion source is driven with a sinusoidal pulse, the ion current pulse should also be sinusoidal, if the extraction field under the outlet hole U (fig. 3) is sufficiently strong to avoid space charge limiting. Fig. 2b shows an oscillogram of the sinusoidal discharge current I_u and fig. 7b shows an oscillogram of the corresponding ion current I_j. It is apparent that I_j is proportional to I_u.

If the pressure in the ion source is varied one can distinguish three types of discharge which will be called I, II and III (fig. 7). All three have cylindrical plasmas of the type shown in fig. 6b. The highest yield is obtained

Fig. 7. Ion current including secondary electrons to electrodes L + Sk + C of fig. 3, for three different types of discharge. Extraction voltage 50 kV. (a) High pressure, 30 mT H_2, discharge type I with several bursts of discharge of type II. (80 mA, 60 μsec). (b) Medium pressure, 12 mT H_2, discharge type II (120 mA, 60 μsec). (c) Low pressure, 6 mT H_2, change from discharge type II to type III after about half the pulse (140/80 mA, 60 μsec).

for discharge type II (see fig. 7b). The pressure is not too high (in this case 7–20 mT H_2) and the ion current is proportional to the discharge current with only slight modulation by superimposed oscillations. If the pressure in the ion source is increased above a certain limit, in this case 50 mT H_2, the yield falls somewhat and the ion current pulse is modulated with a relatively low-frequency oscillation (about 100 kp/s). This is discharge type I and is shown in fig. 7a. If on the other hand the pressure is reduced below a certain value, in this case 7 mT H_2, the nature of the discharge changes while the pulse is in progress, the change-over occurring earlier for lower pressures (see fig. 8) going over from discharge type II to discharge type III, with lower yield. The ion current is modulated with an oscillation of about 1 Mp/s (see fig. 7c).

The change from discharge type II to type III is favoured by a high current amplitude (see figs. 8a and 8b), and low gas pressure (see figs. 8a and 8c). In the oscillogram in fig. 8d a combination of both these factors causes discharge type III to extend throughout almost the whole pulse.

From a–b there is increased discharge current but constant pressure.

From a–c there is reduced pressure for the same current.

From a–d there is both reduced pressure and increase in discharge current.

The change from discharge type II to III is not so clearly marked in the oscillograms of the voltage or current at the ion source. The discharge voltage oscillogram however changes with decreasing pressure, showing superimposed high frequency oscillations of amplitude increasing as the pressure is reduced (see figs. 2a and 9). The high-frequency oscillations also

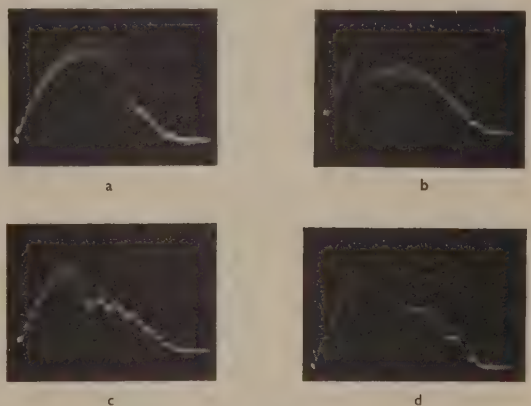

Fig. 8. Oscillogram of ion current to electrode c of fig. 3, not including secondary electrons, showing the change from discharge type II to III for different operating conditions (extraction voltage 50 kV), $T = 60$ μsec. (a) $p = 6$ mT; $I_u = 6.2$ A; $I_j = 32$ mA. (b) $p = 6$ mT; $I_u = 9$ A; $I_j = 37$ mA. (c) $p = 4$ mT; $I_u = 6.2$ A; $I_j = 23$ mA. (d) $p = 3.5$ mT; $I_u = 9$ A; $I_j = 20$ mA.

Fig. 9. Voltage across ion source, discharge type III. $p = 7$ mT, $I_u = 11$ A.

modulate the ion current (see fig. 8). It was also noticed that when the ion current pulse was modulated with high-frequency oscillations there was always a change to discharge type III sooner or later in the duration of the pulse.

The change from discharge type II to III occurs at such a low pressure that the condition

$$2 \cdot j_e \leq \frac{1}{2} \cdot j_+ \cdot \sqrt{M/me} \qquad (1)$$

does not hold.

This is eq. (2) in article I, where the condition is discussed.

M/m is the ratio of ionic to electronic mass. $\frac{1}{2} j_+$ is the positive-ion current reaching one of the cathodes from the plasma, and j_e is the component of the oscillating electron current in one direction. (This current is assumed to consist of two equal but opposite components each $= j_e$.) If the condition expressed in eq. (1) is to be met it is shown in article I that

$$\frac{S}{\lambda} \leq 2 \sqrt{\frac{m_e}{M}} \qquad (2)$$

In ion source type III the spacing between the cathodes $S = 4.5$ cm, and assuming that for electrons up to 500 eV energy a mean value is $p\lambda = 0.4$ Torr·cm in hydrogen (1), it follows that the lowest pressure at which the condition of equation (2) is met is 2×10^{-3} Torr of D_2 or 3×10^{-3} Torr of H_2, if the atomic ion content is 0%, or 3×10^{-3} and 4×10^{-3} Torr respectively if the atomic ion content is 100%.

The high frequency oscillations in the discharge voltage of the ion source and in the emitted ion current which occur when the discharge has a tendency to change from discharge type II to type III (see figs. 8 and 9) would thus appear to be due to the instability in the outer ranges of the plasma opposite the cathodes, due to the fact that condition (2) is no longer fulfilled. It was found experimentally that in agreement with eq. (2) the limiting pressure for D_2 gas was lower than for H_2 gas, and that these pressure were approximately in the ratio $1:\sqrt{2}$ (5 and 7 mT).

The types of discharge just discussed were observed with ion source type III (see fig. 1). It was found on the other hand that with ion sources of type I (fig. 5 part I) and type II (fig. 6 part I) with uranium covered cathodes, this pressure could be reduced until the discharge was broken off without the appearance of any noticeable high frequency oscillation of the types shown in figs. 8 and 9 in the ion current and voltage oscillograms respectively. Down to the lowest pressure 2×10^{-3} and 3×10^{-3} Torr respectively at which the discharge could be maintained, these sources give an ion current pulse very similar to that shown in fig. 7b.

It is not clear why this is so. It may be noted that type III has a more symmetrically located anode than type II. It was also observed that ion source type I could maintain a stable discharge at the lowest pressure only if the extraction voltage was more than 5 kV, so that its field extended into the discharge chamber, or the upward going secondary electron current from stray gas molecules ionized in the acceleration tube, could be able to influence the operation of the ion source.

5. Delay in Striking

Using a pulse generator which gave rectangular voltage pulses the delay in striking was measured, as shown in fig. 10.

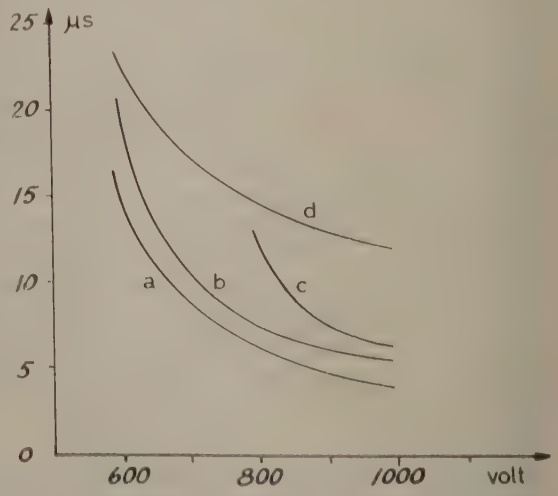

Fig. 10. The delay in striking as a function of the anode voltage.

Recesses in the cathodes, which help to stabilize the discharge, as discussed, increase the delay in striking (see curve c).

The delay can be reduced somewhat by

pre-ionisation. The pulse generator which was used for subsequent testing of the ion sources gives a striking pulse of about 2000 V, as shown on the oscillogram fig. 2, which shows a delay in striking of only about 3 μsec. The values shown on the lowest curve of fig. 10 were measured with a slight continuous current superimposed on the pulse current. This curve holds for a continuous current between 1–10 mA, but if the current is increased above these values there is no further reduction in the striking delay.

If pulses shorter than 20 μsec are required it is necessary to pulse the acceleration system as well as the ion source, or to save the striking by means of the electron emission from a filament.

6. Extraction of Ions

The electrode field between the extraction electron L and the bottom of the ion source (see fig. 3) is determined by the extraction voltage V_e. If this voltage is removed the plasma extends out through the outlet hole. For small extraction voltages the extracted ion current is space charge limited, i.e. it varies as the 3/2 power of the extraction voltage. If the extraction voltage is so large that the current is saturated, the plasma is forced back into the outlet channel, the boundary of the plasma taking up a position such that the field strength in its neighbourhood is just sufficient to withdraw all the ions which diffuse there from the body of the plasma. If the outlet channel has a length H approximately equal to the diameter $2r$, ions will drift from the plasma into the walls of the channels.

Of the ion current $J_0 = J \cdot \pi r^2$ which enters the top of the outlet channel, only a fraction J_1 reaches the surface of the plasma filling the extraction field. One gets, using the symbols of fig. 11,

$$J_1 = \frac{\pi r^2}{\pi r^2 + 2\pi r h} \cdot J \pi r^2 \qquad (3)$$

(r = radius of the channel and h = the downwards penetration of the plasma). The full curve in fig. 12 shows the peak ion current as a function of the radius for $h = H = 2.5$ mm. The ion current density J has been taken to correspond to the discharge current used in an experiment which gave the results shown by crosses in fig. 12.

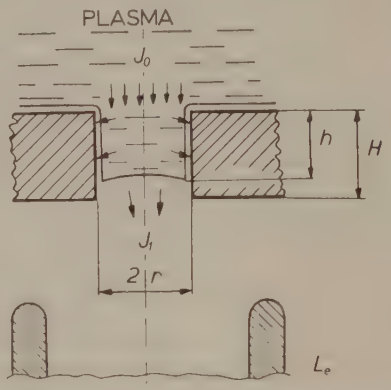

Fig. 11. The mechanism of the ion extraction from the discharge plasma through the outlet hole in the cathode of the ion source.

It should be noted that for large r, h will be somewhat smaller than H (see fig. 11) because of the penetration of the extraction field.

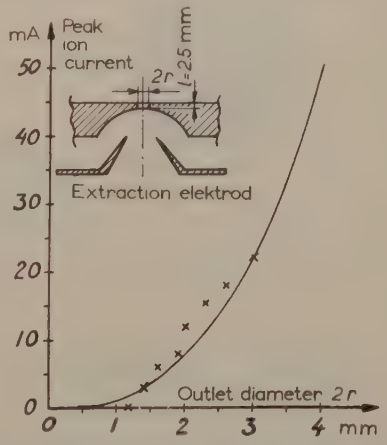

Fig. 12. Ion current at constant extraction voltage (25 kV) and constant discharge currents (2.5 A peak) for various diameters of the outlet channel. Length of outlet channel 2.5 mm.

Like the gas leakage through a hole, the ion current is proportional to r^2 as long as $r \gg 2h$ and to r^3/h when $r \ll h$. Therefore the extracted

ion current is proportional to the gas consumption, the outlet shape not influencing. As the electron loss in the discharge is proportional to the area of the outlet, this is to be chosen as small as possible. At the same time the length of the outlet channel shall be considerably smaller than its diameter, so that the loss of ions to its walls will be as small as possible.

If the extraction voltage is increased while the diameter of the outlet hole is kept constant, the plasma is forced back into the channel. The penetration of the extraction field into the outlet channel is however proportional to the logarithm of the extraction voltage. This means that when the extraction voltage is sufficiently large to saturate the ion current, this current increases only slowly with extraction voltage. With the ion source type III, which had an outlet channel 2 mm in diameter and 2 mm long, the voltage dependence of the current was as shown in the lower curve of fig. 13, corresponding to:

$$J_1 = k \cdot V_e^{1/2} . \qquad (4)$$

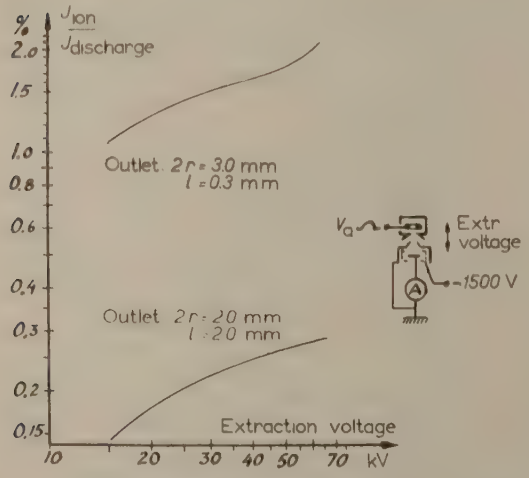

Fig. 13. Total ion current expressed in % of the discharge current at different extraction voltages. Both curves are for ion source III, but with different outlet holes. The theoretical ratio between the ion currents from these two holes is $J_3/J_2 = 8$ as follows from eq. (3).

Measurements on ion source type III with a short channel (upper curve in fig. 13), and on type I with an outlet channel 3.5 mm in diameter and 0.5 mm long (not shown in fig. 13 but of the same shape), showed how the ion current increased with extraction voltage in these cases. The similar shape as for the long and narrow hole can be explained as follows. When the extraction voltage is increased the plasma is forced back and forms a dome over the outlet hole, and its concave boundary surface, from which the ions are released, becomes greater.

The extent to which the extraction field penetrates through the outlet hole is proportional to the logarithm of the extraction voltage, as it was for the 2×2 mm channel. The ion current thus increases as a function of the extraction voltage in much the same way for different outlet channels, as may be seen from fig. 13.

The ion current (eq. (3)) which enters the top of the outlet channel (of area $A_1 = \pi r^2$) at a given discharge current should be a function of A_1/A_2 of the ion current to the lower cathode surface, where A_2 is the cross sectional area of the discharge. The diameter of the column of the plasma which determines A_2 is slightly less than the inner diameter of the anode. The ion current to the lower cathode surface of a geometrically symmetric source is half the discharge current minus the electron current which is emitted from the cathode, and which in this case can be estimated to be 1/5 of the ion current, so that the ion current on the lower cathode $0.5/1.2 = 0.4$ of the discharge current.

In ion source type III with a 3 mm outlet hole, A_1/A_2 is about $(3/10)^2 = 0.09$, which gives $J_0/J_d = 0.036$. After making the correction expressed by eq. (3), we get $J_1/J_d = 0.025$. The ion current which was found experimentally, corresponded to $J_1/J_d = 0.015$–0.02, see upper curve of fig. 13.

With a 2 mm outlet hole A_1/A_2 is equal to 0.04, which gives $J_0/J_d = 0.016$. After making the correction of eq. (3) we get $J_1/J_d = 0.0032$. The experimental value is 0.002–0.003 (see fig. 13 lower curve).

The oscillograms in fig. 14 show the ion current pulses for different extraction voltages. They are sinusoidal, i.e. proportional to the discharge current even at the lowest extraction

voltages. At an extraction voltage of 2.5 kV the discharge changes type and has a considerably smaller ion yield. A plasma density such that the extraction voltage is insufficient has not been reached, but if it were, the pulse form would show flattened peaks.

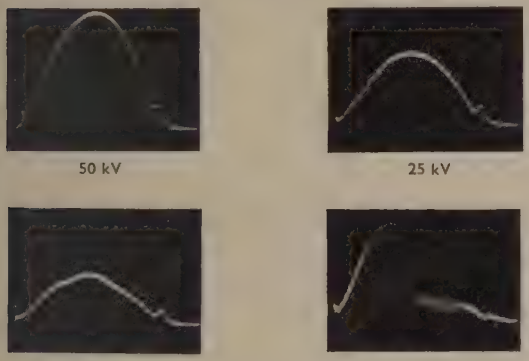

Fig. 14. Total ion current including secondary electrons, L + C, fig. 3, at constant discharge current (5.6 A maximum). Pulse length 60 μsec, but different extraction voltages, 50, 25, 15 and 2.5 kV. Amplitudes: 100, 60, 40 and 7 mA respectively.

7. Focusing

The lens consisting of the bottom of the ion source and the extraction electrode should be designed so that the ion current is emitted from the ion source with a suitable divergence.

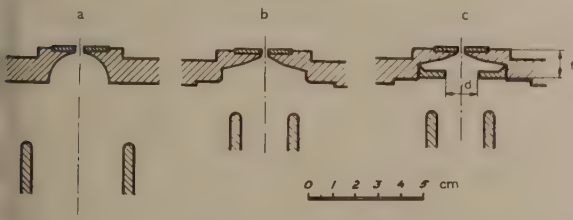

Fig. 15. Different bottom design of the ion source for focusing tests.

Several different designs, shown in fig. 15, were tested in an arrangement which is shown schematically in fig. 3. In these measurements the magnitude of the current reaching the collector C was determined when the stop B1 was 25 mm in diameter, i.e. when the ion beam was limited to a cone of angle $2 \times 10°$.

The focussing action of an electrostatic lens of which one electrode (the bottom of the ion source) has almost zero potential, is to a first approximation independent of the voltage on the other electrode (L. fig. 3).

The form of the ion beam should thus not be dependent on the extraction voltage at the current densities in question here. However, the spreading of the beam because of its own space charge becomes of importance. In a field-free region the spreading in a given distance (eq. (7) of part I) is a function of $J_1/V^{3/2}$ where J_1 is the total current in the beam and V its energy, here equal to the extraction energy. If this fraction is constant the form of the beam should also be constant.

From the oscillogram of the ion current pulse to collector C (fig. 3) it is possible to calculate the amplitude of the largest pulse which can

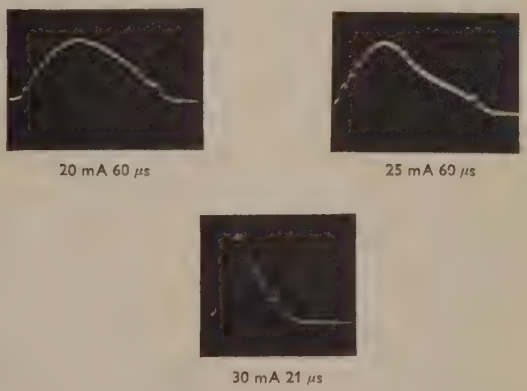

Fig. 16. The current into a cone of angle $2 \times 10°$ when the amplitude of the emitted ion current is varied by varying the discharge current. Extraction voltage (50 kV) and geometry (type C fig. 15) are the same in all three cases.

pass the stop B1 (fig. 3) without striking its edges. Fig. 16a shows a pulse which has passed a stop without distortion, the aperture of the beam being less than that of the stop. In fig. 16b the amplitude is so large that the beam begins to be cut down, and one sees a slight inflection shortly after the current maximum. In this case the diameter of the beam is slightly larger than that of the stop. Finally in fig. 16c the diameter of the beam at the current maximum is considerably larger than that of the stop,

resulting in a severe cutting down of the pulses. The slope of this part of the curve is presumably due to a reduction of the extraction voltage during the pulse, caused by too small a capacity in the high voltage supply.

An investigation of the maximum amplitude which could be passed without distortion showed that within $\pm 10\%$ it was proportional to $V^{3/2}$, as might be expected if the spread due to space charge determines the form of the beam. The actual width of the beam also depends on its initial focusing, i.e. on the focusing power of the first lens, so that each electrode discharge gives a different value for the ratio $J_1/V^{3/2}$. The values for this ratio are shown in the following table: $J_1/V^{3/2}$ for various different forms of the bottom of the ion source.

J_1 is the amplitude of the highest current which will pass through a 25 mm stop placed 75 mm below the outlet for the extraction voltage V.

$$c_1: \begin{matrix} d = 14 \\ f \quad 6 \end{matrix} \qquad c_2: \begin{matrix} d = 14 \\ f = 10 \end{matrix}.$$

Electrode type see fig. 15.

$J_1/V^{3/2}$ mA/kV$^{3/2}$	a	b	c_1	c_2
	0.11	0.03	0.10	0.11

NUCLEAR INSTRUMENTS 2 (1958) 237-248; NORTH-HOLLAND PUBLISHING CO. - AMSTERDAM

USE OF $Li^6I(Eu)$ AS A SCINTILLATION DETECTOR AND SPECTROMETER FOR FAST NEUTRONS

R. B. MURRAY

Oak Ridge National Laboratory†, Oak Ridge, Tennessee

Received 9 November 1957

The scintillation response of europium activated crystals of Li^6I to neutrons in the energy range 1–14MeV has been investigated with the crystals maintained at various temperatures. The pulse-height spectrum from monoenergetic neutrons incident on a crystal at room temperature demonstrates a poorly defined and broad fast-neutron peak. Upon cooling the crystal, the fast-neutron peak becomes sharper and assumes a nearly Gaussian shape at temperatures below about —140° C. This behaviour is attributed to an increased scintillation efficiency of LiI(Eu) to alpha particles at low temperatures. Pulse-height spectra from crystals at the liquid nitrogen point are presented for neutrons from the $D(d,n)He^3$, $T(d,n)He^4$, and $Be^9(d,n)B^{10}$ reactions, a Po-Be source, and U^{235} fission. The principal features of $Li^6I(Eu)$ as a fast-neutron spectrometer are a relatively high detection efficiency ($\approx 0.1\%$) and moderate resolution.

1. Introduction

The work which is reported here was initiated in an attempt to develop a more efficient and versatile instrument for measuring the energy distribution of neutrons in the range of about 1 to 14 MeV. This program was motivated largely by the need for a suitable fast-neutron spectrometer for use in studies of reactor physics and reactor shielding where it is necessary to measure the spectrum of escaped neutrons. Considerable attention has been devoted in the past to fast-neutron spectral measurements, particularly at laboratories engaged in studies of nuclear reactions and nuclear level structures. The most widely used techniques have been those employing recoil protons, either in photographic emulsions or in counter "telescopes". A review of these techniques is available elsewhere[1,2]). In order to obtain a differential neutron energy spectrum from the observed energy distribution of recoil protons, it is generally necessary to know the direction of the incoming neutrons. In the case of a neutron source widely distributed in space (e.g., a reactor shield) it is then necessary to collimate the neutrons prior to incidence on the detector. This has a twofold disadvantage in that, first, the detector must be removed from the source point by a distance equal to the collimator length, resulting in a geometrical attenuation of the neutron flux of order 10^{-2} to 10^{-3}; second, neutron scattering from the collimator walls may perturb the incident neutron spectrum. The required use of a neutron collimator in conjunction with a recoil-proton "telescope" may result in an over-all detection efficiency of order 10^{-8} or smaller, leading to a prohibitively low counting rate for many problems of current interest. The use of photographic plates provides a very reliable technique, but one which requires a large investment in reading time in order to extract the desired information. It is therefore of interest to seek a more efficient spectrometer whose detecting element is insensitive to the direction of the incoming neutron

† Operated by Union Carbide Nuclear Company, Division of Union Carbide Corporation, Oak Ridge, Tennessee.

[1]) J. L. Fowler and J. E. Brolley, Jr., Revs. Mod. Phys. 28 (1956) 103.

[2]) C. D. Swartz, Spectrometry of Fast Neutrons, NYO-3863 (1954).

and whose output can be directly recorded on a multi-channel analyzer for rapid data taking.

Scintillation crystals of $Li^6I(Eu)$ provide a candidate for such an instrument. Neutron capture takes place through the $Li^6(n,\alpha)T$ reaction ($Q = 4.78$ MeV), whose cross section has been measured in the energy range of interest[3,4]). The magnitude of the scintillation pulse resulting from neutron capture depends upon the total energy released, $E_N + Q$, so that in principle a one-to-one correspondence

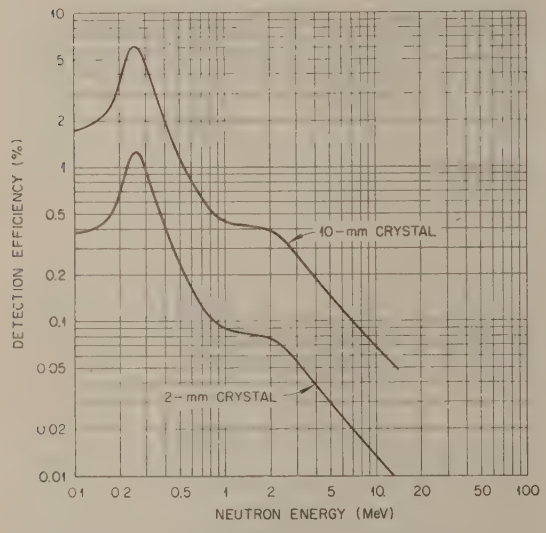

Fig. 1. Neutron detection efficiency of $Li^6I(Eu)$ as a function of neutron energy, assuming neutrons to be incident normal to the plane face of a crystal. Curves are calculated from the reported (n,α) cross section and assume 100% isotopic concentration of Li^6.

should exist between the pulse size and the energy of the incoming neutron. A pulse-height analysis of fast-neutron pulses should then provide a measure of the energy distribution of the incident neutrons. A particular advantage in the use of $Li^6I(Eu)$ is its relatively high detection efficiency compared to the previously mentioned techniques. A plot of neutron detection efficiency of $Li^6I(Eu)$ *vs.* neutron energy is given in fig. 1.

In order to examine the scintillation response of $Li^6I(Eu)$ to fast neutrons, a series of experiments, described below, has been carried out with various neutron sources.

2. Crystals

The crystals used in this work were obtained by growing at this Laboratory and from Harshaw Chemical Company. Crystals enriched in Li^6 to 96% were available from both sources. The crystals prepared at this Laboratory were grown and made available for this work by J. Schenck. These crystals were grown by the Stockbarger method starting with anhydrous lithium iodide to which a small quantity of activator in the form of europium chloride had been added. The starting material was prepared by reacting high purity lithium carbonate with freshly distilled hydriodic acid; the resulting lithium iodide trihydrate was dehydrated by heating slowly in a vacuum to about 325°C. This preparation has been previously described[5]). Crystals were grown with varying amounts of activator, the europium content ranging from about 0.01 to 0.1 mole percent. The best results, in the sense of sharp resolution, are realized with a europium content of about 0.05 mole percent or greater. The very hygroscopic nature of lithium iodide requires that the crystals be carefully mounted and maintained in a moisture-free environment.

The scintillation response of LiI(Eu) crystals to slow neutrons and gamma rays has been reported by Schenck[6]). A properly activated crystal used in connection with a selected photomultiplier will produce a slow-neutron peak of resolution 6%. (*Resolution* is defined here as $\Delta E/E$, where ΔE is the full width at half-maximum of a peak occurring at pulse height E.) The emission spectrum of LiI(Eu), upon excitation by X-rays, is centered near 4 750 Å. The absorption spectrum shows that LiI(Eu) absorbs strongly below a sharp cut-off at about 4 500 Å.

[3]) F. L. Ribe, Phys. Rev. **103** (1956) 741.

[4]) D. J. Hughes and J. A. Harvey, Neutron Cross Sections, BNL-325 (1955).

[5]) R. H. Sampley, Preparation of high purity anhydrous LiI, ORNL-1673 (1954).

[6]) J. Schenck, Nature **171** (1953) 518.

The crystals used in the experiments to be described were in the form of thin discs, 2 to 3 mm in thickness by about 30 mm in diameter. Normally the crystals were mounted on a polished cylindrical lucite light piper whose walls, as well as the reverse face of the crystal, were loosely covered by an aluminum foil reflector. The crystal was always sealed from the atmosphere by a suitable thin cap.

It should be pointed out that considerable difficulty has been encountered in preparing and keeping good LiI(Eu) crystals. The pulse-height spectra shown in this paper were recorded with selected crystals, the criterion for acceptance being a symmetrical slow-neutron peak with resolution of 8% or better. It is hoped that improved crystal-growing technology will result in a more uniform product in the future.

3. Electronics

Two-inch-diameter photomultiplier tubes were used throughout the study; best results were obtained with a selected Dumont 6292 and a selected RCA 6342. The photomultiplier pulses were fed to a cathode-follower preamplifier, then to a linear amplifier in which the pulse was clipped by a shorted delay line. Since the decay time of LiI(Eu) is about 1.2 μsec, it was necessary to use 4 μsec delay line clipping in the amplifier in order to obtain a pulse which was flat on top before being clipped. The amplified 4 μsec pulses were then fed to a multi-channel pulse-height analyzer for analysis and recording. Since 4 μsec pulses were analyzed it was necessary to restrict the over-all counting rate to a few thousand counts per second to avoid an appreciable over-lapping of pulses. Linearity and zero checks of the electronic system were made prior to each experiment.

4. Room Temperature Scintillation Response to Fast Neutrons

The pulse-height spectra resulting from monoenergetic neutrons on a thin $Li^6I(Eu)$ crystal at room temperature were recorded for neutron energies in the range 0.63 to 14.9 MeV. Monoenergetic neutrons in this energy region were obtained from the $T(p,n)He^3$, $D(d,n)He^3$, and $T(d,n)He^4$ reactions, using the ORNL 3-MeV Van de Graaff generator as the charged particle accelerator. A typical pulse-height spectrum, from 1.57-MeV neutrons, is shown in fig. 2. The fast-neutron peak, which appears as a broad and "rectangular" band, is accompanied

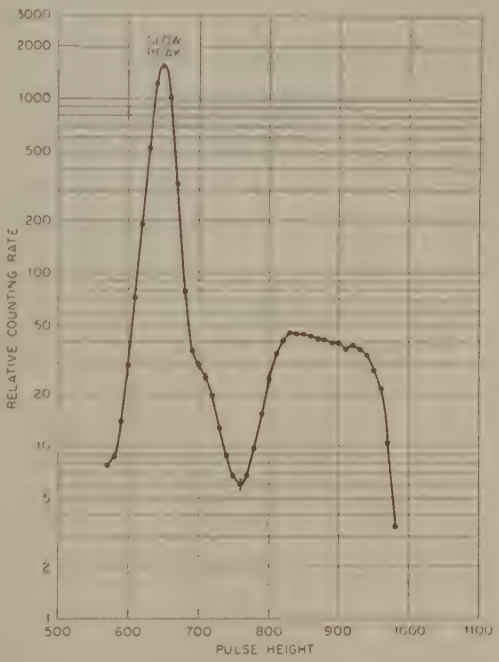

Fig. 2. Pulse-height spectrum from 1.57-MeV neutrons on a $Li^6I(Eu)$ crystal at room temperature.

by a slow-neutron peak arising from a background of epithermal neutrons scattered to the crystal by nearby apparatus. The magnitude of the slow-neutron peak is due to the very large $Li^6(n,\alpha)T$ cross section at low energies (945 barns at thermal). The small hump on the side of the slow-neutron peak at about 700 pulse-height units is presumably due to the (n,α) resonance at 0.25 MeV. The width and poor definition of the fast-neutron peak is attributed to a difference in the scintillation efficiency of LiI(Eu), at room temperature, to the alpha and triton. For the fast-neutron induced reaction both the alpha and triton have

a range of energies available to them, since the energy division between the reaction products depends upon their angular distribution. For very slow neutrons, however, the energy distribution between the alpha and triton is uniquely specified, so that the epithermal peak appears as a sharp Gaussian. A difference in the scintillation efficiency of LiI(Eu) to the alpha and triton may very reasonably be expected on the basis of studies of NaI(Tl), where it was found that the efficiency to alpha particles is considerably lower than that to protons or deuterons[7]). Experiments at this Laboratory on the excitation of LiI(Eu) by natural alpha particles indicate that such a difference does indeed exist in this case, and that the efficiency to alphas is lower than that for tritons or electrons. Further, the width of the fast-neutron peak in fig. 2, as well as spectra recorded at other neutron energies, can be correlated with the energy spread available to the reaction products if the ratio of the alpha to triton scintillation efficiency is about $\frac{1}{2}$.

Pulse-height spectra resulting from monoenergetic neutrons of various energies are quite similar to the spectrum shown in fig. 2. In each case a broad band from the fast neutrons is accompanied by a sharp slow-neutron peak. At 14.3-MeV neutron energy, a large continuous background from competing nuclear reactions is observed. This background will be demonstrated and discussed later. Measurements of fast-neutron pulse-height spectra have been carried out on other crystals of LiI(Eu) with various concentrations of europium activator, Li^6 isotope, and different thicknesses ranging from 2 to 10 mm. The spectra observed were all basically similar and are characterized by the general features shown in fig. 2. The results of these experiments do not encourage the use of Li^6I(Eu) as a fast-neutron spectrometer by virtue of the width and poor definition of the fast-neutron peak.

5. Low Temperature Studies

Another variable which can affect the scintillation properties of a crystal is its temperature. Some recent experiments[8, 9]) on temperature dependent effects in alkali halides suggested the possibility of improving the scintillation response of LiI(Eu) to fast neutrons by operating the crystal at a reduced temperature. Preliminary experiments were carried out with an apparatus in which the crystal could be maintained at any chosen temperature between room temperature and about —190°C. A schematic diagram is shown in fig. 3; the design

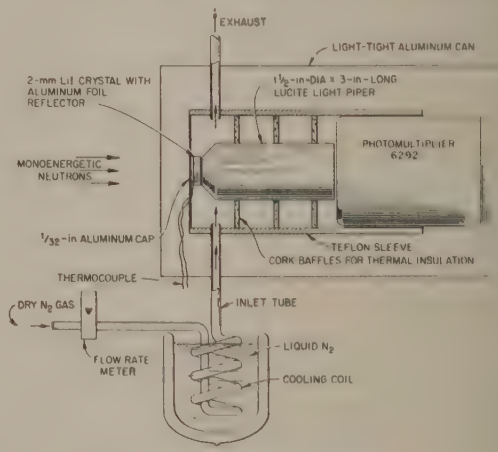

Fig. 3. Cooling apparatus.

of this equipment was dictated by the fact that conventional photomultipliers (with a transparent photocathode made of a semiconducting material) do not function below about —140°C. With the scheme shown here the photocathode is maintained near room temperature, while the crystal may be cooled to the desired point. The crystal temperature, which is measured by a copper-constantan thermocouple, is set by adjusting the flow rate of the cooling gas.

Two effects are observed upon cooling a crystal. First, the scintillation efficiency increases with decreasing temperature. This effect has been previously observed in all the alkali

[7]) C. J. Taylor, W. K. Jentschke, M. E. Remley, F. S. Eby and P. G. Kruger, Phys. Rev. **84** (1951) 1034.

[8]) W. Van Sciver, I. R. E. Trans. Nuc. Sci. NS-3 (Nov. 1956) 39.

[9]) E. der Mateosian, M. McKeown and C. O. Muehlhause, Phys. Rev. **101** (1956) 967.

iodides[10]). Second, the fast-neutron peak assumes a nearly Gaussian shape at about —140°C, with a marked improvement in resolution. This behaviour is shown as a function of temperature

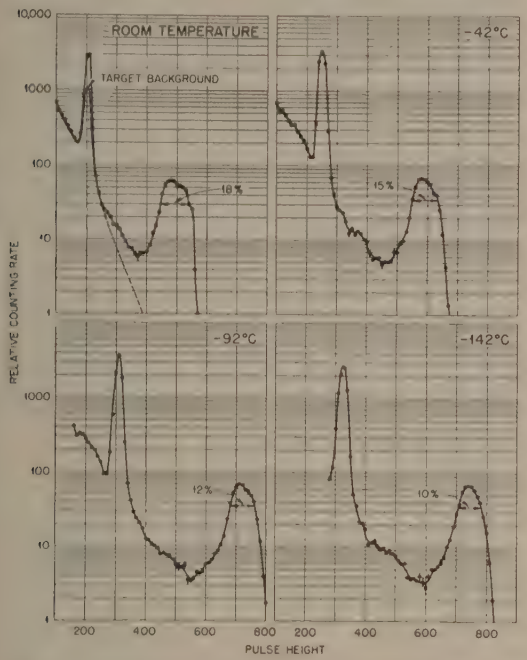

Fig. 4. Pulse-height spectra at various temperatures from 5.3-MeV neutrons.

for a $Li^6I(Eu)$ crystal of 2 mm thickness in fig. 4. The continuous background in fig. 4 is due in part to neutrons and gamma rays resulting from the penetration of the deuteron beam through a thin nickel foil in the gas target which was used for the $D(d,n)He^3$ reaction. This background was recorded by replacing the deuterium gas in the target with helium. The target background is indicated in the room temperature spectrum.

The resolutions indicated in fig. 4 are somewhat deceptive in that they represent the full-width at half-maximum divided by the pulse height of the maximum, following the usual convention. From the standpoint of neutron energy, however, the zero of energy occurs at the position of the slow-neutron peak, so that the *neutron energy* resolution is broader than that shown. For example, the neutron energy resolution at —142°C (fig. 4) is 18%.

The considerable improvement in fast-neutron response suggests that the ratio of the alpha to triton scintillation efficiency is temperature dependent, and that the difference in scintillation efficiency to the two particles is minimized at low temperatures. In order to check this, an experiment was carried out in which a LiI(Eu) crystal was simultaneously excited by 1.12-MeV gammas from Zn^{65}, U^{233} alpha particles from a thin, external source, and the alpha-triton pair from slow-neutron capture. The peaks observed in the pulse-height spectrum resulting from these three modes of excitation were followed as a function of temperature. The results are shown in fig. 5, in which the pulse heights of the three peaks are normalized to the same value at room temperature. Fig. 5 shows that the scintillation efficiency to alpha particles increases faster with decreasing temperature than that for gammas or the alpha-triton pair from neutron capture. The results of this experiment are thus consistent with the proposed explanation for the observed fast-neutron response.

In order to take advantage of the results indicated in figs. 4 and 5, a low-temperature apparatus was built which would permit routine operation at the liquid nitrogen point,

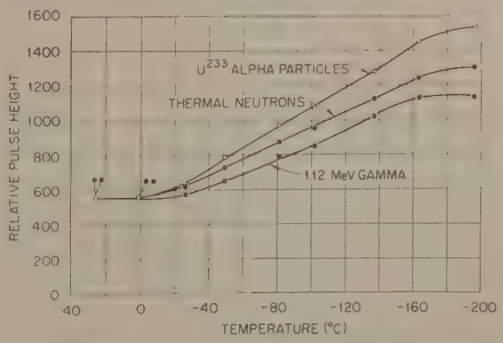

Fig. 5. Relative pulse height as a function of temperature for LiI(Eu) excited by alpha particles, gamma rays, and thermal neutrons.

and which would require minimum attention. A drawing of this instrument is shown in fig. 6. The LiI(Eu) crystal is mounted on a polished

[10]) J. Bonanomi and J. Rossel, Helv. Phys. Acta **25** (1952) 725.

lucite light piper 1¼ in. long. The light piper is optically coupled to the photomultiplier by DC 200 silicone grease. The photomultiplier is held firmly against the lucite by spring tension, as shown. A flow of compressed air around the

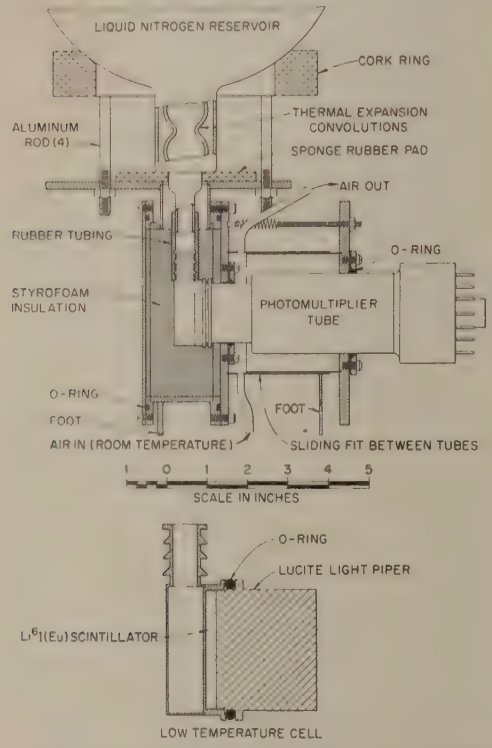

Fig. 6. Scintillation spectrometer for use at liquid nitrogen temperature.

photomultiplier and light piper maintains the photocathode surface near room temperature. The "cold" end of the light piper is provided with a flange and is threaded so that the crystal may be sealed from the atmosphere by a thin-wall brass cap which seats on a rubber "0" ring against the flange. This cap is part of the liquid nitrogen system and communicates directly with the liquid nitrogen reservoir. The reservoir is a glass Dewar vessel of two liters capacity and requires filling about every four hours. The Dewar vessel is connected to the liquid nitrogen cell adjoining the crystal by a short length of rubber hose. Partial thermal insulation is achieved by surrounding the low-temperature cell with styrofoam.

It is necessary to mount the crystal directly on the light piper without the use of an optical coupling fluid, since the various greases normally used for this purpose solidify upon cooling and may break either the optical seal or the crystal. In the case of thin LiI(Eu) crystals mounted on lucite, it was found that the room-temperature resolution (for slow neutrons) of a crystal mounted dry is very little different from that of the same crystal mounted with an optical grease.

The crystal unit is cooled slowly to a temperature near —196°C before pouring liquid nitrogen into the reservoir. Gradual cooling is accomplished by blowing gas through a liquid nitrogen heat exchanger, as in fig. 3, and into the low temperature cell.

6. Neutron Spectra

The spectrum of neutrons from various sources has been recorded using the apparatus shown in fig. 6. Neutrons from nuclear reactions were obtained in this case by accelerating deuterons in the ORNL 625-keV cascade generator. The pulse-height spectrum from 2.92-MeV neutrons from the D(d,n)He^3 reaction is shown in fig. 7. The counts observed in fig. 7 between the fast- and slow-neutron peaks are attributed to neutrons scattered to the crystal by the surrounding apparatus. Probably the most offensive piece of apparatus in this respect is the lucite light piper, which is immediately adjacent to the crystal and which contains hydrogen. The light piper also is largely responsible for the slow-neutron peak which is always found to accompany fast neutrons. The counts due to these degraded neutrons constitute, of course, a background in the form of a low-energy "tail" which must be taken into account in a measurement of a continuous spectrum.

The spectrum from 14.3-MeV neutrons from the T(d,n)He^4 reaction is shown in fig. 8. The very large continuous background observed here is due to competing nuclear reactions which are excited by such high-energy neutrons,

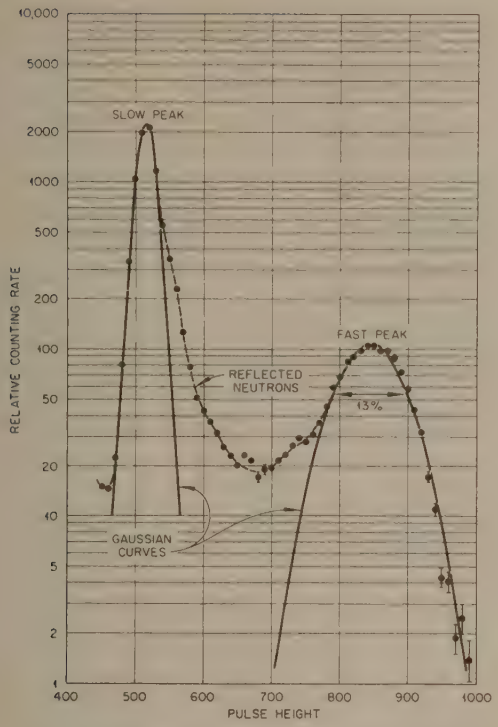

Fig. 7. Pulse-height spectrum from 2.92-MeV neutrons, with $Li^6I(Eu)$ crystal at liquid nitrogen point.

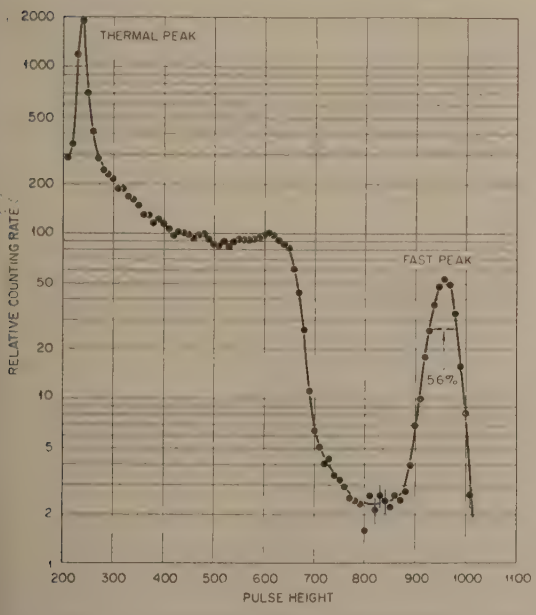

Fig. 8. Pulse-height spectrum from 14.3-MeV neutrons, with $Li^6I(Eu)$ crystal at liquid nitrogen point.

viz., $Li^6(n,dn)He^4$, $Li^6(n,p)He^6$, and Li^6 elastic recoils, as well as degraded neutrons scattered to the crystal. These reactions, however, will contribute counts to a pulse-height spectrum which can be confused with a $Li^6(n,\alpha)T$ event only in the case of a continuous spectrum containing neutrons above ≈ 7 MeV. This, of course, is a result of the positive Q of almost 5 MeV for the (n,α) reaction, combined with negative Q values for the competing reactions. Li^6 elastic recoils can give possibly spurious counts only for neutrons above 10 MeV, since the maximum energy of a Li^6 recoil is 0.49 E_{neutron}. For many continuous neutron spectra of interest (e.g., fission-like spectra) the number of high-energy neutrons is small compared to the number in the 2- to 3-MeV region, so that the above-mentioned effects will give rise to a minor correction. The severity of the background problem arising from competing reactions, then, depends entirely on the nature of the incident spectrum, and each case must be treated individually.

The $Be^9(d,n)B^{10}$ reaction ($E_d = 535$ keV) provides a source of five groups of monoenergetic neutrons. The energies of the various neutron groups can be predicted from the known level structure of the B^{10} nucleus. The scintillation response of the $Li^6I(Eu)$ spectrometer to neutrons from this reaction is shown in fig. 9. The calculated energies of the neutron groups are indicated by arrows. The neutron energy scale at the top of fig. 9 is determined by a plot of pulse height versus neutron energy (see fig. 10). The separation between the 2.52- and 2.90-MeV peaks shown in fig. 9 occurred in each of the several runs on this reaction, and is thus considered to be real. The small peak observed just above 5 MeV is attributed to contamination of the Be target by N^{14}.

The ordinate of fig. 9 is the relative counting rate and has not been corrected for the energy dependence of the $Li^6(n,\alpha)T$ reaction. This correction has the effect of multiplying the ordinate by a factor which increases with energy. Upon application of this correction, the relative number of neutrons observed in

the three principal groups of fig. 9 compares well with the relative intensities estimated from neutron spectra and angular distributions previously measured by nuclear emulsion techniques[11,12]).

In order to examine the scintillation response of $Li^6I(Eu)$ to a continuous neutron distribution,

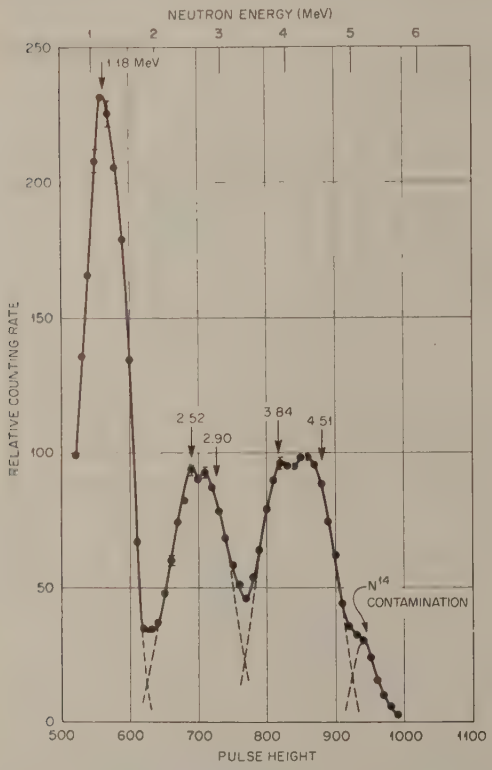

Fig. 9. Pulse-height spectrum from $Be^9(d,n)B^{10}$ neutrons on $Li^6I(Eu)$ crystal at liquid nitrogen point. Slow-neutron peak and correction for scattered neutrons have been subtracted.

the spectrum of neutrons from a Po-Be source was recorded, using the apparatus of fig. 6. The neutron spectrum from Po-Be sources is known from previous work[13,14]) to extend from low energies up to about 11 MeV, with a maximum intensity in the 3–5 MeV region. In this case the relatively large number of neutrons from 3 to 5 MeV gives rise to a significant background in the pulse height spectrum at lower energies due to scattered neutrons. As a result it is necessary to perform a spectrum "unfolding" to go from the $Li^6I(Eu)$ pulse-height spectrum to the incident neutron spectrum. The spectrum "unfolding" was carried out by starting at the high-energy end of the pulse-height spectrum, lumping together the counts in a $\frac{1}{2}$-MeV energy interval, and constructing the continuous background associated with this number of counts. This background was then subtracted from the initial spectrum, and the procedure was repeated for the next lowest energy interval. The shape and magnitude of the background correction associated with monoenergetic neutrons of a given energy can be inferred from various pulse-height spectra as in figs. 4 and 7. Upon completion of this process, the final pulse-height spectrum was corrected for the energy dependence of the $Li^6(n,\alpha)T$ cross section. The resulting neutron spectrum is shown in fig. 11. The background discussed above amounted to about 60% of the counts at 1.5 MeV, 17% at 3 MeV, and was negligible above 5.5 MeV. The neutron energy

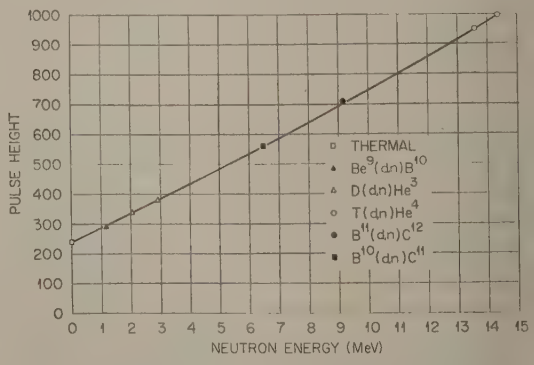

Fig. 10. Pulse height as a function of neutron energy for a $Li^6I(Eu)$ crystal at liquid nitrogen point.

scale was determined by a calibration as in fig. 10. The spectrum presented in fig. 11 is quite similar to those previously reported[13,14]).

As a further check on the applicability of the

[11]) A. J. Dyer and J. R. Bird, Aus. J. Phys. **6** (1953) 45.
[12]) J. Genin, Compt. Rend. **240** (1955) 2514.
[13]) B. G. Whitmore and W. B. Baker, Phys. Rev. **78** (1950) 799.
[14]) R. J. Breen, M. R. Hertz and D. U. Wright, Jr., The spectrum of polonium-beryllium neutron sources, MLM-1054 (1955).

$Li^6I(Eu)$ technique to the measurement of fission-like spectra, an experiment was carried out to measure the spectrum of neutrons from U^{235} fission. The experiment was performed with the 3-MeV Van de Graaff accelerator as a source of neutrons; this method was chosen so that the fission source and detector would be far away from floors, walls, and concrete shields.

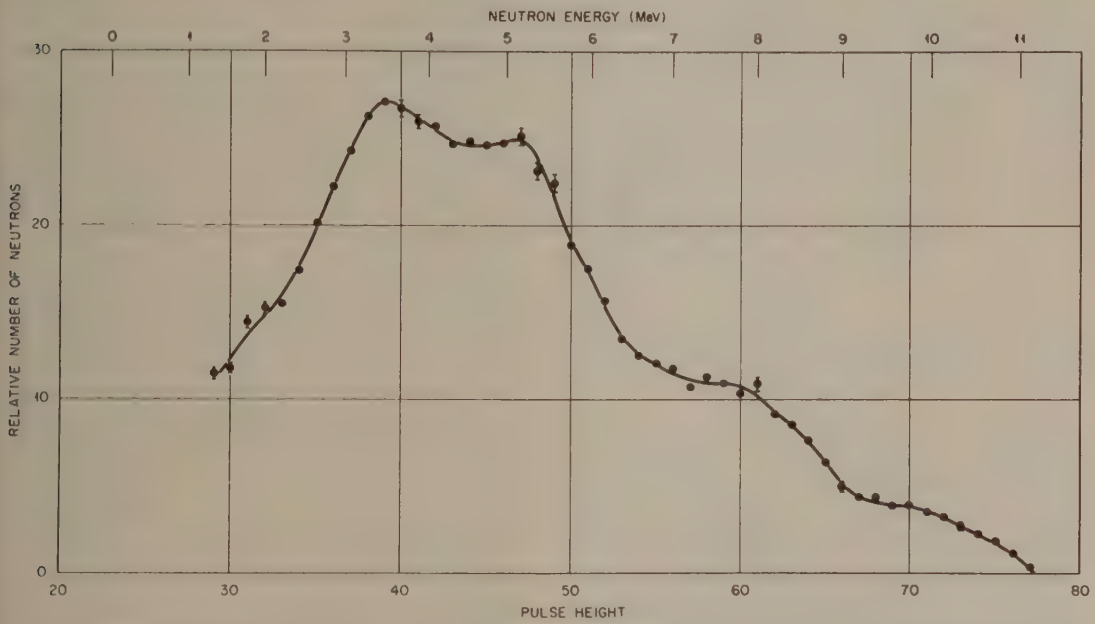

Fig. 11. Neutron spectrum of 1-curie Po-Be source. Data were recorded on a 20-channel analyzer in 5 hours. Standard deviation shown on some points represents counting statistics only.

Protons were accelerated to an energy above the threshold of the $T(p,n)He^3$ reaction, producing low-energy (< 200 keV) neutrons in a forward cone. These neutrons initiated fission events in a $^5/_8$-inch thick by 1 inch diameter U^{235} slug. The $Li^6I(Eu)$ detector, in the apparatus of fig. 6, was placed outside the neutron cone and was 8 cm from the fission source. The pulse-height spectrum was unfolded in the same manner as the Po-Be data, and was corrected for the $Li^6(n,\alpha)T$ cross section. The scattered neutron correction amounted to 15% at 1.5 MeV, 5% at 3 MeV, and was negligible above 4 MeV. The resulting fission neutron spectrum is presented in fig. 12. For comparison, the U^{235} fission neutron spectrum as measured by photographic plates at Los Alamos[15]) is also shown. These two sets of data were normalized by requiring the areas under the curves above 2 MeV to be equal. An additional uncertainty in these data (and in the spectra discussed above) is introduced by probable errors in the $Li^6(n,\alpha)T$ cross section of 11 to 18%, combined with the fact that no cross section data at all are available between 6.5 and 14 MeV. The cross section in this region was taken from a smooth curve joining the data below 6.5 MeV with the one point at 14 MeV. The parallel curves in fig. 12 represent bounds of $\pm$ 11 to $\pm$ 18% on a smooth curve drawn through the $Li^6I(Eu)$ data points. The two sets of data in fig. 12 really should not be compared directly, as the thick source used in the $Li^6I(Eu)$ experiment is expected to modify the spectrum. Within the uncertainties mentioned above, however, the spectra are in reasonable agreement.

[15]) L. Cranberg, G. Frye, N. Nereson and L. Rosen, Phys. Rev. **103** (1956) 662.

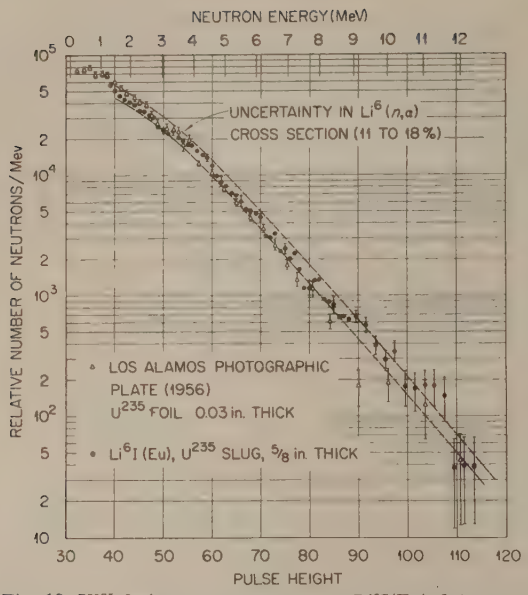
NEUTRON ENERGY (MeV)
0 1 2 3 4 5 6 7 8 9 10 11 12
RELATIVE NUMBER OF NEUTRONS/Mev
UNCERTAINTY IN Li⁶ (n,α) CROSS SECTION (11 TO 18%)
LOS ALAMOS PHOTOGRAPHIC PLATE (1956) U²³⁵ FOIL 0.03 in. THICK
Li⁶I (Eu), U²³⁵ SLUG, 5/8 in. THICK
PULSE HEIGHT

Fig. 12. U^{235} fission neutron spectrum. $Li^6I(Eu)$ data were recorded on a 100-channel analyzer in 6 hours. Standard deviation shown on $Li^6I(Eu)$ points represents counting statistics only.

7. Background and Gamma-Ray Corrections

It should be pointed out that no attempt has been made in the present work to determine a precise and detailed picture of the low-energy "tail" due to neutrons scattered to the crystal. The exact shape of this background is determined by the immediate environment of the crystal and, as such, is a property of each individual low-temperature apparatus. It was previously stated that the lucite light piper was chiefly responsible for the large number of slow-neutron counts. The use of a glass or quartz light piper has the effect of reducing the size of the slow-neutron peak, but increases slightly the background in the MeV region. Clearly the most desirable solution is to eliminate the light piper entirely. In this direction, a device has been constructed in which the cold $Li^6I(Eu)$ crystal is mounted inside a cylindrical, thin-wall aluminum sleeve which slips over the photomultiplier. The interior wall of the sleeve is polished to provide a reflecting surface. Preliminary results indicate that one can achieve quite satisfactory resolution with such a scheme, with a substantial reduction in slow-neutron background. An alternative approach would be to mount the crystal directly on a photomultiplier which will operate at the low temperatures desired. Such photomultipliers are available from commercial suppliers on special order. This scheme, however, has not proved satisfactory in our experience, in the sense that it is difficult to achieve acceptable resolution.

A further step to reduce the number of slow-neutron counts would be simply to surround the crystal with a slow-neutron absorbing material, such as Li^6 or B^{10} in a suitable compound. This shield could be chosen so that it would have little effect on the fast-neutron spectrum.

A major issue which remains to be discussed is that of the gamma-ray background which inevitably accompanies neutron sources. Three main points may be made on this subject: (1) The slow-neutron peak in a properly activated crystal occurs at a gamma-ray equivalent pulse height of above 4MeV. The large Q value thus provides a built-in bias against gamma rays up to this energy. (2) Thin crystals of $Li^6I(Eu)$ may be used (≈ 2 or 3 mm) so that the probability that a high-energy gamma ray (say 8 MeV) will deposit its full energy in the crystal is very small indeed. (3) An auxiliary crystal of $Li^7I(Eu)$ can be used as a gamma-ray monitor. Subtracting the $Li^7I(Eu)$ pulse-height spectrum from that recorded with $Li^6I(Eu)$ should eliminate the gamma-ray counts from the neutron spectrum. It is not necessary to operate the gamma-ray monitor at a reduced temperature.

In order to demonstrate the validity of the latter two points, some experiments were carried out with gamma-ray sources. The crystals chosen were a $Li^7I(Eu)$ crystal (99.9% Li^7) grown at ORNL, and a normal LiI(Eu) crystal supplied by Harshaw. Both crystals were slightly over 2 mm thick. The first question considered was whether the pulse-height response of these two arbitrarily selected crystals would be sufficiently similar to justify point

(3) above. The pulse-height spectra from 1.12-MeV gammas from Zn^{65}, 4.43-MeV gammas from a Po-Be neutron source, and high-energy gammas from the $B^{11}(p,\gamma)C^{12}$ reaction were recorded. For each of these sources, the two gamma-ray spectra were identical and could be well superimposed. It was, of course, necessary to adjust the amplifier gain slightly to match the pulse height from the two crystals. The superposition of the two spectra from $B^{11}(p,\gamma)C^{12}$ gammas is shown in fig. 13. In this

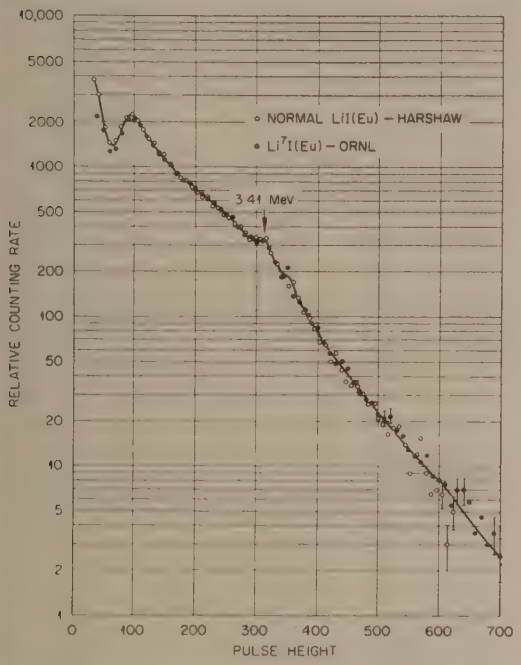

Fig. 13. Pulse-height spectra from $B^{11}(p,\gamma)C^{12}$ gamma rays on LiI(Eu) and $Li^7I(Eu)$. Both crystals were at room temperature. Gamma rays were incident normal to the plane face of the crystal.

case protons were accelerated in the cascade generator to 175 keV, producing gamma rays at 16 MeV and an 11.6 + 4.43 MeV cascade. It is seen in fig. 13 that the gamma-ray counting rate falls off very rapidly with increasing energy, in spite of the presence of the high-energy gammas. This fact is taken as evidence in support of point (2) above.

The gamma-ray background in the fission experiment was monitored with an auxiliary crystal of $Li^7I(Eu)$. At a neutron energy of 1.5 MeV, the gamma-ray counting rate was 10^{-3} times the neutron counting rate. Similarly, the gamma-ray background was negligible in the Po-Be spectrum.

It is not necessary to use a $Li^7I(Eu)$ crystal with almost 100% Li^7 content as a gamma-ray monitor. One might instead use a normal LiI(Eu) crystal, taking into consideration neutron counts from the small Li^6 content. In this case, the pulse-height response of the LiI(Eu) crystal should be matched to that of the $Li^6I(Eu)$ crystal by intercalibration with *gamma rays* and not neutrons. This is a result of the fact that the relative scintillation efficiency of a crystal to neutrons and gammas is a function of activator content, and may be expected to vary from one crystal to another.

8. Summary

The experiments described here indicate that the use of $Li^6I(Eu)$ provides a technique suitable for fast-neutron detection and for certain types of fast-neutron spectral measurements. The principal advantage to be gained in the use of $Li^6I(Eu)$ as a fast-neutron spectrometer is the relatively high detection efficiency which may be orders of magnitude greater than that afforded by currently used recoil-proton methods. As a spectrometer, this method would be appropriate for experiments where high resolution is not required. The technique appears to be applicable to the measurement of continuous neutron spectra as well as line spectra. The low energy limit of usefulness is about 1 MeV; below this energy the distinction between fast- and slow-neutron counts is not clear.

As an energy sensitive fast-neutron detector, $Li^6I(Eu)$ might find application in various neutron scattering experiments; it might further be useful as a fast-neutron monitor. For such purposes it probably would not be necessary to operate the crystal at a reduced temperature.

Finally, the relatively few $Li^6(n,\alpha)T$ cross section points in the energy range of interest leads to some uncertainty in the detector

efficiency. It is hoped that the use of the experimental techniques described here will permit a remeasurement of the (n,α) cross section in more detail.

9. Acknowledgements

This work was initiated largely as a result of conversations with E. P. Blizard and F. C. Maienschein. The author is especially indebted to J. J. Manning for his assistance and participation in all of the experimental work described here. The initial phases of this program were carried out jointly with J. Schenck. The author wishes to thank C. D. Moak and C. H. Johnson for their cooperation during the use of the ORNL high-voltage accelerators.

NUCLEAR INSTRUMENTS 2 (1958) 249–260; NORTH-HOLLAND PUBLISHING CO. – AMSTERDAM

ELECTROMAGNETIC ISOTOPE SEPARATOR IN GOTHENBURG

O. ALMÉN, G. BRUCE and A. LUNDÉN

Department of Physics, Chalmers University of Technology, Gothenburg

Received 28 October 1957

A 90° electromagnetic isotope separator with a beam radius of 100 cm is described. Using an acceleration voltage of 50 kV, ion currents of up to a few hundred μA can be handled. The ion current and resolving power can be varied within wide limits by adjusting the position of the lens system during operation. Two types of magnetic ion sources have been used to prepare targets for nuclear reaction studies and samples for beta- and gamma-ray spectroscopy.

1. Introduction

Twenty three years ago, in 1934, Oliphant, Shire and Crowther[1]) and Smythe, Rumbaugh and West[2]) carried out the first experiments with isotopes separated in mass spectrographs In principle the production of pure isotopes for many purposes is possible by mass spectrographs where the ion current intensity has been increased at the expense of the resolving power[3]). The demand for large quantities of uranium 235 in U.S.A. during the war made electromagnetic isotope separation a large scale process. The rapid expansion of all fields of nuclear physics after the war has caused a great demand for very pure samples of stable isotopes in microgram and milligram quantities, suitable e.g. as targets for particle accelerators. Another field of great importance is the separation of radioactive isotopes to produce samples for beta- and gamma-ray spectrometers. Therefore a large number of isotope separators have been built during the last decade and new instruments are under construction or in the stage of planning. The development of electromagnetic isotope separators has been reviewed elsewhere[3, 4, 5, 6]). A monograph on the field is in course of publication[7]).

Among modern electromagnetic isotope separators there is a distinction between those working with a 180° magnetic field for the deflection of the ions and those with a sector field. The main difference between these two groups of instruments is that in the 180° instrument the ion source is operated within the magnetic field which means that only a few types of ion sources can be used, while in the sector field instruments the ion source is placed at some distance from the magnet, which permits the use of additional types of ion sources.

The calutrons in U.S.A. and England and the Dutch separator in Amsterdam are all of the 180° type. The French separator built by Bernas has a 60° deflecting magnet, while the four Scandinavian separators have 90° magnetic fields. The oldest of these is the one in Copenhagen, Denmark. The first Swedish separator was built in Stockholm. It was followed by the instrument in Uppsala and by our separator at Chalmers University of Technology in Gothenburg. Although the four Scandinavian separators have many features in common, we have thought it of interest to describe our instrument, with some stress on details where different constructions have been chosen for the individual separators.

[1]) M. L. Oliphant, E. S. Shire and B. M. Crowther, Proc. Roy. Soc. A **146** (1934) 922.

[2]) W. R. Smythe, L. H. Rumbaugh and S. S. West, Phys. Rev. **45** (1934) 724.

[3]) H. Ewald und H. Hintenberger, Methoden und Anwendungen der Massenspektroskopie (Weinheim, 1953).

[4]) J. Koch, Thesis (Copenhagen, 1942).

[5]) I. Bergström, S. Thulin, N. Svartholm and K. Siegbahn, Arkiv Fysik **1** (1949) 281.

[6]) C. J. Zilverschoon, Thesis (Amsterdam, 1954).

[7]) J. Koch (Editor), R. H. Dawton, M. L. Smith and W. Walcher, Electromagnetic Isotope Separators and Application of Electromagnetically Enriched Isotopes (North-Holland Publishing Co., Amsterdam, 1958).

Some thirty isotope separators have been described more or less in detail up to August 1957. The site and some general data are given in table 1 for these instruments. It was considered proper to include not only ordinary electromagnetic isotope separators, but all types of instruments where the basic principle is that ions are extracted from an ion source, accelerated and by some electric or magnetic device sorted according to their mass. The distinction between isotope separators and mass spectrometers is always somewhat arbitrary. We have restricted our list to cover instruments where the purpose has been claimed to be the obtainment of separated isotopes.

Except for the mass spectrometers used for the first uranium separations, all instruments listed have produced ion currents of at least the order of 1 μA. For data on mass spectrometers see e.g. ref. [3]).

2. General Principles of Design

The aim when designing the machine was to build an instrument capable of separating isotopes of all elements in quantities that could be used as targets for the electrostatic generator of this Institute[70]). The results already obtained with the separators in Copenhagen[8]) and Stockholm[5]) showed clearly that a similar instrument would be suitable for our purposes. Hence, we decided to construct a separator with a 90° magnetic field and with a beam radius of 100 cm. The ion optics of such an arrangement has been discussed e.g. by Koch and Bendt-Nielsen[8]). (For the general case of focusing, see e.g. ref. [3]).)

A parallel ion beam entering perpendicular to the boundary of a 90° homogeneous magnetic field is focused in one dimension at the exit boundary. The mass dispersion is then

$$D = \frac{r}{2}\frac{\Delta M}{M} \qquad (1)$$

where r = beam radius
M = mass number.

In our case this means about 2 mm between adjacent masses for the heaviest elements. This is about the same as the half width of the mass lines we can expect to obtain at optimal running conditions. Therefore the resolving power, P, would be insufficient for producing pure samples over the whole mass region. P is given as

$$P = \frac{DM}{B} \qquad (2)$$

where B is the line width. (Generally the half width is used when calculating P.)

[70]) N. Ryde and L. Karsberg, Arkiv Fysik 2 (1950) 224.

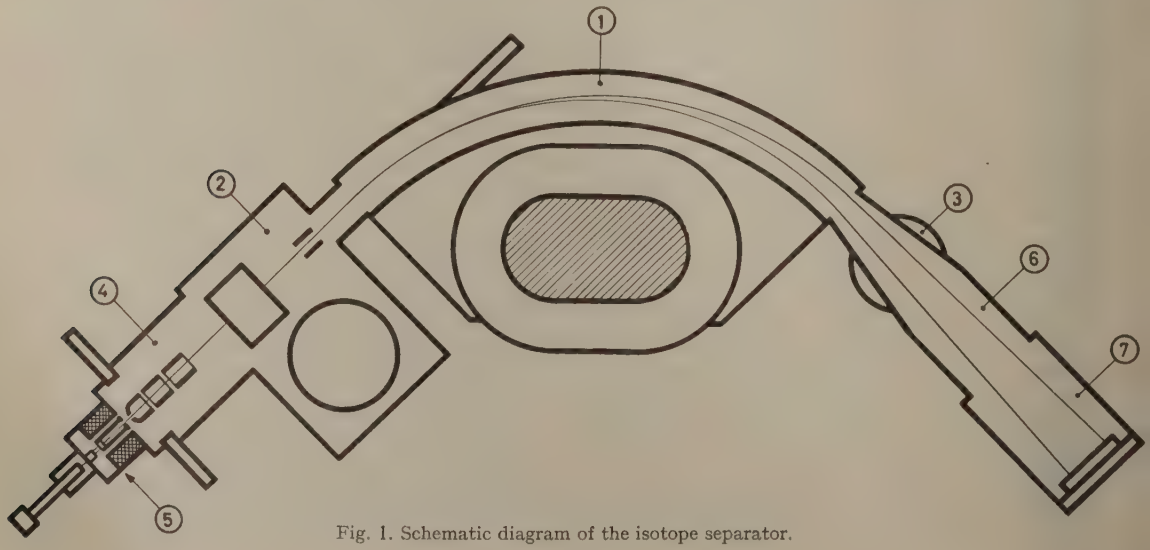

Fig. 1. Schematic diagram of the isotope separator.

TABLE I

ELECTROMAGNETIC ISOTOPE SEPARATORS AND RELATED INSTRUMENTS

General data

Site of instrument	Approx. date of first operation	Magnetic sector field degrees	Beam radius cm	Maximal acceleration voltage kV	Typical ion currents A	Remarks	Still in use	Refs.
Denmark								
Copenhagen	1941	45	18	60	10^{-6} — 10^{-4}		No	[4]
Copenhagen	1943	90	80	70	10^{-6} — 10^{-4}		Yes	[8,9,10,11]
England								
Cambridge	1934	—	—	0.8	2.5×10^{-6}	velocity selector	No	[1]
Cambridge	1934	—	—	10	5×10^{-6}	velocity selector	No	[1]
Cambridge	1938	—	—	10	40×10^{-6}	velocity selector	Yes	[12]
Harwell	1948	180	15			light elements separated	No	[13,14]
Harwell	1955	60	61			preceding instrument rebuilt	No	[14]
Harwell	1950	180	61	30	10^{-1}	calutron type	Yes	[13,14,15,16,17,18]
Harwell	1955	90	122	40	10^{-3}	"Hermes"	Yes	[19,20,21,22]
France								
Saclay	1952	60	50	35	10^{-3}	originally at Fort Chatillon	Yes	[23,24,25,26]
Germany								
Marburg	1937	90	100	10	10^{-6} — 10^{-4}	originally in Berlin	Yes	[27,28]
Bonn	1955	—	—	0.1	10^{-5}	electric mass filter	Yes	[29,30]
Berlin	1957	180	50	40	5×10^{-2}		Yes	[31]
Dresden	1957	60	60	35		starting operation autumn 1957		[32,33,34]
Holland								
Amsterdam	1951	180	100	30	10^{-2}		Yes	[35,6]
Italy								
Rome								[36]
Japan								
Osaka	1956	—	50	20	10^{-3}	Smythe type magnetic lens, cf. ref. [2])	Yes	[37]
Russia								
Moscow		180			10^{-1}	calutron type	Yes	
Sweden								
Stockholm	1948	90	160	60	10^{-6} — 10^{-4}		Yes	[5,38,10,39]
Uppsala	1953	90	100	70	10^{-6} — 10^{-4}		Yes	[40,10,41]
Göteborg	1953	90	100	50	10^{-6} — 10^{-4}		Yes	[42]
U.S.A.								
Pasadena	1934	—	20	4	10^{-4}	similar instrument at Franklin Inst.	No	[2,43,44,45]
Minneapolis	1939	180	18	1	10^{-9}	uranium separation	No	[46]
Schenectady	1939	180	12.5		6×10^{-8}	uranium separation	No	[47,48]
Ithaca	1941	—	—	—	small	modulation separator	No	[49]
Ithaca	1941	—	—	—	10^{-2}	radial magnetic separator	No	[49]
Princeton	1941	—	—	—		isotron	No	[50,51]
					10^{-6}	3 ion sources simultaneously	No	[52]
							No	[53]

Oak Ridge	1943	180	122	35	10^{-1}	time-of-flight	No	[55])
Oak Ridge	1943	180	61	35	10^{-1}	calutrons	Yes	[56,57,58,59,60])
Oak Ridge	1956	180	61			calutrons	Yes	[56,57,58,59])
Oak Ridge	1956	180	61		10^{-3}	improved calutron	Yes	[61])
Oak Ridge	1949	—	—	18	10^{-3}	for radioactive species	Yes	[61])
Yugoslavia						time-of-flight in a magnetic field	No	[62])
Belgrade	1957	60	75	60	10^{-3}		Yes	[63])

COMMENTS TO TABLE 1

The data given here on the instruments are to be considered only as approximate figures giving rough information on the type and size of instrument. Alternations have often been made during the course of years the instruments have been in operation. For this or other reasons the references occasionally give diverging information concerning acceleration voltage. ion currents etc. Since the obtainable ion currents vary from element to element, the figures given here are to be used only for a rough comparison between the different instruments.

Many other versions of isotope separators have been discussed, e.g. by Martelly [64]), Ewald [65,32a]), Heil [66]), Hofmann and Walcher[67]), Slepian [68,69]) and von Ardenne[32a, 32b]).

The list of references is not complete, as many papers dealing with ion sources or other details of the separators or with other special problems such as concerning the separation of certain elements have been omitted.

[8]) J. Koch and B. Bendt-Nielsen, Mat. Fys. Medd. Dan. Vid. Selsk. **21** (1944) no. 8.

[9]) J. Koch, Circ. U.S. nat. Bur. Stand. No. 522 (Washington, 1953).

[10]) J. Koch, Proc. 1955 Harwell Isotope Conf., Chapter 25.

[11]) K. O. Nielsen, Nuclear Instruments (in press).

[12]) E. L. Yates, Proc. Roy Soc. A **168** (1938) 148.

[13]) W. D. Allen, Nature **168** (1951) 451.

[14]) W. D. Allen, R. H. Dawton, M. L. Smith and P. C. Thonemann, Nature **175** (1955) 101.

[15]) J. Cockcroft, Proc. Roy. Soc. A **211** (1952) 165.

[16]) R. H. V. M. Dawton and M. L. Smith, Quart. Rev. Chem. Soc., London **9** (1955) 1.

[17]) M. L. Smith, Proc. 1955 Harwell Isotope Conf., Chap. 7.

[18]) K. E. B. Jay, Atomic Energy Research at Harwell (London, 1955).

[19]) R. H. Dawton, Proc. 1955 Harwell Isotope Conf., Chapter 24.

[20]) M. L. Smith, Proc. 1957 Int. Symp. on Isotope Separation (North Holland Publishing Co., Amsterdam).

[21]) Nuclear Power **2** (1957) 132.

[22]) F. R. Paulsen, Atomics **8** (1957) 178.

[23]) R. Bernas, J. d. Physique **14** (1953) 34.

[24]) R. Bernas, CEA-308 (1955).

[25]) C. H. Cassignol, Proc. 1957 Int. Symp. on Isotope Separation (North Holland Publishing Co., Amsterdam).

[26]) J. L. Sarrouy, CEA-305 (1955).

[27]) W. Walcher, Z. Phys. **108** (1938) 376.

[28]) W. Walcher, Fiat Review of German Science, Nuclear Physics and Cosmic Rays, Part II (Wiesbaden, 1948) p. 94.

[29]) W. Paul und M. Raether, Z. Phys. **140** (1955) 262.

[30]) O. Osberghaus, Proc. 1955 Harwell Isot. Conf., Chap 28.

[31]) F. Bernhard, S. Göring, G. Huhn und E. Wilde, Proc. 1957 Int. Symp. on Isotope Separation (North Holland Publishing Co., Amsterdam).

[32]) M. von Ardenne, Tabellen der Elektronenphysik, Ionenphysik und Übermikroskopie, Bd 1 (Berlin, 1956) p. 605.

[32a]) ibid. p. 472. [32b]) ibid p. 471.

[33]) M. von Ardenne, Atomkernenergie (1956) 121.

[34]) M. von Ardenne, priv. comm.

[35]) J. Kistemaker and C. J. Zilverschoon, Circ. U.S. nat. Bur. Stand. No. 522 (Washington, 1953).

[36]) cf. ref. [41]) p. 348.

[37]) J. Okano, J. Phys. Soc. Japan **12** (1957) 390.

[38]) S. Thulin, Arkiv Fysik **9** (1954) 107.

[39]) T. Alväger and J. Uhler, Arkiv Fysik (in press).

[40]) G. Andersson, Phil. Mag. (7) **45** (1954) 621.

[41]) G. Andersson, Arkiv Fysik **12** (1957) 331.

[42]) O. Almén and A. Lundén, Arkiv Fysik **8** (1954) 2.

[43]) L. H. Rumbaugh, Phys. Rev. **49** (1936) 882.

[44]) W. R. Smythe and A. Hemmendinger, Phys. Rev. **51** (1937) 178.

[45]) A. Hemmendinger and W. R. Smythe, Phys. Rev. **51** (1937) 1052.

[46]) A. O. Nier, E. T. Booth, J. R. Dunning and A. V. Grosse, Phys. Rev. **57** (1940) 546 and 748.

[47]) K. H. Kingdon, H. C. Pollock, E. T. Booth and J. R. Dunning, Phys. Rev. **57** (1940) 749.

[48]) K. H. Kingdon, H. C. Pollock, Phys. Rev. **57** (1940) 1072.

[49]) L. P. Smith, W. E. Parkins and A. T. Forrester, Phys. Rev. **72** (1947) 989.

[50]) H. D. Smyth, Atomic Energy for Military Purposes (1945).

[51]) R. R. Wilson, AECD-3373, UCRL-833 (1952).

[52]) H. Lu, Thesis, (University of Minnesota, 1941).

[53]) R. H. Bernas and A. O. C. Nier, Rev. Sci. Instr. **19** (1948) 895.

[54]) W. Whaling and J. E. Evans, Phys. Rev. **73** (1948) 648.

[55]) M. C. Michel and D. H. Templeton, Phys. Rev. **93** (1954) 1422.

[56]) C. P. Keim, Annual Review of Nuclear Science **1** (1952) 263.

[57]) C. P. Keim, J. Appl. Phys. **24** (1953) 1255.

[58]) C. P. Keim, Nature **175** (1955) 98.

[59]) C. E. Normand, Proc. 1955 Harwell Isotope Conf., Chapter 23.

[60]) C. E. Normand, L. O. Love, W. A. Bell and W. K. Prater, Proc. 1955 Harwell Isotope Conf., Chapter 1.

[61]) R. S. Livingston, Proc. 1957 Int. Symp. on Isotope Separation (North Holland Publishing Co., Amsterdam).

[62]) R. S. Livingston, J. A. Martin and R. L. Murray, AECD-3997 (1951).

[63]) I. Ševarac *et al.*, to be published.

[64]) J. Martelly, C. R. Acad. Sc. Paris **215** (1942) 106.

[65]) H. Ewald, unpublished see refs. [3]) and [28]).

[66]) H. Heil, Z. Phys. **128** (1950) 36.

[67]) R. Hofmann und W. Walcher, Z. Phys. **141** (1955) 237.

[68]) J. Slepian, Proc. Nat. Acad. Sci. **41** (1955) 451.

[69]) J. Slepian, J. Appl. Phys. **26** (1955) 1283.

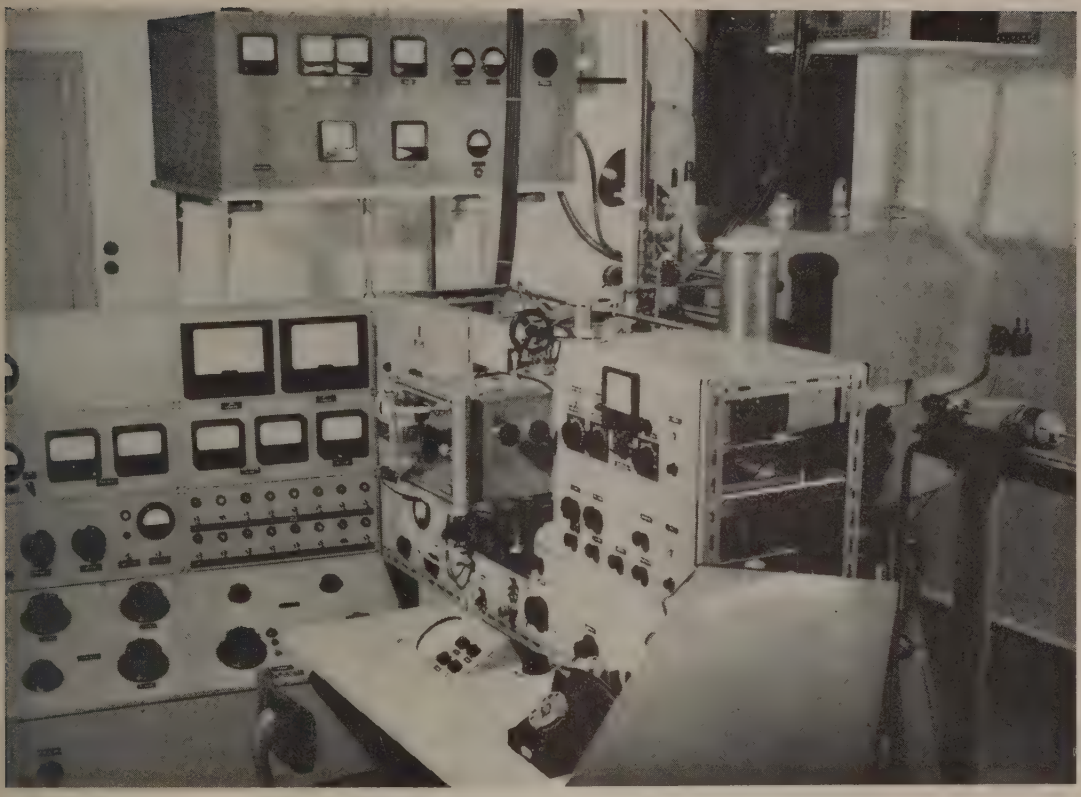

Fig. 2. View of the isotope separator.

The mass dispersion is increased if the image is moved to a distance l from the exit boundary of the magnet. The focusing conditions require that the beam entering the magnetic field is slightly divergent. With perpendicular entrance and exit of the central beam we have (cf. e.g. ref. [3]).

$$D = \frac{r}{2} \cdot \frac{\Delta M}{M} \left(1 + \frac{l}{r}\right). \tag{3}$$

The line width B also depends on l, and the condition for obtaining a higher resolving power is that B increases less than by a factor $(1 + l/r)$. Experiments in Copenhagen[8]) and Stockholm[38]) have shown that B does not change appreciably when the image is moved out to a distance $l = r$ from the magnet. In our present arrangement the collector is thus placed at $l = r = 100$ cm†.

The total line width during a separation depends on several parameters (cf. [38]). E.g., fluctuations of high tension, V_h, and magnet current, I, give the following contributions

$$b_{V_h} = \frac{r}{2} \cdot \frac{\Delta V_h}{V_h} \cdot \left(1 + \frac{l}{r}\right) \tag{4a}$$

$$b_I = r \cdot \frac{\Delta I}{I} \left(1 + \frac{l}{r}\right). \tag{4b}$$

We see that in our case the line width increase is 1 mm by a fluctuation of 1 part in 1 000 for the acceleration voltage or 1 part in 2 000 for the magnet current. This emphasizes the importance of having a good stabilization of both these parameters; see sections 5, 6 and 7.

The general lay-out of the separator is shown

† Our first separations were made with the target close to the magnet. The next arrangement was to move the target to $l = 40$ cm from the magnet, in which position some of the separations listed in table 2 were made.

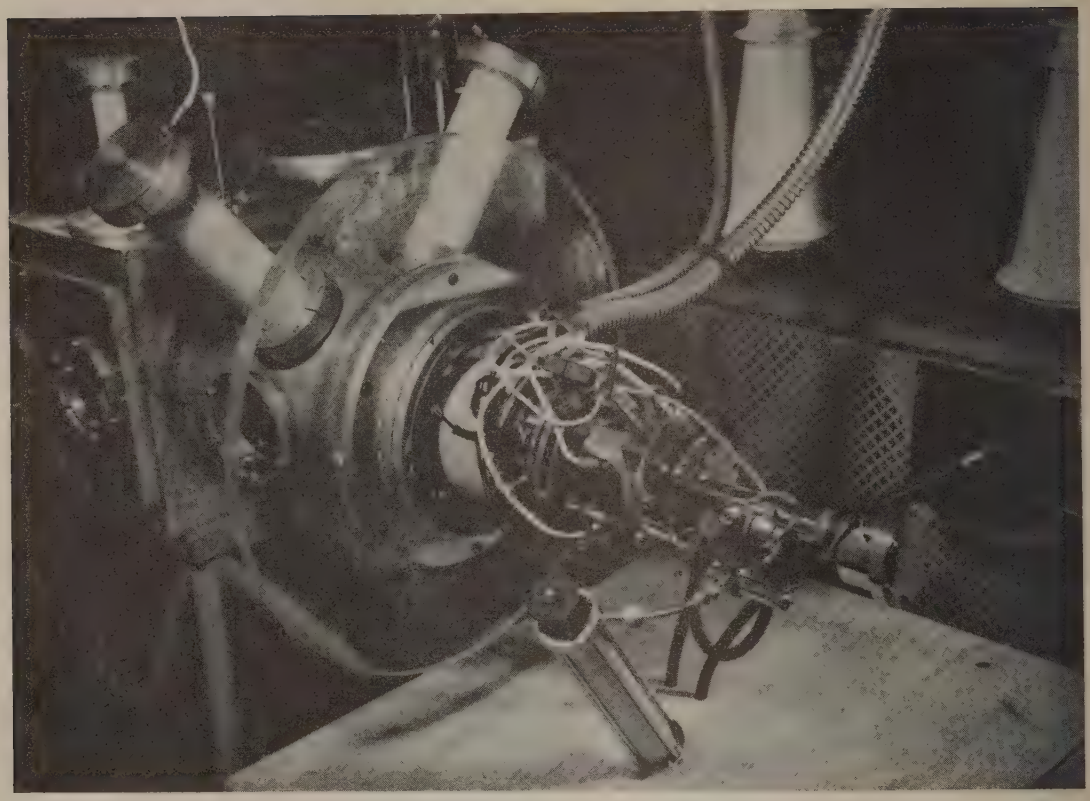

Fig. 3. View of the ion source end of the separator.

in fig. 1, and figs. 2 and 3 show the instrument in its present state.

3. Vacuum System

The main parts of the vacuum system are (see fig. 1):

(1) deflection chamber with a mean radius of 100 cm;

(2, 3) vacuum valves, one for each of the two oil diffusion pumps. The larger pump (1500 l/s at 10^{-4} mm Hg) is near the ion source and the smaller one (500 l/s) is on the collector side;

(4) acceleration chamber; a cylinder made of iron for shielding the acceleration system from the stray field of the deflecting magnet;

(5) ion source with vacuum lock used for charging the oven without breaking the main vacuum;

(6) extension chamber;

(7) collector chamber with vacuum lock for changing collector plates.

One backing pump (pumping speed 1.4 l/s) is in common for both oil diffusion pumps. A small backing pump is used alternatively for the two locks mentioned above. Between the valves (2, 3) and the oil diffusion pumps there are baffles cooled by freon to a temperature of about —25°C. Two liquid air traps are used to reduce the pressure of condensable vapours. One is placed near the ion source and one near the collector.

The total volume of the vacuum system is about 140 l and a vacuum better than 10^{-5} mm Hg can be maintained when the ion source is operated with a gas. The pressure is measured with Pirani, Penning and ionization gauges.

4. Ion Source and its Power Supply

Two types of magnetic ion sources have been used.

(a) In the first ion source the ionization of neutral atoms is caused by electrons oscillating in a direction perpendicular to the extracted ion beam[71]). This ion source has a closed discharge chamber made of pyrophyllite with an outlet plate of stainless steel. The anode and the reflectors at cathode potential inside the chamber are made of thin sheets of tantalum. The whole discharge chamber is heated by the filament. This ion source was built for the separation of gases and solid substances requiring temperatures up to 800°C in the discharge chamber.

Gases are admitted through a needle valve and solids are vapourized from a small oven of pyrophyllite. Normal operating conditions of the ion source are:

arc voltage	80–100 V
arc current	0.2–0.5 A
magnetic field	100–200 gauss.

This ion source was used for the separation of many substances, e.g. Ne, Mg, Zn, As, Hg (see table 2). Furthermore, the ion source has been used with minor modifications for sputtering experiments on Mo[72]) and for production of ions by electron bombardment of high melting solids (Pd)[71]).

A few measurements of the total efficiency of the isotope separator have been made using this ion source. For noble gases and radioactive mercury we have found efficiencies of 1–5 per cent.

(b) The second ion source was built at the Institute for Theoretical Physics in Copenhagen†. Here the ionization is caused by electrons oscillating in a direction parallel to that of the extracted ion beam [71,73]). Measurements on this type of ion source have been made at the isotope separator in Copenhagen[74]).

Two different types of discharge chambers are used with this ion source: the original one which can be used for temperatures up to about 800°C, and a discharge chamber made of graphite with insulators of pyrophyllite for temperatures up to about 1 000°C. This discharge chamber is shown in fig. 4. It is heated by the filament (1) and by an additional heating element (2) surrounding the anode cylinder (3). The heater is insulated by tubings of either

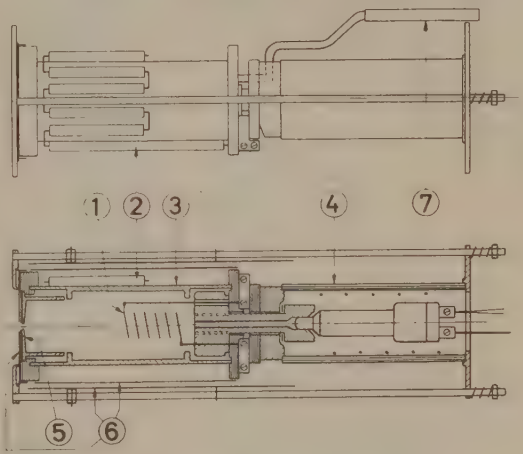

Fig. 4. Discharge chamber built for high temperatures. 1. filament; 2. heating elements surrounding the anode; 3. anode cylinder; 4. oven heater; 5. outlet plate; 6. radiation shields; 7. gas inlet.

degussit or quartz. To enable high temperatures, radiation shields (6) of molybdenum enclose the discharge chamber.

Typical operating conditions are:

arc voltage	100–150 V
arc current	20–200 mA
magnetic field	100 gauss.

This discharge chamber has been used for the separation of the rare earth metals Ce, Er and Yb.

The power units for the source are enclosed in a box standing on four porcelain insulators and connected to high tension (see fig. 5).

† We acknowledge the help of Dr. K. O. Nielsen in this matter.

[71]) O. Almén and K. O. Nielsen, Proc. 1955 Harwell Isotope Conf., Chapter 3.

[72]) cf. J. Druaux and R. Bernas, Proc. 1955 Harwell Isotope Conf., Chapter 4.

[73]) K. O. Nielsen, Nuclear Instruments 1 (1957) 289.

[74]) O. Almén and K. O. Nielsen, Nuclear Instruments 1 (1957) 302.

Power is supplied to the various units in the box by means of four insulating transformers:

(1) arc voltage and magnetic field, maximum 800 W;

(2) filament heating, 800 W

(3) oven heating, 400 W;

(4) heating of the anode cylinder, 800 W.

The currents to the filament and to the anode heater are rectified (R_3 and R_4) with a ripple

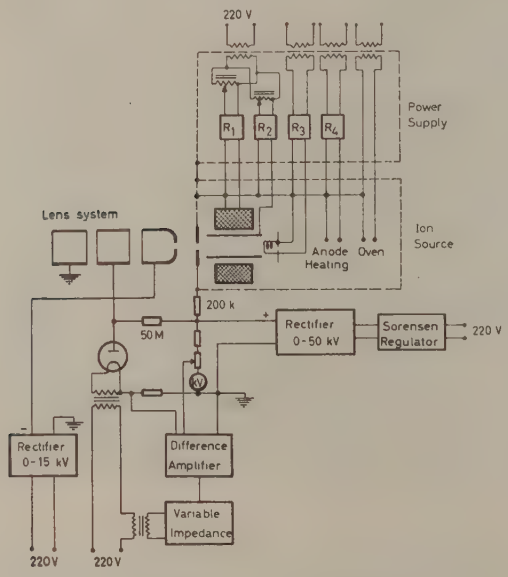

Fig. 5. Circuit diagram showing high tension and ion source supplies.

less than 2 per cent. The magnet current and the arc current are also thoroughly rectified (R_1 and R_2).

The rectification of all these currents is a necessary condition for having a high resolving power[74]).

The power dissipated in the discharge chamber and oven requires an efficient cooling of the outer parts of the ion source. Particularly the vacuum gaskets and the perspex insulator cannot stand high temperatures. Transformer oil is circulated through a copper tubing soldered on the outside of the ion source. The oil is cooled by water in a heat exchanger placed on ground potential together with the circulating pump. To increase cooling, air is blown round the ion source.

5. Acceleration and Electrostatic Focusing

The acceleration of ions is performed by an electrostatic lens system which consists of three cylindrical electrodes made of stainless steel (see fig. 6). The diameter of these cylinders is 70 mm, and their lengths are 80, 70 and 95 mm, respectively. All three cylinders are insulated, the first for about 20 kV, the second for 50 kV and the third for a few hundred volts. The insulators are made of mycalex at the first cylinder and of perspex at the other two. The whole lens system is assembled as one unit which can be moved from outside in three perpendicular directions.

By this arrangement the axis of the lens system and the ion source can easily be adjusted to coincide. Furthermore, the distance between the ion source and the first electrode (10–60 mm) can be varied continously from the control desk during operation.

The acceleration voltage V_h, maximum 50 kV, is fed to the ion source, which is insulated by a circular disc of perspex. The first cylinder of the lens system is at a negative potential, V_n, of 0–15 kV. The second cylinder is at a potential $V_l = \alpha V_h$, called the lens potential. V_l is adjusted to give the best focusing conditions at the collector, corresponding to $\alpha \approx 0.6$. The third cylinder is grounded.

The high tension is produced by a full-wave rectifier. A filter reduces the ripple to about 0.02 per cent. A resistor of 200 kΩ limits breakdown-currents. The rectifier is fed from a Sorensen voltage stabilizer with a regulation accuracy of $\pm$ 0.1 per cent. The lens potential is tapped off from the high tension by means of a 50 MΩ resistor and a diode. This potential is adjusted by varying the heating current (about 5 A) to the filament of the diode, which is done by means of a variable impedance in series with the primary winding of the filament transformer (fig. 5).

Three pairs of plates follow the lens system. Pairs no 1 and 3 are connected in parallel

(see fig. 7) and fed from two ganged potentiometers supplied by a rectifier giving + 150 and — 150 volts to ground. With this arrangement the beam can be deflected in a vertical direction and thus adjusted to strike the collector at a suitable position. Pair no 2 is fed with a positive potential of 0–15 kV, so that the three pairs of plates together form a positive lens, which compresses the beam in a direction parallel to the magnetic field. In this way it is possible to reduce the beam height at the collector to about 10 mm.

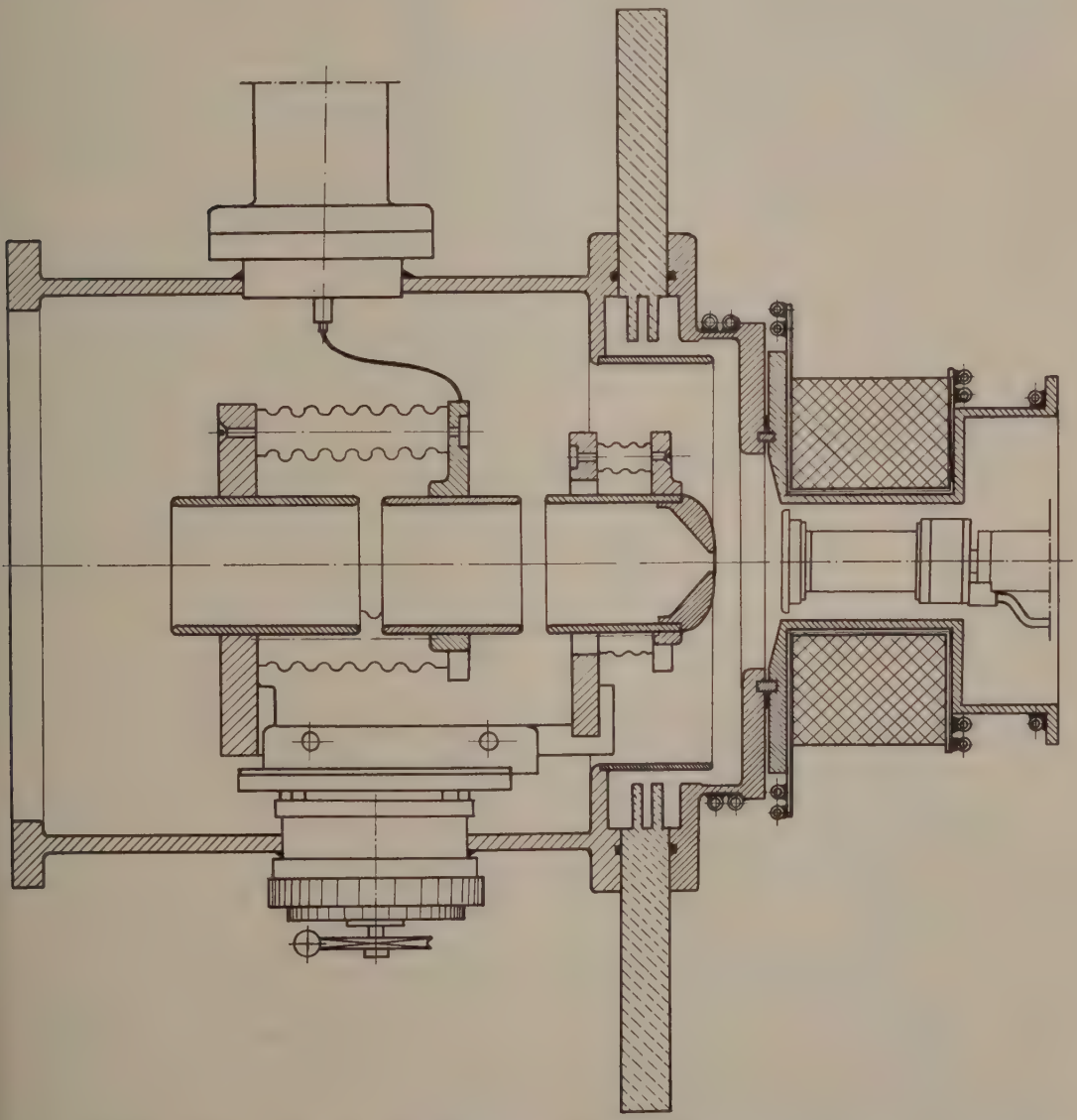

Fig. 6. Acceleration system. From right to left: part of the ion source (magnet coil and discharge chamber), first electrode at a negative potential V_n, second electrode at lens potential V_l, and third electrode at ground. A perspex plate insulates the ion source from the acceleration chamber. The device for adjusting the position of the lens system is shown in the floor of the acceleration chamber. Grounded caps (not shown) shield the insulators from ion bombardment.

It might be of interest to mention that in the beginning we had a lens system with four cylindrical electrodes (cf. refs. [5]) and [41])).

The current extracted from the ion source is determined by two groups of parameters, (a) operating parameters of the ion source (b) parameters of the acceleration gap[74]). If the operating conditions of the ion source and the lens potential are adjusted, so that optimal

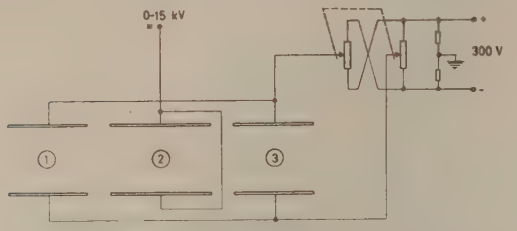

Fig. 7. System of plates for deflection and focussing of the beam.

focusing is obtained, the ion current from the source, I_1, (measured at the collector) is given by the expression,

$$I_1 = C \cdot \frac{A_0 \cdot V^{3/2}}{d^2 M^{1/2}} \qquad (5)$$

where

A_0 = outlet area of the ion source in cm²,
d = distance in cm between ion source and first electrode of the lens system,
V = extraction potential in volts—in our case the sum of V_h and V_n,
M = mass number (single charged ions),
C = a constant depending on the shape of the outlet plate and the first electrode. For plane geometry we find, for I_1 in μA, $C \approx 0.5 \times 10^{-2}$, in agreement with Almén and Nielsen[74]).

With $V = 50$ kV, $A_0 = 6$ mm² and $M = 100$ the ion currents given by eq. (5) vary from 10 to 300 μA, when d is altered from 60 to 10 mm. However, for short distances, $d = 10$–20 mm, current losses in lens system and analyzing magnet cannot be neglected, and the current to the collector is somewhat smaller than I_1.

The resolving power, P, (at optimal focusing) also depends on d, e.i. P increases when d is increased[74]). Since d can be varied during operation, it is possible to make a compromise between the requirements of ion current and resolving power.

Fig. 8 shows the influence of V_n on I_1 and P.

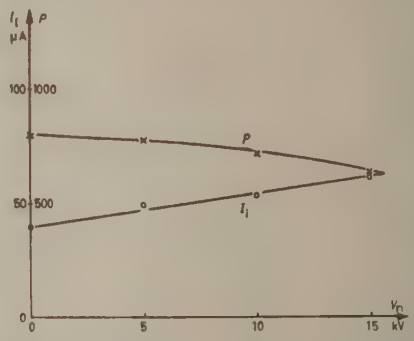

Fig. 8. Ion current I_1 and resolving power P (eq. (2)) for Kr *vs.* negative potential on first electrode of the lens system. $V_h = 50$ kV, $d = 30$ mm, $A_0 = 6$ mm².

I_1 increases with V_n according to eq. (5), which indicates a method to increase I_1 above the value given by V_h alone (in our case max. 50 kV). P decreases slightly, since an increase in I_1 at constant V_h means a greater space charge repulsion.

When a chemical compound is used as charge material in the ion source, several groups of ions normally appear. Hence, the ion current of the desired mass numbers can be much smaller than calculated from eq. (5). E.g. when charging with $CeCl_3$ the current of Ce-ions was only about 10 μA ($d = 30$ mm).

6. Magnet and Stabilization of the Magnetic field

The deflecting magnet has a mean radius of curvature of 100 cm, a pole gap of 6 cm and a pole width of 16 cm. The iron is of the quality Sgj 10 and its total weight is nearly 3 500 kg. A magnetic field of 5 500 gauss is obtained with a current of 100 A in the ten double-layer coils which are connected in series†. There are

† The magnet coils were wound at Elektriska AB Morén (now ASEA), Partille, by courtesy of civ.-ing. S. Lagerkvist to whom we express our gratitude.

496 turns of winding altogether. The coils are separated by copper plates which are cooled with water, flowing in a tubing along the outer edges of the plates. The DC current is supplied by a motor-generator (50 V at 100 A) placed in another room, but remote-controlled from the control desk of the separator. The motor is a 3 phase asynchronous motor of 7.5 kW.

It has already been pointed out that the magnetic field has to be stabilized to prevent the mass lines to drift at the target. The usual arrangement is to stabilize the current from the DC generator by balancing the voltage drop over a resistance against the EMF of a normal element. However, we decided to try a system where a small coil rotates in the field to be stabilized, and where the output EMF from this coil regulates the current through the field-winding of the DC generator.

The stabilization system consists of one coil S_1 (see fig. 9) rotating in the stray-field of the separator magnet and another coil S_2 rotating in the field of a permanent magnet. The two coils are identical and placed on a common shaft, which is driven by a synchronous motor at 1 500 r/m. The outputs from the two coils are rectified mechanically. The coil windings and the field strength of the permanent magnet are designed to give maximum 30 volts DC. The permanent reference field is placed at some distance from the separator magnet, in order to reduce the influence of the stray-field on the reference field.

The output voltage e_1 from S_1 and a suitable fraction e_2 of the output from S_2 are fed to a difference amplifier. e_2 is adjusted by means of a "Helipot" precision potentiometer. From this amplifier the signal is fed to a power amplifier, which supplies the current to the excitation coil of the DC generator. The action of the whole stabilization circuit is to reduce the difference between e_1 and e_2 to a small error signal, which means that the magnetic field will be held at a constant value determined by e_2. By changing the "Helipot" setting, the field can be varied continously.

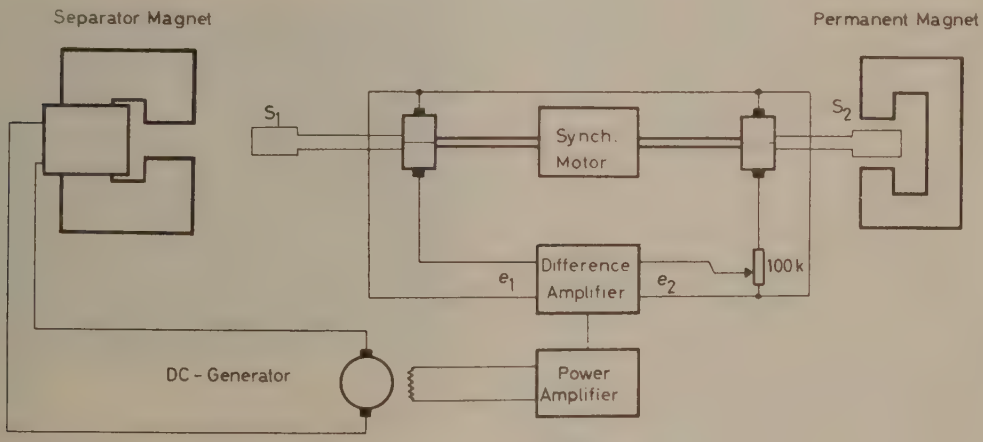

Fig. 9. Block diagram of the magnet stabilization.

The difference amplifier has two stages with 6SL7-tubes specially selected to get equal μ's and g_m's in the two sections of the tubes. Wire wound resistors and high precision carbon resistors of sufficient ratings are used to prevent variations caused by self-heating. The power amplifier consists of six 807-pentodes connected in parallel.

With this arrangement the stability of the magnetic field is about 1 : 5 000. Another version of this principle of stabilizing has been used by van der Walt[75]).

[75]) N. T. van der Walt, Rev. Sci. Instr. 24 (1953) 413.

7. Final Stabilization of the Mass Spectrum

The stabilization described above of the high tension and of the magnetic field is insufficient when a high resolving power is desired. A very sensitive arrangement was obtained by applying

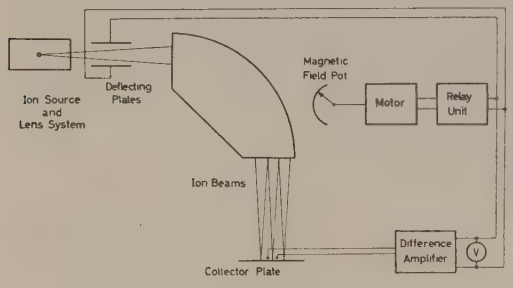

Fig. 10. Principle of beam position stabilization.

a system stabilizing the position of the beam[6, 11, 38, 41]).

One mass number is chosen as a reference beam which passes between two sniffers mounted at the collector. The distance between the two sniffers as well as their position can be changed from outside during operation. When the beam position deviates, the currents to the sniffers are slightly different. The difference is amplified and fed to two deflecting plates in such a way that the position of the beam is nearly restored at the target (see fig. 10). With this arrangement instabilities in both high tension and magnetic field are counteracted.

In principle the deflecting plates can be used to compensate large errors in beam position. However, this gives a defocusing effect when the beam enters the magnetic field at an oblique angle. Therefore, we constructed an arrangement for adjusting the magnetic field automatically. If the potential difference between the deflecting plates rises above a preset value, an on–off system changes the setting of the Helipot potentiometer in the magnetic field stabilization system (see section 6). Thanks to this arrangement only short periods of manual control of the separator were required during 10-hour collections of the rare isotopes A^{36} and Ne^{21} (natural abundance 0.35 and 0.30 per cent).

8. Safety precautions

The high tension parts of the separator are closed off from the rest of the room by chains resting on micro-switches, which are connected in the primary circuit of the high tension supply. In the same circuit there are relays which prevent overloading of the high tension unit at breakdown. When the high tension supply is switched off, a relay automatically discharges the high tension condensors (4 μF) through a one Mohm resistor. Otherwise the time of discharging would be several minutes. To prevent breakdown caused by bad vacuum a relay switches off the high tension, when the pressure in the vacuum chamber exceeds a certain value.

There are relays checking the circulation of water to the cooling system of the magnet and to the oil diffusion pumps. In the system for cooling the ion source the circulation of both oil and water is checked by relays.

9. Collector Arrangements

The collector chamber is shown schematically in fig. 11. A vacuum lock (1) makes it possible to replace the collector without breaking the main vacuum of the separator.

The isotopes are usually collected on foils of Cu, Al or Ag[5]), depending on the further use of

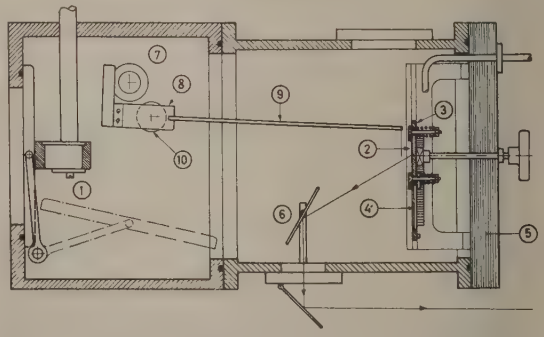

Fig. 11. Collector chamber with vacuum lock and mechanical scanner.

the targets (direct deposition method). The collector plates (2) are mounted on a water-cooled backing (3), which can be moved from outside in a vertical direction. The lower part of this backing consists of a glass plate (4),

which is used as a fluorescent screen[4]). It is covered with a thin wire gauze in order to prevent the beam from being disturbed by charges on the screen. The whole collector is mounted on a perspex plate (5), thus permitting the total ion current to the collector to be measured. By means of two adjustable mirrors (6) the fluorescence from the collector plate can be observed during operation.

A mechanical scanner (7) is used for checking the resolving power of the isotope separator during operation[76]). Its main parts are a leaf

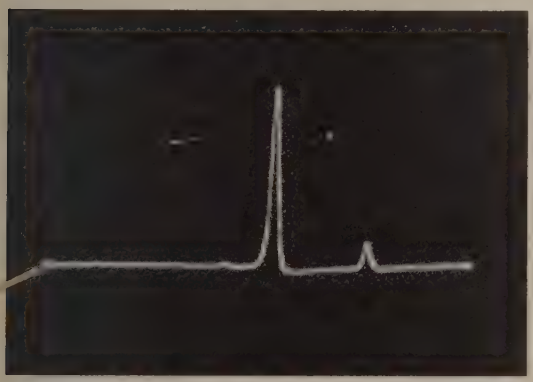

Fig. 12. Ce mass spectrum. Photo of the oscillograph screen. (Mass number 139 does not belong to Ce.)

spring (8), to which a tubing of stainless steel (9) is soldered, with a thin needle at the end, and a magnetic circuit with a winding (10). The leaf spring (and the tubing) oscillates at its fundamental frequency (about 17 c/s), which is picked up by means of a crystal of barium titanate. The signal is amplified and fed to the winding (10). The mechanical amplitude of the scanner can be varied between 20 and 90 mm.

The beam current striking the oscillating needle is amplified and fed to the vertically deflecting plates of an oscillograph. The horizontally deflecting plates are connected to the output of the amplifier driving the scanner. Thus the picture on the screen shows the mass spectrum (see fig. 12).

The mechanical scanner can be moved horizontally from outside, thus allowing different parts of the mass spectrum to be scanned. The depth of the needle can also be adjusted so that a suitable part of the line height is picked up.

When beginning a separation, the ion source and the lens potential are adjusted until the mass spectrum seen on the oscillograph has a suitable shape. At the same time the height and position of the lines are checked on the fluorescent screen. After that the collector is moved into position and the collection is commenced.

10. Separations

Table 2 gives examples of the stable and radioactive isotopes separated in Gothenburg. The references give the particular experiments in which the isotopes have been used.

Table 2

Element	Mass number of isotope		Applications	Ref.
	stable	radioactive		
Nitrogen	14		n	
Oxygen	16		n	
	18		n	[77])
Neon	20		n	[78])
	21		n	
Magnesium	24		n	[78])
	25		n	[78])
Silicon	28		n	
Sulphur	32		n	
Argon	36		n	
Zinc	all		i	
Krypton	all	85	i, c	
Molybdenum	all		i	
Palladium	all		i	
Cerium		141	s	
Tungsten	all		i	
Mercury		203	s	[79,80,81])

c ion collection studies
i ion source studies
n nuclear reaction studies
s nuclear spectrometer studies.

[76]) K. O. Nielsen and O. Skilbreid, Nuclear Instruments 1 (1957) 159.

[77]) K. Ahnlund, Arkiv Fysik 10 (1956) 425.

[78]) S. E. Arnell, J. Dubois and O. Almén, Nuclear Physics, in press.

[79]) C. Nordling, K. Siegbahn, E. Sokolowksi and A. H. Wapstra, Nuclear Physics 1 (1956) 326.

[80]) G. J. Nijgh, Thesis (Amsterdam, 1955).

[81]) G. J. Nijgh, A. H. Wapstra, L. Th. M. Ornstein, N. Salomons-Grobben, J. R. Huizenga and O. Almén to be published.

11. Acknowledgements

This work was financially supported by Svenska atomkommittén and Chalmerska forskningsfonden, which we acknowledge with gratitude. We are much indebted to Professor Nils Ryde for the confidence he has shown us by placing working facilities at our disposal. We owe our warmest thanks to the members of the staff of the Institute who have contributed in various ways to this project. Among these, special mention is to be given to Mr. Henning Liljeqvist for his skilful work. During the first years the advice given by Dr. Ingmar Bergström and Dr. Sigvard Thulin of the Nobel Institute of Physics, Stockholm, was of specially great value for this project. We have always derived much inspiration from the extreme good spirit of cooperation that joins the staffs of the four Scandinavian isotope separators. It is thus a great pleasure to thank the present and former members of these groups for discussions and exchange of ideas and experience.

This work was started in 1949 by one of us (A.L.), who went over to other work in 1952. The next member of our group (O.A.) joined the work in 1951 and the third (G.B.) for a period in 1954–55 and definitely from 1956. The first separation was performed in 1953.

NUCLEAR INSTRUMENTS 2 (1958) 261–269; NORTH-HOLLAND PUBLISHING CO. – AMSTERDAM

ON THE PULSE SHAPE IN A CYLINDRICAL IONIZATION CHAMBER

C. CERNIGOI, G. PAULI and C. POIANI

Instituto di Fisica dell'Università, Trieste, Italy

Istituto Nazionale di Fisica Nucleare, Gruppo di Trieste

Received 23 November 1957

A fast ionization chamber, 60 l in volume, filled with argon at 10 atm, is described. The pulse shapes are calculated assuming the ionization: (a) confined to an infinitesimal volume of the chamber, (b) distributed along a straight line parallel to the axis of the chamber, (c) distributed along a straight line passing through the axis of the chamber and perpendicular to it, (d) distributed along a straight line perpendicular to the axis of the chamber and not passing through it, (e) distributed throughout the volume of the chamber.

A comparison is made between the theoretical pulse shapes and the experimental ones.

1. Introduction

It is well known that the pulse of an ionization chamber is characterized both by its height and shape. From height measurements it is possible to establish the energy dissipated by the ionizing particles in the sensitive volume of the chamber, whereas useful information about the ionization distributions can be obtained by inspection of the pulse shapes[1]). In this connection, it has to be emphasized that if the pulse shapes corresponding to various kinds of ionization events are theoretically known, the ionization chamber is made into a detector capable of separating the recorded events.

With this aim in view, we have undertaken an analitycal study of the pulse shape (sect. 3) with reference to the ionization chamber described in sect. 2. The pulse shapes have been derived for some kind of events particularly simple. The calculations have been carried out assuming the relation

$$v_- = \text{const.} \cdot E^{1/2}$$

between the electron drift velocity, v_-, and the electric field, E, and neglecting diffusion, recombination and attachment processes be-cause they can be experimentally shown to be negligible.

[1]) H. S. Bridge, W. E. Hazen, B. Rossi and R. W. Williams, Phys. Rev. 74 (1948) 1083.

The comparison between the theoretical results and the experimental ones is fairly satisfactory.

2. The ionization chamber

2.1. DESIGN OF THE CHAMBER

The ionization chamber used in the present investigation is of cylindrical type. Its design is schematically shown in fig. 1. The external electrode consists of a cylindrical copper tube 27 cm in diameter, 1 m length and with 0.2 mm thickness. The collecting electrode is a steel wire, 2.5 mm in diameter, stretched along the axis of the outer electrode. The electrodes are contained into an iron vessel of cylindrical shape, with 1 cm walls. The outer electrode is supported by the iron vessel through small cylinders of ceramics, which ensure electrical insulation, and is connected to a high-voltage source by means of a steel wire, supported by one of the vessel covers through a glass-to-kovar seal. The inner electrode is supported by the vessel covers through a porcelain insulator by one side and through a glass-to-kover seal by the other side.

At the vessel wall is fixed a brass box containing a perspex rod which bears a polonium source used for the calibration of the chamber. The rod can be displaced along the direction of the vessel radius so that the radioactive source

can be either placed in different positions between the electrodes or extracted from the sensitive volume of the chamber.

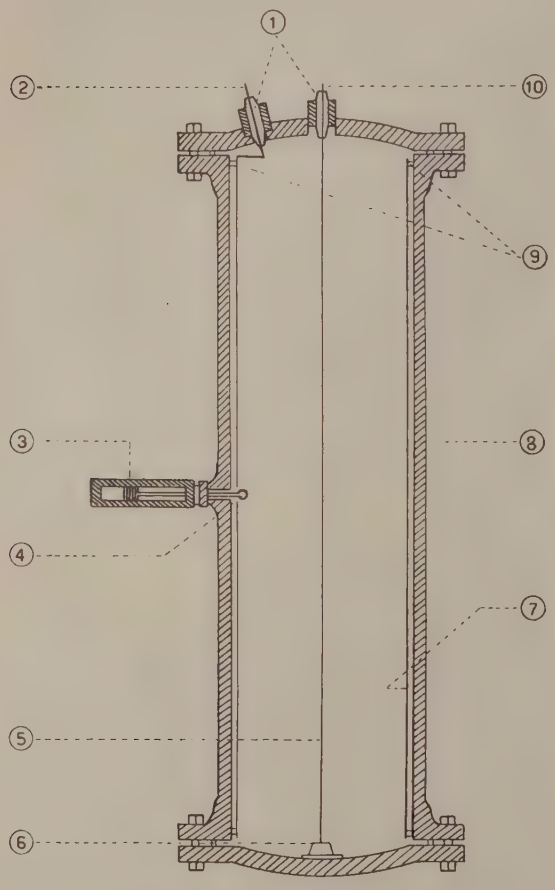

Fig. 1. The ionization chamber. (1) Glass-to-kovar seals. (2) To the high voltage generator. (3) Brass box. (4) Polonium source. (5) Collecting electrode. (6) Porcelain insulator. (7) Outer electrode. (8) Iron vessel. (9) Ceramics insulator. (10) To the electronic amplifier.

2.2. GAS FILLING AND PURIFICATION

The chamber is filled with commercial argon at a pressure of 10 atm. The argon is purified from the oxygen by means of a purifier[2]) which consists of an iron tube containing a copper strap, stretched along its axis, which can be heated electrically up to a temperature at which oxidisation of the copper takes place. The purifier is connected to the chamber through two copper pipes and the gas is allowed to circulate through it by convection.

2.3. OPERATION OF THE CHAMBER

The outer electrode is kept at a fixed negative voltage of 3 500 volts and the inner electrode, connected to the input of the electronic amplifier, at a fixed positive voltage of 280 volts. It follows that the total d–c voltage across the chamber is 3 780 volts. This potential difference is sufficient to ensure saturation and gives no undesirable phenomena like corona and breakdown. The capacity to ground of the outer electrode is 680 pF and that of the inner electrode, disconnected from the amplifier is 20 pF. The insulation of the inner electrode is larger than 10^9 ohms.

The values of the ratio E/p, between the electric field and the pressure, versus the distance r from the axis of the chamber, are plotted in fig. 2. Since the ratio E/p lies practically between 10^{-1} and 10^{-2} volt/cm·mmHg, the electron drift velocity can be safely described according to the following empirical law[3])

$$v_- = k_- (E/p)^{1/3}, \qquad (2.1)$$

where the constant k_- depends on the gas.

According to available experimental data[4]), the electron drift velocity in argon has a value of the order of 10^5 cm/sec, if the condition $E/p < 10^{-1}$ volt/cm·mmHg is verified. Hence, the value of the constant k_- in eq. (2.1) comes out to be of the order of 10^6.

The drift velocity of the positive ions A_+ in argon, v_+, is related to the ratio E/p by the equation

$$v_+ = K_+ (760) (E/p),$$

where K_+ is a constant of the order of some units[3]). In our case, v_+ is easily seen to have a value of the order of 10^2 cm/sec, and therefore it is

$$v_- = 1\,000 \times v_+ . \qquad (2.2)$$

[2]) C. Cernigoi and G. Poiani, Nuovo Cimento **X** 2, (1955) 677.

[3]) D. H. Wilkinson, Ionization chamber and counters (Cambridge, 1950).

[4]) See ref. [3]); B. B. Rossi and H. H. Staub, Ionization chambers and counters, (Mc-Graw, 1949); T. E. Bortner, G. S. Hurst and W. G. Stone, Rev. Sci. Instr. 28 (1947) 103.

Eq. (2.1) gives for the electron collection time, t_1, a value of the order of 10^{-5} sec. Then, eq. (2.2) suggests the collection time of the positive ions A_+, t_2, to be a thousand times longer, i.e., of the order of 10^{-2} sec,

$$t_2 = 1\,000 \times t_1 \,.$$

The time constant RC of the collecting wire has been taken of the order of 10^{-4} sec, so that the condition

$$t_1 \ll RC \ll t_2$$

is satisfied and the chamber may be considered to behave as a "fast chamber".

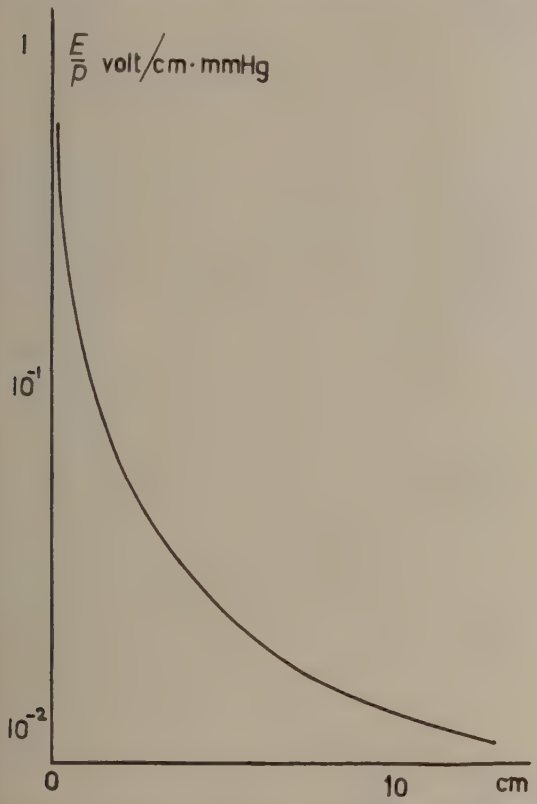

Fig. 2. Ratio E/p between the electric field and the pressure *vs.* the distance r from the axis of the chamber.

2.4. CALIBRATION

The calibration of the chamber is performed using a conventional 5.3 MeV α-particle source. The range of the α-particles in argon at 10 atm is about 0.5 cm and therefore very small compared with the radius of the chamber. It follows that the α-particles are brought to rest in the gas and dissipate their whole energy in the sensitive volume of the chamber. The integral pulse height distribution obtained with an amplification of 1.5×10^5—the electronic amplifier is of the Bell-Jordan type—is shown in fig. 3. Its end point is at 38 volts, which is the pulse height corresponding, under the considered amplification conditions, to an energy of 5.3 MeV dissipated into the chamber by the recorded particle.

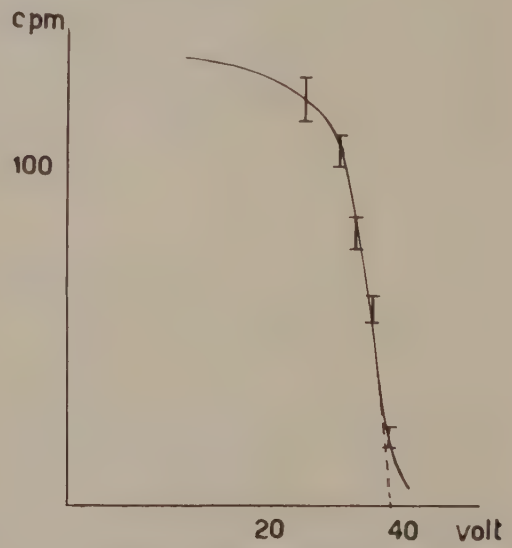

Fig. 3. Pulse height distribution of the particles.

No appreciable change has been observed in the integral pulse height distribution by reducing the gas pressure from 10 to 6 atm. This indicates that the processes of electron diffusion, recombination and attachment are negligible.

3. The Mechanism of the Pulse Formation; the Pulse Shape

3.1. THE PULSE FORMATION

Let us suppose that somewhere in the sensitive volume of the chamber an ion pair is formed at the time $t = 0$. Under the influence of the electric field, the electron and the positive ion drift towards the oppositely charged electrodes. The electron is collected at the time t_1

[5]) See ref. [3]).

and the positive ion at the time t_2. The collecting wire has a time constant RC about tenth times longer than t_1, and hence it can be considered as an insulated conductor during the electron collection time. It will suffer, therefore, a potential change because of the induction effects exerted by the two charges, $-e$ and $+e$. In order to determine such a potential variation, we shall make use of the following consequence of the Green's theorem, i.e., the potential imposed to an insulated conductor A by a charge q located at a point P is equal to the potential that is determined in P by the charge q placed on the conductor A. To demonstrate this statement, consider the following two sets of conditions.

Conductor	A	C	A	C
Charge	0	q	q	0
Potential	V	V'	V^*	V'' .

being C a conductor of indefinitely small dimensions situated at P. Green's theorem gives $qV = qV''$ and hence

$$V = V'' . \tag{3.1}$$

Let us suppose, now, that the insulated conductor A is held near a second conductor B, which is kept at a fixed potential V_B, so that V_A is the potential of A in the field set up by B. Moreover, let the charge q, located at the point P, be small compared with the charge placed on the conductor B, so that the presence of q does not alter the charge distributions consistent with the potentials V_A and V_B. Under these conditions, the principle of superposition is applicable to the fields created by the charge q and by the charged conductor B. Eq. (3.1), therefore, gives the value of the change suffered by the potential V_A of A because of the induction effect exerted by q.

On the same footing it has to be treated the situation arising from the formation of an ion pair at a point P in the ionization chamber. According to section 2.3, the fixed positive voltage of the collecting wire, with respect to the voltage of the outer electrode, is $V_B = +3\,780$ volts, if the latter is made equal to zero, $V_A = 0$. From the above mentioned Green's theorem consequence and the formulas for the cylindrical capacitor, one easily finds that the change of the potential V_A caused by the ion pair located at the point P is given by

$$V = \frac{e}{C}\frac{\log(b/r)}{\log(b/a)} - \frac{e}{C}\frac{\log(b/r)}{\log(b/a)} \tag{3.2}$$

where r is the distance of the point P from the axis of the chamber, b and a are the outer and inner radii of the chamber and C is the capacity of the collecting wire. The two terms in the right-hand-side of eq. (3.2) represent the contributions due to the positive ion and to the electron respectively.

The quantity r appearing in eq. (3.2) has to be regarded as a function of the time, because the ions move within the chamber under the influence of the electric field. However, being the ratio t_2/t_1 about 10^3, we may assume that during the electron collection time the positive ion remains practically stationary at the point r_0 where the ion pair has been created at $t = 0$. Under this assumption, eq. (3.2) will be written, for convenience reasons, in the following form

$$V(t) = \frac{e}{C\log(b/a)}\left\{\log\frac{r(t)}{b} - \log\frac{r_0}{b}\right\} \quad (0 \leqslant t \leqslant t_1) . \tag{3.3}$$

The function $r(t)$ is obtained by integrating eq. (2.1). Being

$$k = \frac{V_A}{r\log(b/a)} ,$$

one has

$$r(t) = [r_0^{3/2} - ht]^{2/3} , \tag{3.4}$$

where

$$h = \frac{3}{2}k = \frac{3}{2}\left[\frac{V_A}{p\log(b/a)}\right]^{1/2} . \tag{3.5}$$

The electron collection time is determined by letting in eq. (3.4) $r(t) = r(t_1) = a$. One has

$$t_1 = h^{-1}[r_0^{3/2} - a^{3/2}] . \tag{3.6}$$

At the instant t_1 the pulse height is

$$V(t_1) = -\frac{e}{C\log(b/a)}\log(r_0/a) . \tag{3.7}$$

For $t > t_1$, the pulse is expected to rise slowly according to the law

$$V(t) = -\frac{e}{C\log(b/a)}\log\frac{r_+(t)}{a} \quad (t_1 \leqslant t \leqslant t_2) .$$

where $r_+(t)$ described the motion of the positive ion. When it is collected at the time t_2, one has $r_+(t_2) = b$ and the pulse reaches its maximum $-e/C$. Since $RC \ll t_2$, the maximum effectively reached by the pulse is given by eq. (3.7), because for $t > t_1$ the pulse falls exponentially down to the value V_A with the time constant RC.

3.2. THE PULSE PROFILE

Eq. (3.3) defines the shape of the pulse produced by one ion pair. We shall now extend the calculation to the case in which n ion pairs are simultaneously produced into the chamber. With this aim in view, the following ionization distributions will be taken into account.

(a) Ionization confined to an infinitesimal volume

In this case, from eq. (3.3) we obtained for the function $V(t)$ the following expression

$$V(t) = \frac{Q}{C \log (b/a)} \left\{ \log \frac{r(t)}{b} - \log \frac{r_0}{b} \right\} \quad (0 \leqslant t \leqslant t_1) , \tag{3.8}$$

being $Q = ne$. The electron collection time, t_1, is still given by eq. (3.6) and the maximum pulse height follows from eq. (3.7), i.e.,

$$V_{\max} = V(t_1) = -\frac{Q}{C \log (b/a)} \log (r_0/a) . \tag{3.9}$$

The curve (a), shown in fig. 6, represents the function $V(t)$ given in eq. (3.8). To plot the curve, the parameter $\tau = t/t_1$ has been used and normalization to the value $V_{\max}$ (3.9) has been carried out.

(b) Ionization distributed along a straight line parallel to the axis of the chamber

Let $\rho(z)$ be the charge density per unit length, being z the coordinate taken along the axis of the chamber. Since all the ions are at the same distance from the axis of the chamber, one has simply, from eq. (3.3),

$$V(t) = \frac{1}{C \log (b/a)} \int_0^l \left\{ \rho(z) \left[\log \frac{r(t)}{b} \right] - \rho(z) \left[\log \frac{r_0}{b} \right] \right\} \mathrm{d}z \quad (0 < t \leqslant t_1) ,$$

where l is the track length and t_1 the electron collection time given by eq. (3.6). For uniform distribution, it is $\rho(z) = \rho_0 =$ constant and the function $V(t)$ is still given by eq. (3.8), being now $Q = \int_0^l \rho_0 \mathrm{d}z$. Hence, the pulse shape is still represented by the curve (a), plotted in fig. 6.

(c) Ionization distributed along a straight line perpendicular to and passing through the axis of the chamber

Let the ions, at the time $t = 0$, be produced with density $\rho = \rho(r_0)$ along the direction of the radius of the chamber, between r_{01} and r_{02}, being $a \leqslant r_{01} < r_{02} \leqslant b$. Since the electrons move towards the collecting wire with a drift velocity which depends on r — eq. (2.1) — i.e.,

$$v_- = \frac{2}{3} h r^{-1/2} , \tag{3.10}$$

it follows that the electron density ρ, equal to $\rho(r_0)$ at the time $t = 0$, becomes for $t > 0$ a function depending on t and on the position r where the electrons find themselves at the time t. In order to determine such a function, let us consider an element of the electron track at $t = 0$, i.e., $\mathrm{d}r_0$, which contains a negative charge $\rho(r_0)\,\mathrm{d}r_0$. At a time $t > 0$, the element $\mathrm{d}r_0$ transform itself into an element $\mathrm{d}r$ along which the original charge is distributed with a density $\rho(r,t)$. Clearly, the following relation has to be satisfied, i.e.,

$$\rho(r,t)\,\mathrm{d}r = \rho(r_0)\,\mathrm{d}r_0$$

or

$$\rho(r,t) = \rho(r_0) \frac{\mathrm{d}r_0}{\mathrm{d}r} . \tag{3.11}$$

Since the inverse of the function $r(t)$ defined in eq. (3.4) is

$$r_0 = [r^{3/2} + ht]^{2/3} , \tag{3.12}$$

the density $\rho(r,t)$ can be explicitly expressed. One has

$$\rho(r,t) = \rho(r_0)\, r^{1/2} [r^{3/2} + ht]^{-1/2} . \tag{3.13}$$

The collection time of the first and the last electron of the track, derived from eq. (3.6), is

$$t_{11} = h^{-1} [r_{01}^{3/2} - a^{3/2}]$$

and, respectively,

$$t_{12} = h^{-1}\,[r_{02}^{3/2} - a^{3/2}]\ .$$

It is convenient to split the time interval from the instant of the track formation, $t = 0$, to t_{12}, into the two intervals

$$0 \leqslant t \leqslant t_{11}$$

and

$$t_{11} \leqslant t \leqslant t_{12}\ .$$

The function $V(t)$ in these time intervals turns out to be

$$V(t) = \frac{1}{C \log (b/a)} \left\{ \int_{r_1(t)}^{r_2(t)} \rho(r, t) \left[\log \frac{r(t)}{b}\right] \mathrm{d}r - \int_{r_{01}}^{r_{02}} \rho(r_0) \left[\log \frac{r_0}{b}\right] \mathrm{d}r_0 \right\} \qquad (3.14)$$

and, respectively,

$$V(t) = \frac{1}{C \log (b/a)} \left\{ \int_{a}^{r_2(t)} \rho(r, t) \left[\log \frac{r(t)}{b}\right] \mathrm{d}r - \int_{r_{01}}^{r_{02}} \rho(r_0) \left[\log \frac{r_0}{b}\right] \mathrm{d}r_0 \right\} + \frac{1}{C} \int_{t_{11}}^{t} \rho(a, t)\, v_{-}(a)\, \mathrm{d}t\ . \qquad (3.15)$$

The first term in the right-hand-side of eq. (3.15) as well as the right-hand-side of eq. (3.14) represents both the contributions to the pulse rise due to the electrons not yet collected at the time t and to the positive ions. The second term of the right-hand-side of eq. (3.15) concerns the contribution to the pulse rise due to the electron charge collected up to the time t. The expressions for the integration limits $r_1(t)$ and $r_2(t)$ are, as follows from eq. (3.4),

$$r_1(t) = [r_{01}^{3/2} - ht]^{2/3}$$

and, respectively,

$$r_2(t) = [r_{02}^{3/2} - ht]^{2/3}\ .$$

The maximum pulse height is obtained by letting in eq. (3.15) $t = t_{12}$, i.e.,

$$V_{\max} = V(t_{12}) = \frac{1}{C \log (b/a)} \int_{r_{01}}^{r_{02}} \rho(r_0) \left[\log \frac{r_0}{a}\right] \mathrm{d}r_0\ . \qquad (3.16)$$

The curves (b) and (c) represent the function $V(t)$, normalized to the value given by eq. (3.16), in the two cases $r_{01} = b$, $\frac{1}{2}r_{02} = b$ and respectively $r_{01} = a$, $r_{02} = b$. The curves are plotted assuming $\rho(r_0) = \rho_0 = \text{constant}$ and introducing into eq. (3.14) the parameter $\tau = t/t_{11}$, which varies from zero to 1, and into eq. (3.15) the parameter $\tau' = t/t_{12}$, which varies from t_{11}/t_{12} to 1.

(d) Ionization distributed along a straight line lying on a plane perpendicular to the axis of the chamber

Let us examine the case in which the ion pairs are distributed along a track perpendicular to the axis of the chamber at a distance OM = $b/2$ from it, represented in fig. 4 by the cord AB.

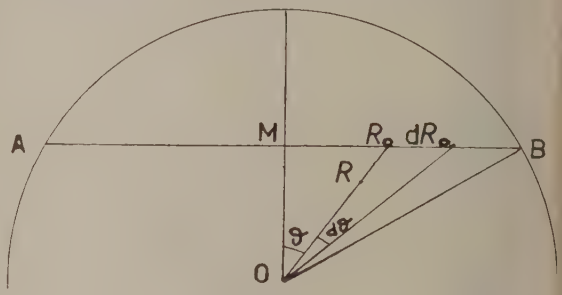

Fig. 4

Because of symmetry reasons, we may consider only the half track MB, since at any instant of time the pulse due to the whole track is twice that one due to the half track. Let the ion pairs be distributed along the track MB with a density ρ given by

$$\rho = \frac{\mathrm{d}q}{\mathrm{d}R_0} = \rho(r_0)\ . \qquad (3.17)$$

In view of the following discussion, it is convenient to substitute the density per unit length by the density per unit angle $\rho(\vartheta) = \mathrm{d}q/\mathrm{d}\vartheta$. During the motion of the electron charge towards the collecting electrode, $\rho(\vartheta)$ remains constant and equal to its original value

$$\rho(\vartheta) = \rho(r_0) \frac{\mathrm{d}R_0}{\mathrm{d}\vartheta}\ . \qquad (3.18)$$

Since

$$OR_0 = r_0 = \frac{\mathrm{OM}}{\cos \vartheta} = \frac{b}{2 \cos \vartheta}\ , \qquad (3.19)$$

$$\mathrm{d}R_0 = [(r_0 \mathrm{d}\vartheta)^2 + (\mathrm{d}r_0)^2]^{1/2} = \frac{b}{2 \cos^2 \vartheta} \mathrm{d}\vartheta\ ,$$

it comes out that

$$\rho(\vartheta) = \rho(r_0) = \frac{b}{2\cos^2\vartheta} . \qquad (3.20)$$

The collection time of the first and the last electron of the track, obtained from eq. (3.6), are

$$t_{\vartheta=0} = h^{-1}[\mathrm{OM}^{3/2} - a^{3/2}] = h^{-1}[(b/2)^{3/2} - a^{3/2}]$$

and, respectively,

$$t_{\vartheta=\pi/3} = h^{-1}[\mathrm{OB}^{3/2} - a^{3/2}] = h^{-1}[b^{3/2} - a^{3/2}] .$$

The rise of the pulse in the time intervals

$$0 \leqslant t \leqslant t_{\vartheta=0}$$

and

$$t_{\vartheta=0} \leqslant t \leqslant t_{\vartheta=\pi/3} ,$$

is pictured by the following equations

$$V(t) = \frac{1}{C\log(b/a)}\left\{\int_0^{\pi/3}\rho(\vartheta)\left[\log\frac{r(t)}{b}\right]\mathrm{d}\vartheta - \int_0^{\pi/3}\rho(\vartheta)\left[\log\frac{r_0}{b}\right]\mathrm{d}\vartheta\right. \qquad (3.21)$$

and

$$V(t) = \frac{1}{C\log(b/a)}\left\{\int_{\vartheta_t}^{\pi/3}\rho(\vartheta)\left[\log\frac{r(t)}{b}\right]\mathrm{d}\vartheta - \int_0^{\pi/3}\rho(\vartheta)\left[\log\frac{r_0}{b}\right]\mathrm{d}\vartheta\right\} - \frac{1}{C}\int_0^{\vartheta_t}\rho(\vartheta)\,\mathrm{d}\vartheta \qquad (3.22)$$

respectively.

The terms in eqs. (3.21) and (3.22) retain the same meaning as in eqs. (3.14) and (3.15). The integration limit ϑ_t is the angular coordinate of the electron collected at the time t; its expression is derived from eq. (3.4) putting $r(t) = a$ and using r_0 given by eq. (3.19). One has

$$\vartheta_t = \mathrm{ar}\cos\frac{b}{2}[a^{3/2} + ht]^{-3/2} .$$

The maximum pulse height is given by eq. (3.22) for $t = t_{\vartheta=\pi/3}$ i.e.,

$$V_{\max} = V(t_{\vartheta=\pi/3}) = -\frac{1}{C\log(b/a)}\int_0^{\frac{b}{2}\sqrt{3}}\rho(r_0)\log\frac{r_0}{a}\,\mathrm{d}R_0 . \qquad (3.23)$$

The function $V(t)$, normalized to the value given by eq. (3.23) is represented by curve (d) plotted in fig. 6, having introduced the parameter $\tau = t/t_{\vartheta=0}$, which varies from zero to 1, into eq. (3.21) and the parameter $\tau' = t/t_{\vartheta=\pi/3}$, varying from $t_{\vartheta=0}/t_{\vartheta=\pi/3}$ to 1, into eq. (3.22). It has done $\rho(r_0) = \rho_0 = \text{constant}$.

(e) Ionization distributed uniformly throughout the chamber

Let the ion pairs be distributed throughout the chamber with constant density $\rho = \rho_0$ and consider the negative charge $\rho_0\,\mathrm{d}\sigma_0$ contained into the infinitesimal volume $\mathrm{d}\sigma_0 = r_0\,\mathrm{d}\varphi\,\mathrm{d}r_0\,\mathrm{d}z$.

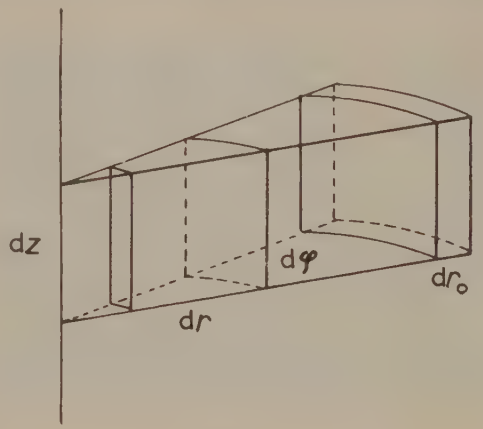

Fig. 5

On the basis of the considerations developed in section 3.2 (*c*), it follows that at the time $t > 0$ the charge $\rho_0\,\mathrm{d}\sigma_0$ is contained into the infinitesimal volume $\mathrm{d}\sigma = r\,\mathrm{d}\varphi\,\mathrm{d}r\,\mathrm{d}z$ with a density $\rho(r,t)$ verifying the relation

$$\rho(r, t)\,\mathrm{d}\vartheta = \rho_0\,\mathrm{d}\vartheta_0$$

or

$$\rho(r, t) = \rho_0\frac{\mathrm{d}\vartheta_0}{\mathrm{d}\vartheta} . \qquad (3.24)$$

From this equation and with the help of eq. (3.12), the density at the time t reads

$$\rho(r, t) = \rho_0 r^{-1/2}[r^{3/2} + ht]^{1/3} . \qquad (3.25)$$

The collection time of the last electrons is given by

$$t_1 = h^{-1}(b^{3/2} - a^{3/2})$$

and the pulse profile is pictured by the following equation

$$V(t) = \frac{2\pi}{C \log (b/a)} \left\{ \int_a^{r(t)} \rho (r, t) \left[\log \frac{r(t)}{b} \right] r(t) \, dr \right.$$

$$\left. \int_a^b \rho_0 \left[\log \frac{r_0}{b} \right] r_0 \, dr_0 \right\} + \frac{1}{C} \int_0^t \rho(a, t) \, v_-(a) \, 2\pi a \, dt, \quad (3.26)$$

where the terms retain the same meaning as in eq. (3.15). The maximum pulse height is given by eq. (3.26) for $t = t_1$, i.e.,

$$V_{max} = V(t_1) = \frac{2\pi\rho_0}{C \log (b/a)} \int_a^b r_0 \left[\log \frac{r_0}{a} \right] dr_0 \, . \quad (3.27)$$

The function $V(t)$, normalized to the value given by eq. (3.27), has been plotted in fig. 6 (curve e) using the parameter $\tau = t/t_1$ which varies from zero to 1.

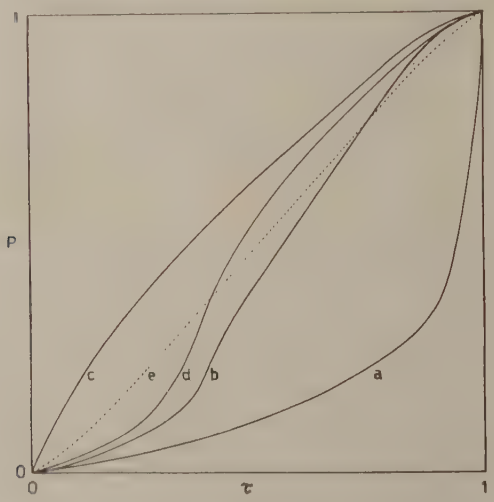

Fig. 6. Pulse shapes corresponding to various kinds of ionization events.

4. Experimental Tests

In order to draw a qualitative comparison between the theoretical pulse shapes and the experimental ones, pulses araising from cosmic radiation have been recorded using the electronic equipment whose block diagram is shown in fig. 7.

The pulse of the chamber is presented both to the vertical deflecting plates of the oscilloscope, through an 8 μsec delay line, and to a pulse height discriminator, adjusted to select pulses higher than a determined value. The signal from the discriminator triggers both the circuit which provides the linear sweep for the

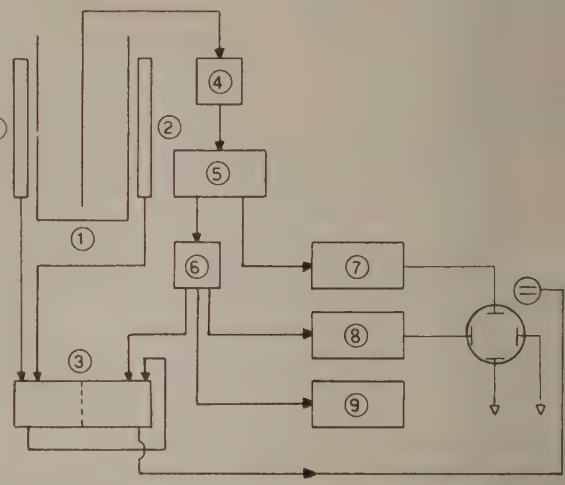

Fig. 7. Block diagram of the electronic equipment used for the recording of the experimental pulses. (1) Ionization chamber. (2) Geiger counters. (3) Mixer circuit. (4) Preamplifier. (5) Amplifier. (6) Discriminator. (7) Delay line. (8) Linear sweep of the oscilloscope. (9) Fotographic recording.

oscilloscope and the photographic recording. The chamber is surrounded by four GM counters. The output pulses of the ionization chamber and those of the GM counters are fed to a mixer circuit, which gives a signal whenever the chamber and the counters are simultaneously discharged. This signal is used to switch on a neon lamp placed before the oscilloscope screen. The electronic amplifier is of the type described in section 2.4; the amplification is 16.250.

In fig. 8 are the reproductions of pictures showing pulses of four different shapes. These experimental shapes are of the type represented in fig. 6 by the curves (a) (c) (d) and (e) respectively and can be explained taken into account the physical assumptions made in the theory. Pulse (a′) may correspond either to a nuclear disintegration which gives rise to some short-range ionizing particles, or to an ionizing particle passing almost parallel to the wire.

A simple ionizing particle traversing the

chamber neither very close nor parallel to the collecting wire may account for a pulse of the type (d'), whereas a pulse of the type (c') may be produced by a particle passing very close to the wire and forming with it a large angle.

A pulse of the type (e') is clearly produced by a group of many ionizing particles passing through the chamber and the GM counters. This can be easily understood by considering that the neon lamp has been switched on.

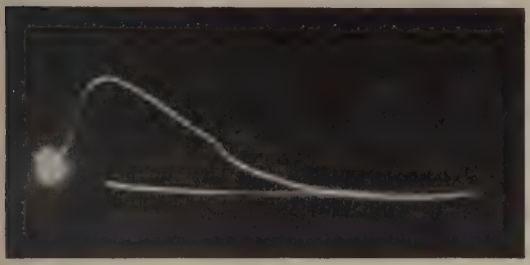

Fig. 8a'

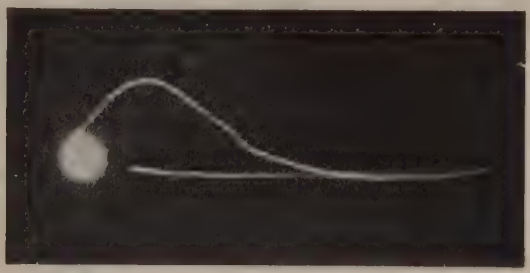

Fig. 8c'

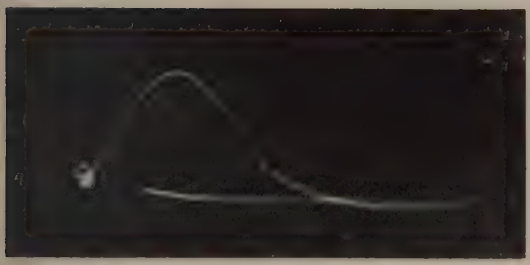

Fig. 8d'

Fig. 8e'

Fig. 8. Experimental pulses.

NUCLEAR INSTRUMENTS 2 (1958) 270–274; NORTH-HOLLAND PUBLISHING CO. – AMSTERDAM

APPARATUS FOR PROCESSING NUCLEAR EMULSIONS

E. BUJDOSÓ† and L. MEDVECZKY

Institute of Nuclear Research of the Hungarian Academy of Science, Debrecen

Received 11 November 1957

The authors built an apparatus for processing nuclear emulsions. Its functioning is shown by describing the processing of an Agfa K2 emulsion of 200 μ thickness.

1. Introduction

The reliability of the nuclear emulsion method, particularly the precision of the measurements depends in high degree on the processing of the plates. The technique may be regarded adequate if

(a) the grade of development is uniform in all points of the plate,

(b) the tracks are not affected by distorsion of the emulsion,

(c) the fog background is low, thus it is easy to distinguish the grains of the tracks from the grains of the background,

(d) the emulsion is translucient, no colloidal silver was developed during processing in the emulsion, thus the optical resolution is uniform in all layers of the emulsion, further

(e) above conditions may be reproduced exactly and efficiently.

From the methods[1–5] different in principle, the temperature cycle development devised by C. C. Dilworth, G. P. S. Occhialini and R. M. Payne[6] is widely used. The process varies according to type and thickness of the emulsion. The maximum variation of temperature in different phases of processing should be less than $\pm$ 0.5 °C. Change of temperature in given time, circulation and gradual dilution of processing solutions etc. are required. These factors involve a complicated apparatus for processing the plates.

2. Apparatus

Our aim was to construct a precision apparatus, which is suitable for processing emulsions of different type and thickness and thus may be used universally. Fig. 1 shows the diagram of our processing apparatus. The vessels containing developer (D) and hypo (F) are made of stainless steel. Double spiral pipes are soldered on the outer surface of both tanks. The pipes are joined to two separate circulating systems. Pump P_1 circulates the water of the thermostatmantle adjusted to 37 °C. Pump P_2 circulates the working fluid from the refrigerator. The evaporator of the refrigerator is immersed in a water-glicerin-alcohol mixture and keeps it at —10° C.

Detailed diagram of the developer tank is shown in fig. 2. Wooden jacket (a) and air serve as heat insulators. Plates are held by stainless steel trays. The trays are perforated when simple temperature method is applied, while flat trays without holes are used in the "hot plate" method. There is place for two fix-contact thermometers (c) in the tank. A third thermometer serves for temperature control. Mixing and uniform heating is carried out by letting nitrogen bubbles[7] through the solution. Nitrogen enters the solution through G_1 glass filter (d)

[1] M. Blau and J. A. de Felice, Phys. Rev. **74** (1948) 1198.
[2] H. Yagoda, Rev. Sci. Instr. **26** (1955) 263.
[3] M. B. Summerfield, Phys. Rev. **89** (1953) 340
[4] A. Bernet and M. Chastel, J. Phys. Rad. **15** (1954) 781.
[5] W. Lohmann, Zs. Naturf. **11A** (1956) 174.
[6] C. C. Dilworth, G. P. S. Occhialini and R. M. Payne, Nature **162** (1948) 102.
[7] M. J. Wilson and W. Vanselow, Phys. Rev. **75** (1949) 1144.

† Now at the Hungarian Research Institute for Non-Ferrous Metals, Budapest.

forming bubbles of uniform small size. The tank is filled through funnel (e) and the solution leaves it through opening (f) in the bottom. The other tank used for fixing is larger but otherwise similar in construction. It contains 3 l hypo,

borings are regulated by the same axis. They connect one way the developing tank, the other way the fixing tank. While methods described in the literature[8–10]) control the water-baths surrounding the tank, in our process we regulate

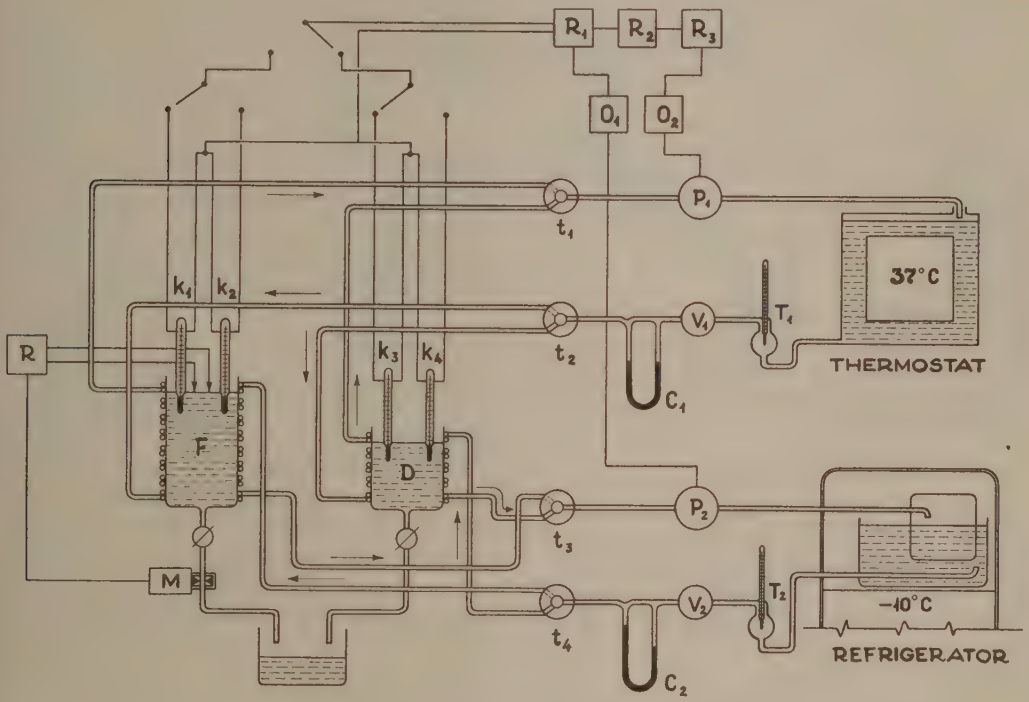

Fig. 1. Diagram of the processing apparatus.

while the volume of the former is only 0.8–1 l.

Thermometers T_1 and T_2 measure the temperature of the circulating liquids (fig. 1). The valves V_1 and V_2 serve to regulate the quantity of the liquids, which is measured by flow-meters C_1, C_2 of Venturi tube type. To facilitate the reading of the thermometer scales T_1, T_2 and flow-meters C_1, C_2 they are lit from the backside by red electric bulbs. The taps t_1–t_4 with twin-

the temperature of the solution directly. Fix contact thermometers k_1–k_4 immersed in the developer and hypo may be connected with electronic relay systems R_1, R_2, R_3 according to the temperature required. Their use is advantageous as no electric current passes through the mercury of the thermometers. Relays R_1 and R_3 control the pumps through magnetic oil-switches O_1 and O_2. Relay R_2 prevents the simultaneous action of the pumps. When the mercury does not touch the contact, pump P_1 circulates hot water until the contact closes, then pump P_2 is switched on and it prevents overheating of the system by circulating cold fluid through the pipes.

[8]) C. C. Dilworth, G. P. S. Occhialini and L. Vermaesen, Fundamental Mechanism of Photographic Sensitivity (Butterworth Scientific Publications, London, 1951) p. 297.

[9]) A. Bonetti, C. C. Dilworth and G. P. S. Occhialini, Bull. Centr. Phys. Nucléaire (Bruxelles 13b., 1951).

[10]) B. Stiller, M. M. Saphiro and F. W. O'Dell, Rev. Sci. Instr. 25 (1954) 340.

The length of time of temperature changes, cooling or heating my be regulated by opening

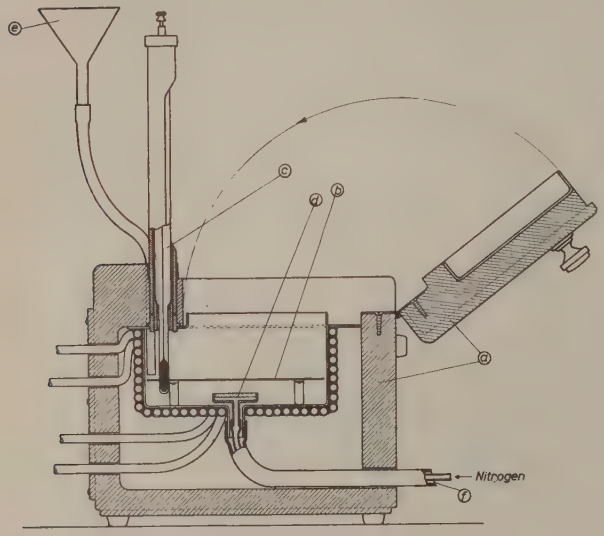

Fig. 2. The developing tank.

or closing valves V_1 and V_2. When keeping a definite temperature the valve is screwd tight and only a small quantity of liquid passes through a narrow opening of 0.5 mm diameter in the valvebody. Thus the system oscillates only slightly round the temperature fixed by the contact thermometer.

3. Processing the Emulsions

Our apparatus is equally suitable to effect slow or fast temperature changes, or to stabilize constant temperature-values exactly, using properly adjusted contact thermometers. Thus various processing problems may be solved using our apparatus. As an example we shall describe the processing of Agfa K2 plates with an emulsion of 200 μ thickness. The temperature diagram of processing this emulsion is shown in fig. 3. The temperature oscillations round the four given temperatures are shown in fig. 4.

3.1. DEVELOPING

The plates are first immersed into distilled water on room-temperature. The water is cooled down slowly at 5° C (1), and when the emulsion is soaked thoroughly, water will be replaced by cold developer solution[11]). In this phase the emulsion is saturated with cold developer. Before beginning the effective devel-

[11]) E. Bujdosó and L. Medveczky, Acta Physica Hungarica **VII** (1957) 135.

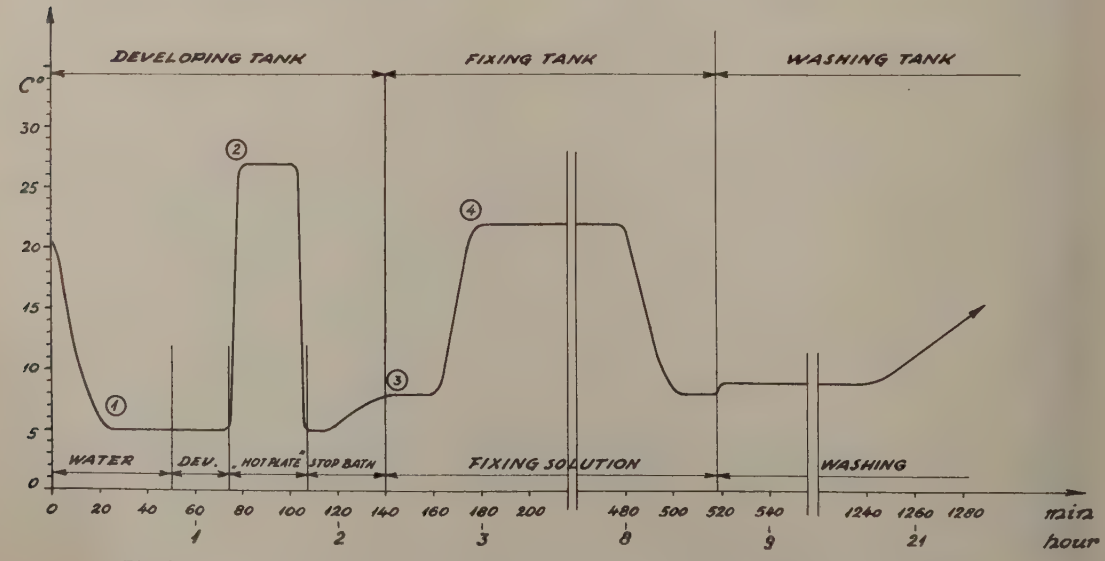

Fig. 3. Temperature graph of the development of Agfa K2 nuclear emulsion, 200 μ thickness.

oping process, a part of the solution is let out until emulsions and trays are clear. We blot the surface of the emulsion with filter paper and rapidly raise the temperature to 27° C (2). A stream of nitrogen bubbles is applied during the whole process. The nitrogen atmosphere formed thus prevents advantageously oxidation of the developer. Latter is particularly dangerous in the hot phase. The solution carried by bubbles to the bottom of the trays ensures temperautre of the trays.

3.2. STOP BATH

Development is first checked by fast temperature decrease then acetic acid cooled to 5° C will be added and the process continued.

3.3 FIXING

From acetic acid bath warmed to 8° C (3) plates pass into the fixing tank. Fixing begins at the same temperature, then after slow warming, it will be continued at 22° C (4).

Some authors[9, 10, 12, 13]) circulate fixing bath with slow laminar motion to exchange used solution for fresh one and thus speed up fixing of the plates. We prefer immersion of the plates into a large quantity of solution. Silver concentration should not exceed 6 g Ag/l. We control concentration from time to time[14]). Solution with higher concentration should not be used[15]). Agitation is worked also by nitrogen bubbles.

After complete clearing of the plates slow and gradual dilution of the fixing bath follows. To avoid sudden swelling of the gelatin dilution is effected by 2% Na_2SO_4 solution poured into the tank. Overflow is prevented by special devices. Two silver contacts reach into the tank (fig. 1). When the level of the liquid reaches the contacts relay R breaks current in the coils of the magnetic pipe-pincer (M) and no liquid passes until the contact ceases. Fixing is finished by

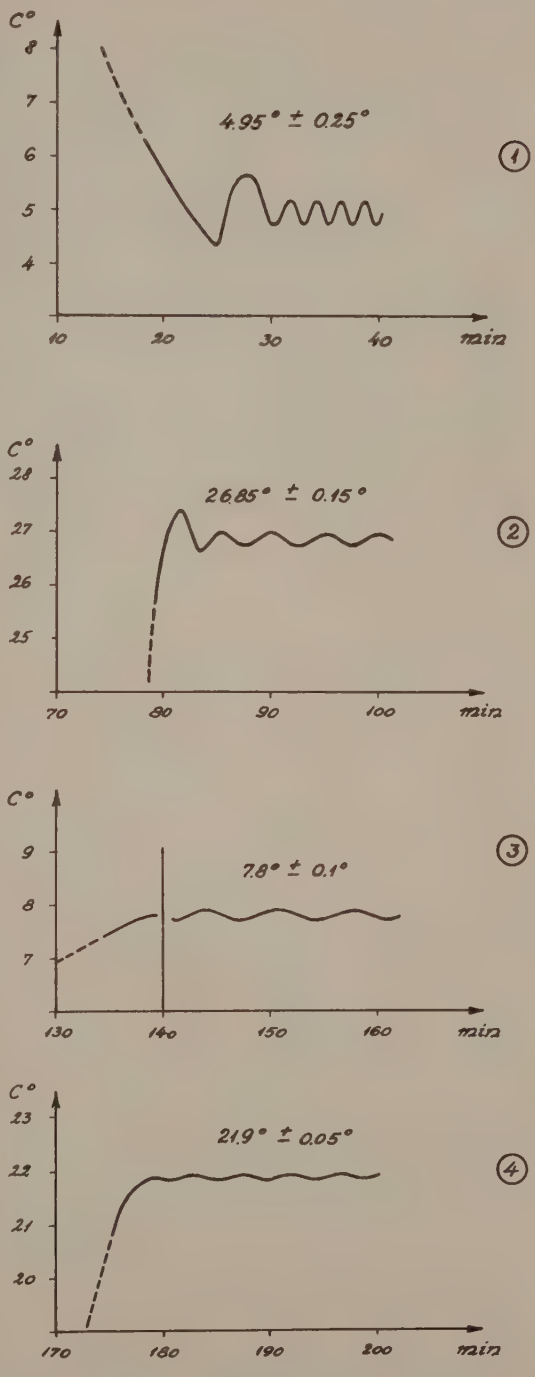

Fig. 4. Temperature oscillations. Figures in the graph refer to points in fig. 3.

[12]) G. Marguin, J. Phys. Rad. **14** (1953) 43.

[13]) F. Thuro, Jour. Sci. Instr. **33** (1956) 296.

[14]) E. Bujdosó and L. Medveczky, Magyar Fizikai Folyóirat **V** (1957) 353.

[15]) A. D. Dainton, A. R. Gattiker and W. O. Lock, Phil. Mag. **42** (1951) 396.

dilution of the hypo, then the temperature of the solution is lowered to about 8° C.

3.4. WASHING

Washing is done by water in laminar flow in a tank made of vinidur. Water from the tap first passes through spiral pipes in the fixing tank, taking up $9 \pm 1°$ C temperature. Washing is finished when no hypo can be traced in the water. Then the control of the fixing tank temperature is switched off and the whole system slowly takes up the temperature of the room. Photograph of the whole apparatus is shown in fig. 5.

Last stage of the process is drying, done by lukewarm air current (20° C).

The apparatus described here proved to be efficient in practice. For more detailed description see literature[14]).

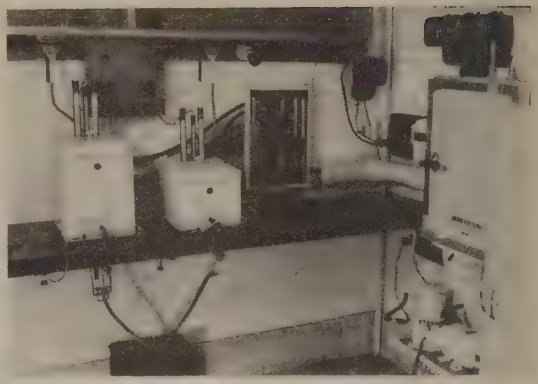

Fig. 5. Photograph of the apparatus with developing and fixing tanks.

Further development and simplification could be effected by direct electric heating instead of water circulation.

NUCLEAR INSTRUMENTS 2 (1958) 275–281; NORTH-HOLLAND PUBLISHING CO. – AMSTERDAM

AUTOMATIC-RECORDING APPARATUS FOR FISSION-FRAGMENT TIME-OF-FLIGHT MEASUREMENTS

J. S. FRASER and J. C. D. MILTON

Atomic Energy of Canada Limited, Chalk River, Ontario

Received 27 November 1957

An apparatus has been constructed to measure the velocities of both members of a fission-fragment pair. A zero-time signal is obtained at the expense of about one per cent of the fragment energy by detecting delta rays ejected by the fragment from a thin plastic foil placed near the source. The fragment times of flight are converted to pulse heights for analysis. An overall time resolution of 3.5 mμsec is obtained. A third variable, e.g. gamma-ray energy or prompt neutron time of flight, may also be recorded, the three pulse heights being punched consecutively on paper tape. Three-dimensional analysis is therefore possible but in practice sorting is done taking two variables at a time.

1. Introduction

An experimental study of the correlation between kinetic energies of a fission-fragment pair and some property of the prompt neutrons or gamma rays requires a three-dimensional analysis. This paper describes a multi-channel automatic-recording apparatus which measures the times of flight of coincident fission fragments as well as a third quantity which may be the gamma-ray pulse height from a scintillation counter or a prompt neutron time of flight. As this type of experiment frequently involves low counting rates while requiring a large number of total counts, the apparatus has been designed to run unattended for many hours.

The record of each event consists of a set of three channel numbers punched on paper tape which, if desired, may be transferred subsequently to punched cards. Analysis of the data can then be performed conveniently on punched-card accounting machinery or on a high speed computer. Sorting is done on a selected pair of variables as the storage requirements for three-variable sorting increase as the triple product of channels used for the variables.

2. General Description

The measurement of the velocities of both coincident fragments by a time-of-flight method requires the production of a fast "zero-time" signal to announce the fission event. This should be done with a minimum loss of energy by the fragments. The use of prompt neutrons or gamma rays is ruled out by the possibility of variation of their intensities among the many fission modes. In fact, this property of the prompt radiations is one that is to be studied in the experiments. A suitable detector has been developed by Stein and Leachman[1]). A modified version of this device has been used in the present apparatus.

The time-of-flight apparatus is shown in fig. 1. At the centre of the apparatus the source holder supports a sample of fissile material deposited on a thin foil of VYNS[2]) which is coated with gold. The gold layer provides a sufficiently low electrical resistance to prevent charge accumulating on the source. The source material covers a circular area about 1/4 in. diameter and is laid down on the gold coating. A collimator is placed on one side of the source. Fragments emerging from the collimator pass through a second foil placed at 45° to the trajectory. Both of these foils are approximately 8 μg/

[1]) W. E. Stein and R. B. Leachman, Rev. Sci. Inst. 27 (1956) 1049.

[2]) A vinyl chloride-acetate co-polymer obtainable from Canadian Resins and Chemicals Ltd., Montreal, Canada.

cm² of VYNS with a coating of 8 μg/cm² of gold. The energy loss in each foil is about 500 keV.

The second foil forms part of the cathode of an electrostatic einzel lens. Secondary electrons or delta rays ejected from the foil by the fragment are accelerated to 10 keV and focused on a thin plastic phosphor[3]). The pressure in the apparatus was maintained at less than 10^{-5} mm of mercury in order to avoid gas discharges in the lens system. The small dimensions of the source and the collimation imposed on the fragments by the and passes down the other drift tube to a similar detector.

3. The Zero-Time Detector

The efficiency of the zero-time detector was measured by comparing the double coincidence rate between the two 4 in. detectors with that between the zero-time detector and one 4 in. detector. For this measurement the drift tube shown on the right of fig. 1 was removed and the scintillation counter fixed to the box. The larger solid angle of the right-hand counter thus

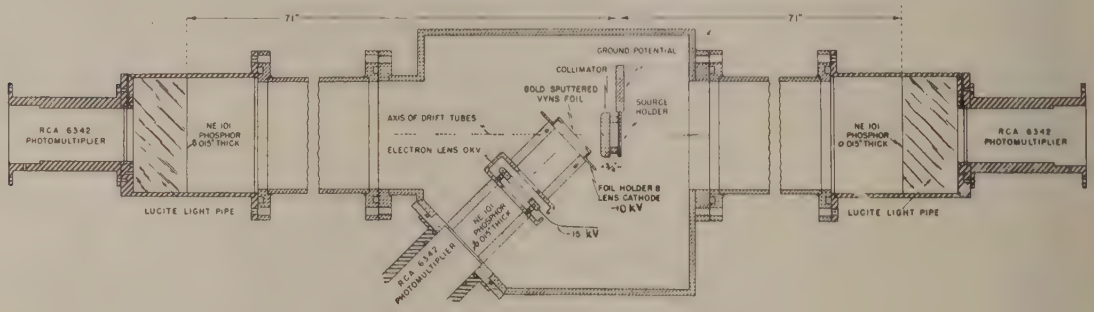

Fig. 1. Fission fragment time-of-flight apparatus.

solid angle of the remote detectors ensure that the delta rays will be produced only in the central region of the foil. The calculated transit time in the lens system for an electron leaving the foil with zero energy is about 4 mμsec. The difference in transit time between such an electron travelling along the axis of the lens system and one taking an extreme paraxial path is 0.1 mμsec. The average initial energy of the delta rays may be estimated to be less than 100 eV[4]). Thus one may expect little variation in the trajectories.

After passing through the foil the fragment proceeds down the drift tube at the end of which it is detected by a 4 in. diameter disk of plastic phosphor coupled to a 2 in. photomultiplier through a 2 in. long light pipe. The complementary fragment penetrates the source backing ensured that any fragment passing through the VYNS foil and being detected in the left-hand counter would have been paired with a fragment detected in the right-hand counter. The two measured coincidence rates differed by less than the statistical standard deviation of 10 per cent. The efficiency of the zero-time detector, therefore, is at least as great as 90 per cent.

It is also of interest to know how many delta rays are collected in the detector. To obtain this from the measured pulse height one needs to measure the response of the scintillation counter to a known number of 10 keV electrons. As it is difficult to procure radioactive sources of monoenergetic electrons in this energy range a pulsed electron gun was mounted on the cathode of the accelerator in place of the plastic foil. Fig. 2 shows schematically the arrangement used for this measurement. A 6BN6 tube, with glass bulb and anode removed, proved quite suitable as an electron gun of small dimensions A careful outgassing of the tube structure,

[3]) Type NE 101 supplied by Nuclear Enterprises Limited, Winnipeg, Manitoba.

[4]) See for example, E. Segrè, Experimental Nuclear Physics, Vol. I (Wiley, 1953) p. 248.

usually lasting overnight, ensured that the cathode was not damaged by positive ion bombardment when the heater voltage was applied.

Pulses 1 μsec wide at a low repetition rate were applied to the grid to form pulses of

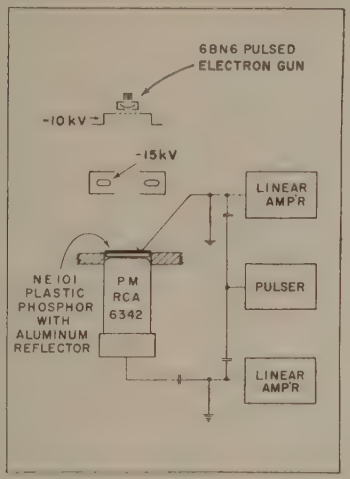

Fig. 2. Schematic diagram of apparatus for studying the "zero-time" detector.

electrons. The back surface of the phosphor was coated with aluminum to act as a reflector. In this measurement the coating also served as a collecting electrode to measure the number of electrons incident on the phosphor. A positive bias of six volts was applied to the collector to eliminate loss of electrons from the surface by secondary emission.

The number of electrons in the pulse incident on the phosphor was measured by comparing the electron collection pulse with that from a calibrated pulse generator coupled through a known small capacitance. The pulse size was adjusted to contain approximately 10^5 electrons in order to reduce the effects of the linear amplifier noise. With the photomultiplier operating at low gain its output pulse was related to that of the pulse generator coupled through a second small capacitance.

The apparatus was then reassembled with a VYNS foil on the lens cathode and a spontaneous fission source mounted in the source holder. The photomultiplier output due to delta rays from the VYNS was measured with respect to the pulse generator, the photomultiplier now being operated at high gain.

These measurements yield a value of 115 ± 15 for the most probable number of electrons collected in the pulse produced by a fission fragment. The pulse-height distribution is shown in fig. 3. The same distribution is observed with either light or heavy fragments passing through the thin foil, the fragments having been identified by their times of flight. The device clearly fulfills the requirements outlined in section 2. The performance of this detector is qualitatively similar to that described by Stein and Leachman[1]).

These measurements together with a knowledge of the absolute gain of the photomultiplier give a value of the efficiency of NE-101 phosphor for 10 keV electrons. The absolute gain at an applied voltage of 600 volts was obtained by measuring the cathode current (produced by a small light source) with an electrometer and the

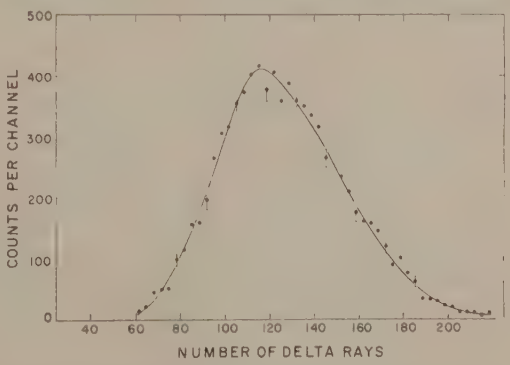

Fig. 3. Distribution of number of delta rays detected.

anode current with a microammeter. On the average a 10 keV electron incident on the phosphor through a few $\mu g/cm^2$ of aluminium produced 2.0 ± 0.1 photoelectrons at the cathode of the photomultiplier (RCA Type 6342).

4. The Time-To-Height Converter

The fission fragment times of flight are determined by converting the time intervals between detector pulses to pulse amplitudes in a linear circuit and subsequently measuring

the amplitudes in a multi-channel analyzer. The circuit to be described is similar in principle to one developed by Moody[5]) but makes use of the properties of the 6BN6 tube. An adaptation of the present circuit for use with a pulsed accelerator has been described by Weber *et al.*[6]).

The construction of the 6BN6 tube results in a very low spread in transit time. Either one of the two grids controls the anode current from cut-off at about —2 volts to saturation at zero volts, with normal anode and focusing electrode voltages of +60 volts. The saturation current is determined essentially by the anode and focusing electrode voltages.

The conversion of time to pulse height is accomplished by allowing the constant anode current to flow into an integrating RC network for a time determined by the interval between the leading edges of the detector pulses. Fig. 4(a) illustrates the shape and time relationship of the two pulses at the fast amplifier outputs

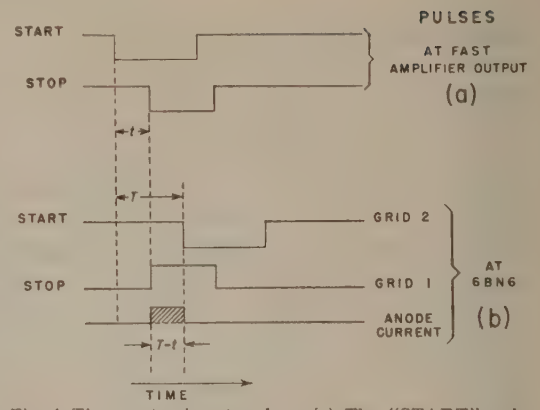

Fig. 4. Time-sorter input pulses. (a) The "START" pulse announces the emission of a fission fragment into the drift tube; the "STOP" pulse is produced at the end of the flight path after a time t. (b) The "START" pulse is delayed by a fixed amount T; the time-sorter output pulse is proportional to $(T - t)$.

when the time of flight of the fragment between the two detectors is t. Between this point and the time-sorter input the "START" pulse is delayed relative to the "STOP" pulse by a fixed amount T whereas the "STOP" pulse is simply inverted. As indicated in fig. 4(b) the

[5]) N. F. Moody, Electronic Eng. 24 (1952) 289.
[6]) Weber, Johnstone and Cranberg, Rev. Sci. Inst. 27 (1956) 166.

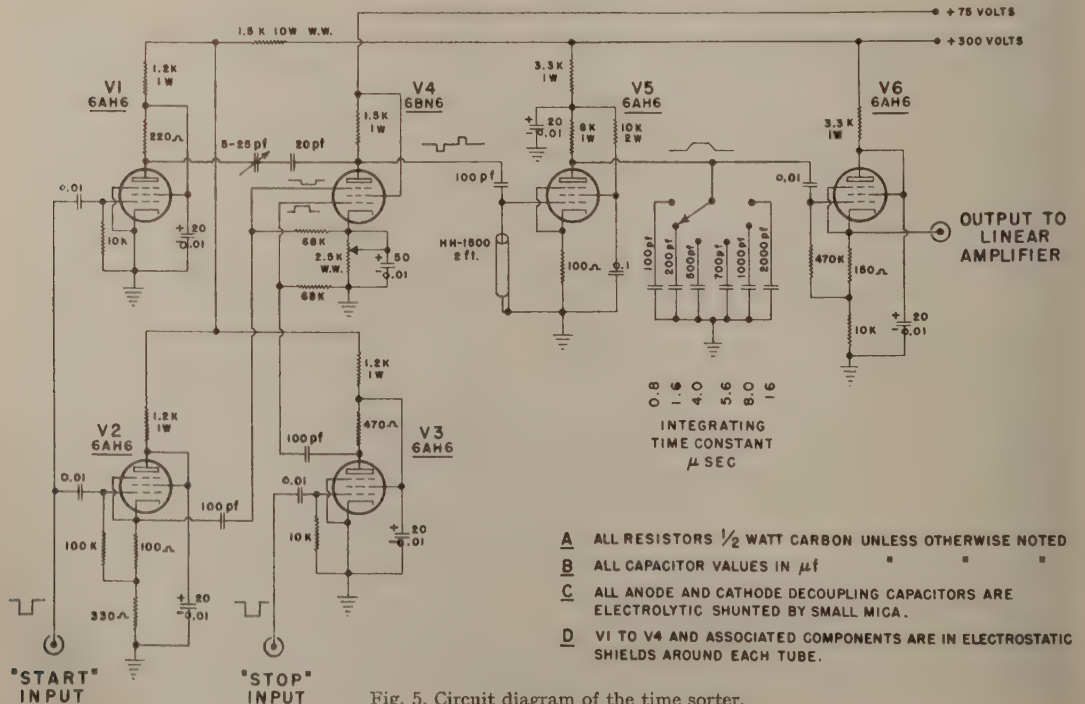
+75 VOLTS
+300 VOLTS
1.5 K 10W W.W.
V1 6AH6
V2 6AH6
V3 6AH6
V4 6BN6
V5 6AH6
V6 6AH6
OUTPUT TO LINEAR AMPLIFIER
"START" INPUT
"STOP" INPUT
INTEGRATING TIME CONSTANT μSEC
A ALL RESISTORS ½ WATT CARBON UNLESS OTHERWISE NOTED
B ALL CAPACITOR VALUES IN μf
C ALL ANODE AND CATHODE DECOUPLING CAPACITORS ARE ELECTROLYTIC SHUNTED BY SMALL MICA.
D V1 TO V4 AND ASSOCIATED COMPONENTS ARE IN ELECTROSTATIC SHIELDS AROUND EACH TUBE.

Fig. 5. Circuit diagram of the time sorter.

"STOP" pulse, applied to grid 1 of the 6BN6, turns on the anode current which flows at a constant rate until cut off by the delayed "START" pulse.

Fig 5 shows the essential parts of the time-sorter circuit. The two inputs are negative pulses from Hewlett-Packard Type 460B amplifiers. The "STOP" pulse is inverted and limited by V3 and applied to grid 1 of V4. This grid is biased to cut-off while grid 2 is at zero bias. The delayed "START" pulse is limited by V2 and applied to grid 2 of V4 to cut off the anode current. V1 provides an inverted version of the "START" pulse which is coupled to the anode of V4 through a trimmer capacitance to compensate for the interelectrode capacity between the second grid and the anode.

V5 is the integrating stage. The integration time constant is adjusted to be at least 10 times as long as the largest time interval to be measured in order to ensure that the deviation from linearity is less than one per cent. The shorted delay line in the grid circuit returns the integrated pulse rapidly and smoothly to the base line eliminating the long exponential tail that would otherwise result.

The high electric field in the zero-time detector produces a high background rate in the "START" channel, but this input will tolerate a higher counting rate than the "STOP" input. A time-sorter output pulse amplitude proportional to t may easily be obtained by interchanging the input leads as well as the fixed delay T; it was chiefly the above considerations of input counting rates that led to the choice of a scale proportional to $(T - t)$ (see section 5.2).

5. Time Resolution

5.1. THE ZERO-TIME DETECTOR

The zero-time detector is potentially very fast. Time spreads arise from the following causes:

(1) Different flight paths through the lens.

(2) Spread in initial energies of delta rays.

(3) Phosphor light emission time constant.

(4) Time spreads introduced by the photomultiplier.

(5) Obliquity of the cathode foil.

Rough estimates have been made of these spreads for the system used here. (1) Different flight paths through the lens introduce a maximum spread of 0.1 mμsec. (2) The spread in initial energies of delta rays gives an approximately exponential distribution in flight times with a 1/e width of less than 0.1 mμsec. The fact that the high energy delta rays will emerge peaked in the direction of the fission fragment has not been taken into account but would tend to decrease this estimate. (3) The decay time of NE-101 is quoted by the manufacturer as 4 mμsec. According to the considerations advanced by Post and Schiff[7]) the variation in time of emission of the first photoelectron is then

$$\frac{\tau}{R} = \frac{4 \times 10^{-9}}{2 \times 115} = 0.02 \text{ m}\mu\text{sec}\,.$$

As there is always a high background in this type of detector resulting from the high voltage applied to the lens it is probably necessary to raise the threshold to something like the tenth electron of the pulse. This would increase the r.m.s. spread to about 0.06 mμsec. There is a considerable spread in the number of delta rays emitted (see fig. 3) and this results in an estimated contribution to the spread of about 0.1 mμsec. (4) Since the lens can be arranged to focus electrons on a small area of the phosphor, say a $\frac{1}{2}$ in. diameter disk, the transit time spread in the photomultiplier will give a contribution to the time resolution of 0.1 mμsec[8]). (5) The obliquity of the cathode foil and finite source size give a semi-circular distribution in time with a calculated spread at the base of 1.0 mμsec for the light fragment rising to 1.4 mμsec for the heavy fragment.

5.2. THE TIME-TO-HEIGHT CONVERTER

From V5 on in the circuit it is essential to avoid base line disturbances. The time scale has been converted to a pulse-amplitude scale so that fluctuations in amplitude introduced in any subsequent circuit result in an effective

[7]) R. F. Post and L. I. Schiff, Phys. Rev. 80 (1950) 1113.
[8]) R. V. Smith, Nucleonics 14, No. 4 (1956) 55.

loss in time resolution. It should be noted that every "STOP" pulse greater than about one volt in amplitude produces an output pulse. In a typical experiment the number of single "STOP" pulses will be enormously greater than the number of true "coincidences". This means that there will be a large number of large unwanted pulses in the integration and linear-amplifier stages. The use of delay-line clipping reduces the pile-up effect of these pulses on the true pulses. A time distribution curve taken with calibration pulses (see section 6) in the presence of about 50 000 counts per minute in each input channel was 0.5 mμsec full width at half maximum.

5.3. THE FRAGMENT "STOP" COUNTERS

The use of light pipes to couple the 4 in. diameter phosphors to 2 in. diameter photo multipliers results in a considerable loss in pulse height.

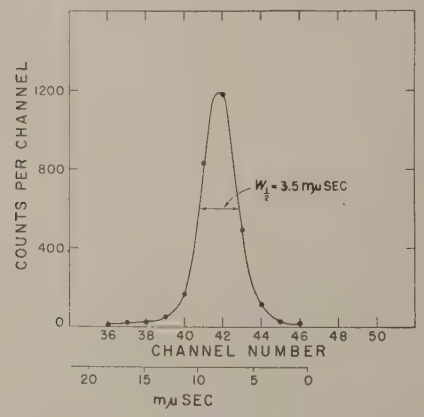

Fig. 6. Resolution curve obtained with a fission-fragment flight path of 15 cm.

No estimate has been made of the contribution of these counters to the overall time spread.

The time resolution shown in fig. 6 represents the distribution in time of coincidences produced by light fission fragments in the zero-time detector and one scintillation counter separated by 15 cm. The light fragments were resolved from the heavy fragments in this short flight path by observing them in coincidence with heavy fragments traversing the full flight path in the opposite direction.

This curve was taken with a "STOP" input rate of about 30 000 counts per minute, most of which were photomultiplier noise pulses. The width at half maximum is 3.5 mμsec.

From the considerations of this section it would appear that the major contribution to the time spread comes from the fission fragment detectors and results from the relatively poor efficiency of the conversion of the fragment energy to photoelectrons.

6. Calibration

It is necessary to calibrate the pulse-amplitude scale of the time sorter in terms of time intervals. A time calibrator was constructed in which a fast rising step wave from a mercury relay was fed into two 100-ohm cables, one of fixed length, the other variable. The difference in time delay of the two circuits was variable in steps of 0.5 mμsec from zero to 500 mμsec. The electrical length of each section of cable was adjusted to be within 0.1 per cent of the required value. This was done by measuring the fundamental and several harmonics of the resonant frequencies of the cable, short- and open-circuited with a heterodyne frequency meter checked against radio station WWV.

The zero of the calibrator was checked by plotting the calibration dial readings as a function of time-sorter output with (a) the calibrator output cables in their normal position and (b) in reversed position. The extrapolated curves intersected at zero relative delay within about 0.5 mμsec.

The true time zero for the fragments was found by measuring the position in time of the light and heavy peaks as a function of the distance from the source of one of the detectors. Meanwhile, the other detector was left at the full distance and enabled one to resolve the two peaks in the near counter even at very small distances. This procedure was then repeated reversing the role of the two detectors. In this way it was found that the time zero for the light fragments was about 3 mμsec earlier than that for the heavy fragments. This was probably due to the large difference in pulse heights for

the two groups in the 4 in. scintillation counters. The average light fragment pulse was about four times as large as the average heavy fragment pulse. As the heavy fragment pulses were not far above the time-sorter threshold it seems plausible that the rise time of the pulses could account for the apparent relative delay between light and heavy fragments. The shift in the intercept was assumed to vary linearly with flight time. Using the indicated times of flight of both light and heavy fragments for two flight distances a single intercept and slope were derived for the linear relationship between time and channel number.

At three-hour intervals during the course of an experiment about 40 calibration pulses were fed into the three channels, time calibration pulses into the time sorters, and voltage pulses into the NaI counter preamplifier (see fig. 7).

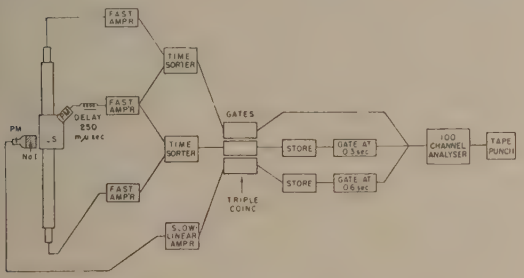

Fig. 7. Block diagram of electronic and recording apparatus for an experiment to correlate prompt gamma-ray spectra with fission-fragment energies measured by the time-of-flight method.

As described in section 7 the calibration pulses could be distinguished from normal pulses on the punched tape.

7. Data Recording and Processing

Fig. 7 is a block diagram of the electronic and recording apparatus used in an experiment to measure the kinetic energies of coincident fission-fragment pairs and at the same time to record the energy of the prompt gamma rays in a large NaI crystal. In this arrangement two time-to-height converter circuits derive a common pulse from the "START" detector and a "STOP" pulse from one of the counters at the ends of the drift tubes. The NaI gamma-ray spectrometer output is amplified by a conventional linear amplifier.

Not shown in the diagram are three linear-amplifier discriminator circuits which handle slow pulses from the three detectors of the time-of-flight apparatus. The three discriminator outputs (0.6 μsec long) actuate a triple-coincidence circuit which in turn gates the three pulses that are to be measured.

In an experiment of this type a three-dimensional pulse-height analysis is required. If one desired N channels for each variable, a total of N^3 channels or cells would be needed, each of which should have a storage capacity of at least 1 000 counts. In order to cope with the sorting problem with a more modest storage capacity the following system was developed:

(a) The three pulses were analyzed consecutively in a 100-channel kicksorter which used a punched paper tape memory. One pulse was fed directly to the kicksorter, the other two to condenser storage units gated subsequently at 0.3 and 0.6 sec following the event. This allowed ample time for the tape punch to operate. A five-channel tape was employed with a binary-decimal code. The record of one event consisted of (i) a code to identify the beginning of the event or calibration and (ii) six binary numbers representing the decimal digits of the analyzer channel numbers for the three pulses.

(b) The data were transferred to punched cards and any portions of the run showing calibration drifts removed.

(c) The data were sorted taking two variables at a time on a computer, the Chalk River Datatron[9]). The computer memory capacity dictated the use of only 60 channels of the kicksorter. The final results were obtained on punched cards and conveniently tabulated[10]) in a 60×60 matrix, each number of which represented a relative frequency of concidence between two pulse-height channels.

[9]) Datatron 205, manufactured by Electrodata Corporation, Pasadena, California.

[10]) On an IBM 407 tabulator.

NUCLEAR INSTRUMENTS 2 (1958) 282–286; NORTH-HOLLAND PUBLISHING CO. – AMSTERDAM

PULSED BEAM DEFLECTION SYSTEM FOR A LINEAR ELECTRON ACCELERATOR

M. J. POOLE, G. DEAN and W. HOWE

Atomic Energy Research Establishment, Harwell, Didcot, Berks.

Received 28 August 1957

A method has been developed to permit the simultaneous use of two targets with a pulsed linear electron accelerator. A magnet is arranged to deflect the beam onto one or the other target, and this magnet is electronically switched on or off in the interval between the beam pulses. A "count-down" circuit is used to select which pulses shall be directed to each target.

1. Introduction

It is required to use the Harwell linear accelerator for two classes of neutron time-of-flight experiment. These are:

(a) Resonance analysis experiments. Here the accelerator is usually run at 400 pps, and the target consists of a uranium block surrounded by a small amount of moderating material.

illustrated in fig. 1 was adopted. A is the uranium target used in the resonance analysis work. Normally the beam is deflected by the electromagnet at B, and emerges through a thin window to fall on A. However before every eighth pulse magnet B is de-energised and this electron pulse travels down the drift tube C to fall on to the lattice target D. The switching operations are

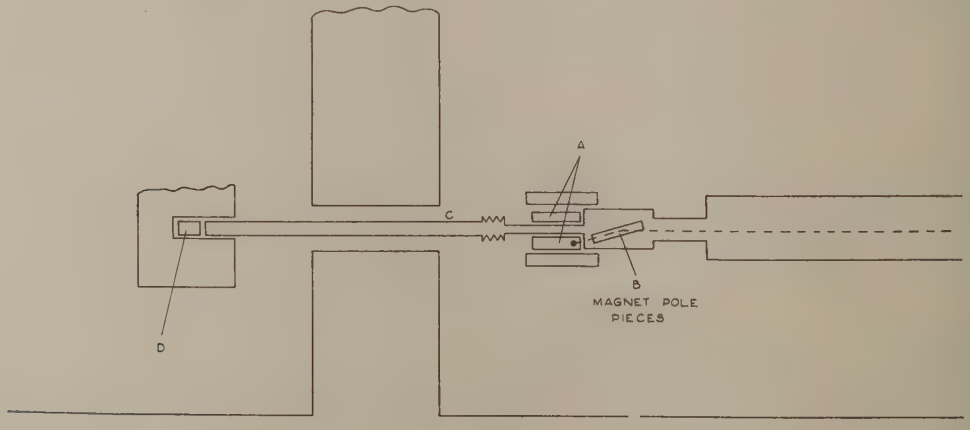

Fig. 1

(b) Lattice spectra determinations. These experiments demand running at 50 pps on to a uranium block target located at the centre of a lattice tank measuring $\approx 18'' \times 18'' \times 18''$. Very long running times are required.

To effect economy in the use of machine time, the arrangement for simultaneous running all completed in the intervals between the pulses. In order to prevent interference between the two experiments, A and D are located in separate concrete cells, with a 4 ft thick concrete dividing wall between them. Thus with the accelerator running at 400 pps, a 50 pps pulsed source is produced at D and a 350 pps source

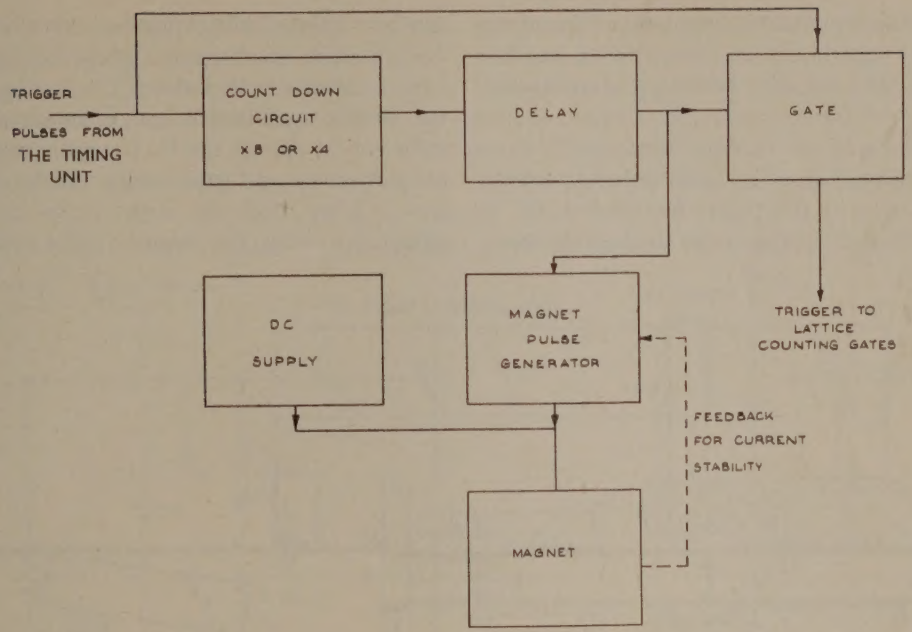
TRIGGER
PULSES FROM
THE TIMING
UNIT
COUNT DOWN
CIRCUIT
x 8 OR x4
DELAY
GATE
DC
SUPPLY
MAGNET
PULSE
GENERATOR
TRIGGER TO
LATTICE
COUNTING GATES
FEEDBACK
FOR CURRENT
STABILITY
MAGNET

Fig. 2

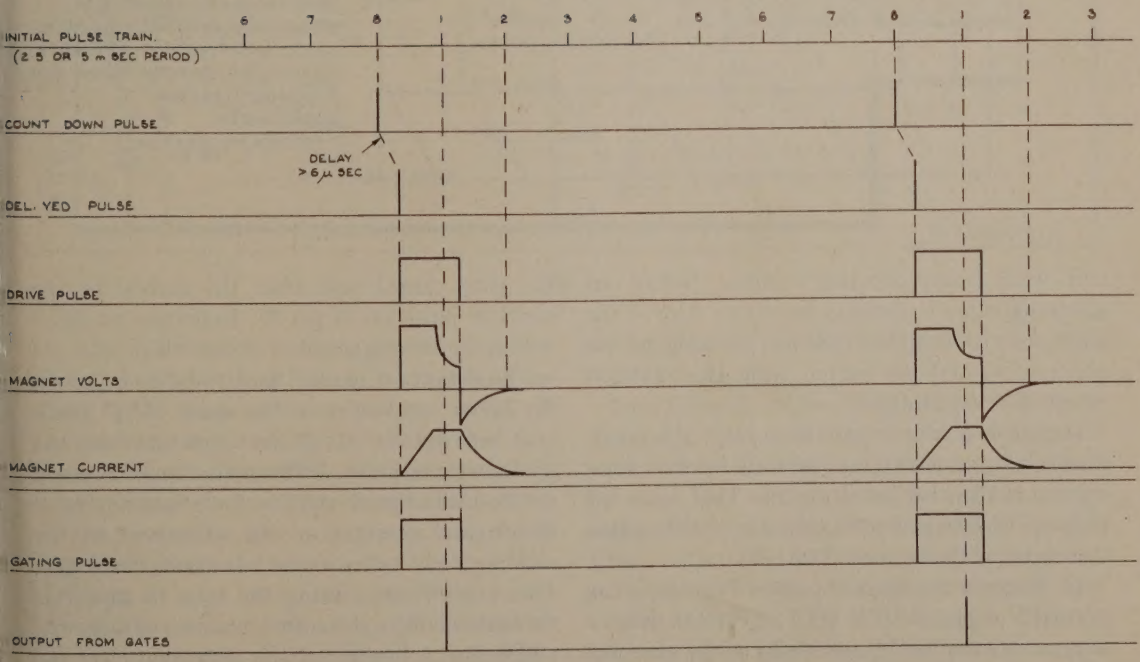
6 7 8 1 2 3 4 5 6 7 8 1 2 3
INITIAL PULSE TRAIN.
(2.5 OR 5 m SEC PERIOD)
COUNT DOWN PULSE
DELAY
> 6 μ SEC
DEL. YED PULSE
DRIVE PULSE
MAGNET VOLTS
MAGNET CURRENT
GATING PULSE
OUTPUT FROM GATES

Fig. 3

at A. In this way full time running of the lattice spectrum experiment is achieved by a sacrifice of only 12½% intensity from the normal target.

2. Circuit

A schematic layout is shown in fig. 2, and the time relation of the pulses involved in fig. 3. A pulse train from the linear accelerator timing unit (each pulse occuring ≈ 6μsec before an electron pulse) is divided by either 8 or 4 (to allow for either 400 or 200 pps working of the accelerator) and the output from this division circuit does two things.

(1) Opens a gate to gate the *next* in the train, thus setting up a 50 pps pulse train in exact time register with the initial train. This train of pulses is used to provide a time zero for the gates associated with the second target.

(2) Triggers the magnet pulser. The magnet is normally energised (5A D.C. 2.5 volts) from a separate power pack, and deflects the electron pulses into the main target. The pulser circuit produces a large voltage pulse in such a direction as to reduce the magnet current. A feedback circuit automatically reduces this voltage when the current has fallen to zero, to an amount just sufficient to oppose the D. C. power pack. The magnet pulser and gate remain on for 2 msec, and a delay after the count down circuit is adjusted so that the magnet pulse ends (and the gate closes) just after the arrival of the electron pulse on target D. Reference to fig. 3 will make the sequence of events clear.

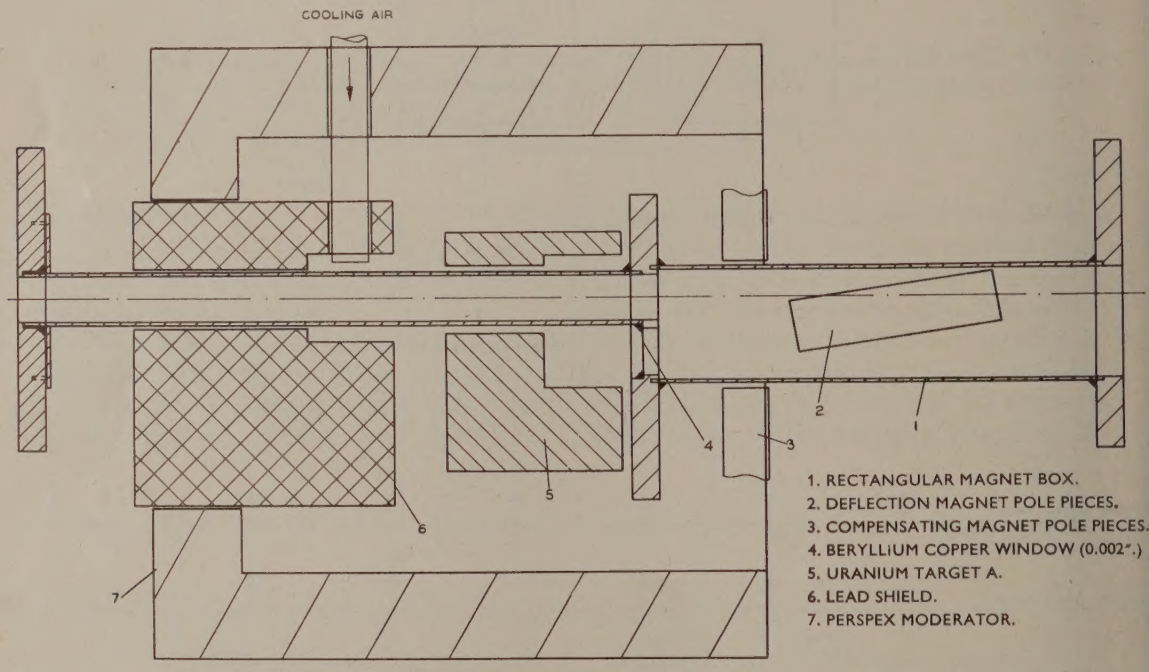

Fig. 4

The deflection magnet had to be installed on the linear accelerator in the space of 6½" available between the end of the accelerator and the position for target A. Additionally target A could not be moved more than ≈ 1 cm laterally from its original position, or the alignment of the existing flight tubes would have been destroyed. This necessitated taking the tube to target D through a hole in the actual uranium of target A, and led to a design for the deflection chamber shown in fig. 4. This chamber is made of thin

stainless steel in order to minimise eddy currents set up by the rapidly varying field, while to allow room for coils, supports etc. the magnet pole pieces were made only 6 cm long, with a gap of 2 cm.

The electron path must have a radius of curvature of 45 cm in order to give the required lateral displacement of 1.5 cm (at the position of A) to the beam. For an electron energy of 13.5 meV this requires a field of 1000 gauss, and to keep down the inductance of the magnet, and so the voltage required to charge the field in the time available, the pole pieces were made only 1.5 cm wide.

A magnet was made using standard transformer laminations as the core, and proved to have an inductance of 25 mH and a D.C. resistance of 0.5 ohms. It produced a field of 1000 gauss with a D.C. current of 5a. To pulse it up to this current in 1.25 msec a voltage of 100 V is required, falling to 7.5 volts when the required field is reached. (It is immaterial for the purposes of argument whether the magnet is considered permanently "on" and is pulsed "off" or vice versa.) The circuit to produce this pulse is given in fig. 5.

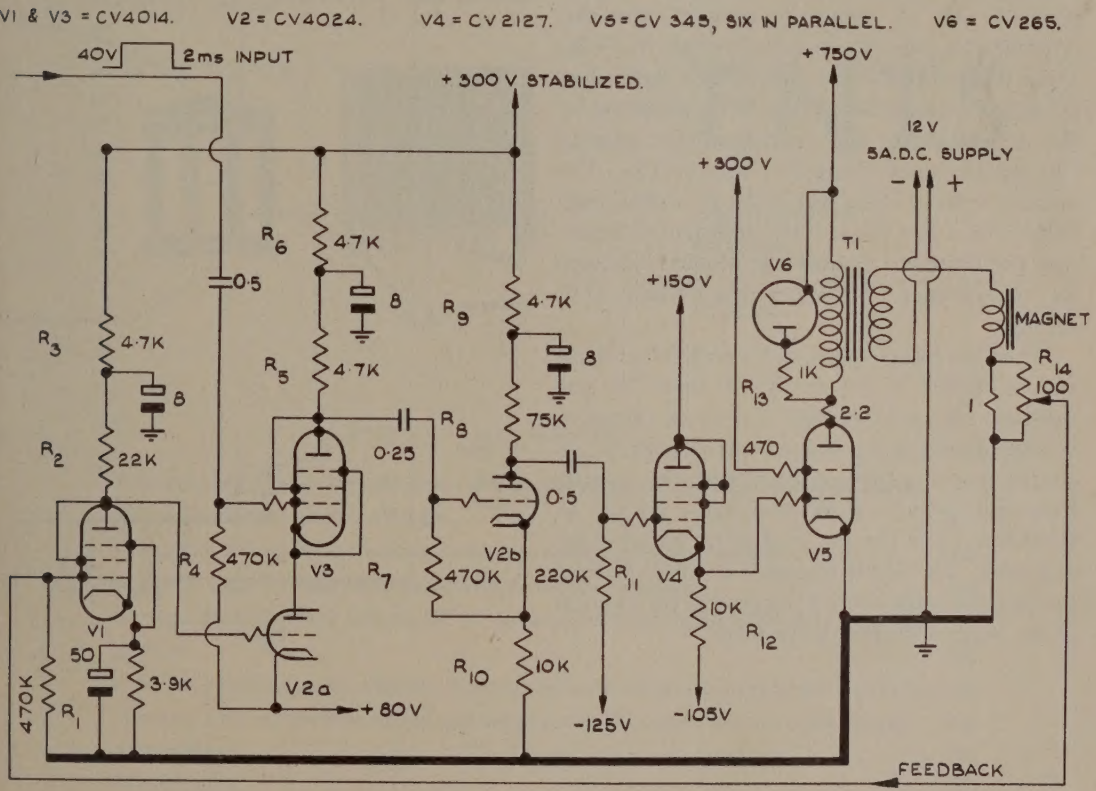

Fig. 5

The delayed pulse from the count down circuit (fig. 3) is used to initiate a +40 V square pulse, whose duration is 2 msec, and controls the time that voltage is to be applied to the magnet. This pulse is fed to the grid of V3, V2b being bottomed, and the resulting negative pulse at its anode after phase reversal and amplification by V2b is fed via a cathode follower V4 to the control grid of the output valves V5. This consists of six CV345 strapped

in parallel so as to obtain the necessary output, and is normally cut off. On the arrival of the positive pulse at its grid, V5 conducts and a 100V square is applied to the magnet, causing an initial linear rise in current (see fig. 6). Potentiometer R_{14} is set so that when the magnet current reaches the required value i, valve V1 which is normally cut off, begins to conduct, and this establishes a negative feed back chain via V2a, which holds the current constant at this value. (It must be remembered that V3 is bottomed by the input square, and so the current passing through R_5 is now controlled only by V2a.) The magnet voltage then falls from its initial high value V to a low value v just sufficient to maintain the current i against the ohmic resistance (or, in practice, to cancel the steady D.C. supply).

When the input square to V3 ends, V3 cuts off and so causes V5 to cut off. A diode V6 and resistance R_{13} are included to prevent excessive voltage arising as the magnet current falls. R_{13} is chosen to give a time constant with the magnet inductance which allows the magnet current to be restored to a few per cent of its initial value in 2 msec. The whole sequence is timed so that the electron pulse arrives during the flat portion of the magnet current wave-form.

This equipment has now been operating satisfactorily for 2 years.

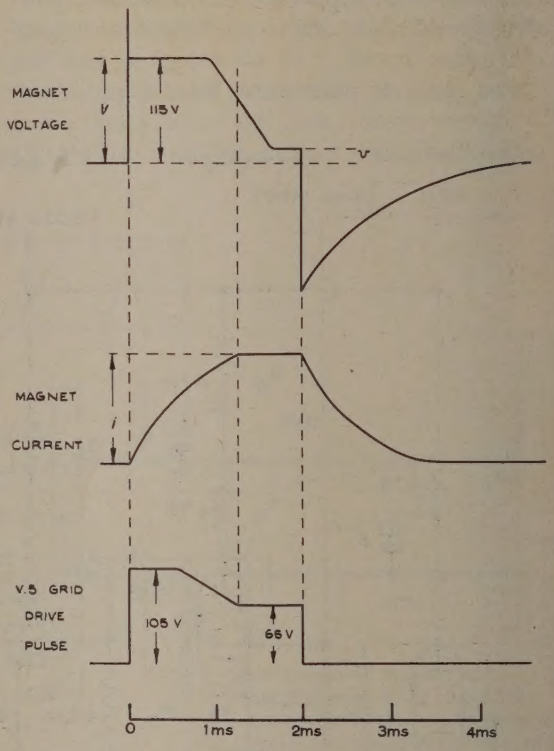

Fig. 6